

The Ups and Downs of Early Dark Energy solutions to the Hubble tension: a review of models, hints and constraints circa 2023

Vivian Poulin,¹ Tristan L. Smith,^{2,3} and Tanvi Karwal⁴

¹*Laboratoire Univers & Particules de Montpellier (LUPM),
CNRS & Université de Montpellier (UMR-5299),*

Place Eugène Bataillon, F-34095 Montpellier Cedex 05, France

²*Department of Physics and Astronomy, Swarthmore College,
500 College Ave., Swarthmore, PA 19081, USA*

³*Center for Cosmology and Particle Physics, Department of Physics,
New York University, New York, NY 10003, USA*

⁴*Center for Particle Cosmology, Department of Physics & Astronomy,
University of Pennsylvania, Philadelphia, PA 19104, USA*

We review the current status of Early Dark Energy (EDE) models proposed to resolve the “Hubble tension”, the discrepancy between “direct” measurements of the current expansion rate of the Universe and “indirect measurements” for which the values inferred rely on the Λ CDM cosmological model calibrated on early-universe data. EDE refers to a new form of dark energy active at early times (typically a scalar-field), that quickly dilutes away at a redshift close to matter-radiation equality. The role of EDE is to decrease the sound horizon by briefly contributing to the Hubble rate [How ??](#) in the pre-recombination era. We summarize the results of several analyses of EDE models suggested thus far in light of recent cosmological data, including constraints from the canonical *Planck* data, baryonic acoustic oscillations and Type Ia supernovae, and the more recent hints driven by cosmic microwave background observations using the Atacama Cosmology Telescope. We also discuss potential challenges to EDE models, from theoretical ones (a second “cosmic coincidence” problem in particular) to observational ones, related to the amplitude of clustering on scales of $8h/\text{Mpc}$ as measured by weak-lensing observables (the so-called S_8 tension) and the galaxy power spectrum from BOSS analyzed through the effective field theory of large-scale structure. We end by reviewing recent attempts at addressing these shortcomings of the EDE proposal. While current data remain inconclusive on the existence of an EDE phase, we stress that given the signatures of EDE models imprinted in the CMB and matter power spectra, next-generation experiments can firmly establish whether EDE is the mechanism responsible for the Hubble tension and distinguish between the various models suggested in the literature.

CONTENTS

I.	Introduction to the “Hubble tension”	3
II.	General considerations for models that attempt to address the Hubble tension	5
III.	Overview of Early Dark Energy models	6
A.	Axion-like Early Dark Energy	7
B.	Rock ‘n’ Roll Early Dark Energy	7
C.	Acoustic Early Dark Energy	8
D.	New Early Dark Energy	8
E.	Dissipative Axion Early Dark Energy	9
F.	Early Dark Energy Coupled to Dark Matter	9
G.	α -attractors EDE	10
H.	Early Modified Gravity	10
I.	Decaying Ultralight Scalar	11
J.	Other models	11
IV.	Phenomenology of Early Dark Energy	12
A.	Background and perturbations evolution	12
B.	Understanding the dynamics of EDE	14
C.	Impact of EDE perturbations on the Weyl potential	15
D.	Impact on the CMB and matter power spectra	17
E.	Beyond the phenomenological model: the axion-EDE case	19
V.	Early Dark Energy in light of <i>Planck</i> data	21
A.	What does it mean to resolve a tension?	21
B.	Preliminary study: results for a phenomenological EDE model	22
C.	Axion-like EDE in light of <i>Planck</i> and SH0ES data	22
D.	Profile likelihood analysis of axEDE	24
E.	Role of <i>Planck</i> polarization	26
F.	Understanding the EDE- Λ CDM degeneracy in the CMB	28
G.	A summary of <i>Planck</i> constraints on the EDE dynamics	32
VI.	Early Dark Energy in light of ACT and SPT data	34
A.	Hints of EDE in ACT	35
B.	Impact of SPT	35
C.	A new tension between ACT and <i>Planck</i> temperature data?	35
D.	ACT and SPT constraints on other EDE models	36
VII.	Challenges to the EDE models	39
A.	A second cosmic coincidence problem	39
B.	Fine-tuning problems of some scalar-field EDE models	39
C.	The trouble with S_8	40
D.	Is Early Dark Energy excluded by BOSS?	40
E.	Age of the Universe tension	44
F.	An extended EDE model to restore cosmic concordance	45
VIII.	Conclusions	46
	Acknowledgments	47
A.	Appendix: Impact of f_{EDE} , a_c and w_f on the power spectra	47
1.	Impact of f_{EDE}	47
2.	Impact of z_c	47
3.	Impact of w_f	48
	References	49

I. INTRODUCTION TO THE “HUBBLE TENSION”

Over the last two decades, our physical description of the Universe on the largest scales has made tremendous progress. The application of General Relativity to the Universe as a whole under the assumption of statistical homogeneity and isotropy has led to the establishment of a standard cosmological model known as the Λ cold dark matter (Λ CDM) model. The Λ CDM model – which includes a cosmological constant Λ and cold dark matter (CDM), along with baryons, photons, and neutrinos – has made predictions that can be tested with cosmological observables up to a very high degree of accuracy. This is especially true for our observations of the cosmic microwave background (CMB), primordial element abundances from big bang nucleosynthesis (BBN), baryon acoustic oscillations (BAO) and uncalibrated luminosity distances to Type Ia supernovae (SNIa). In less than 50 years, these measurements have reached percent-level precision, allowing us to enter an “era of precision cosmology” [1]. However, despite its many successes, our cosmological model remains parametric and the natures of its dominant components – dark matter and dark energy – are yet to be understood.

As measurement precision improves, several tensions have emerged between probes of the early and late universe in recent years, possibly hinting at the underlying nature of these components (for a recent review, see Ref. [2]). Loosely speaking, the “Hubble tension” refers to the inconsistency between “direct” measurements of the current expansion rate of the Universe, *i.e.* the Hubble constant H_0 , made with a variety of probes in the late-universe and “indirect measurements” for which the values inferred rely on the Λ CDM cosmological model calibrated on early universe data. More precisely, it is now understood that the tension arises between measurements which are calibrated using the so-called “sound horizon”, imprints of acoustic waves propagating in the primordial plasma until recombination – under the assumption of the Λ CDM model – and those that rely on different calibration methods¹. This tension is predominantly driven by the *Planck* collaboration’s observation of the cosmic microwave background (CMB), which predicts a value in Λ CDM of $H_0 = (67.27 \pm 0.60)$ km/s/Mpc [4], and the value measured by the SH0ES collaboration using the Cepheid-calibrated cosmic distance ladder, whose latest measurement yields $H_0 = 73.04 \pm 1.04$ km/s/Mpc [5]. Taken at face value, these observations alone result in a 5σ tension.

Great efforts have been mounted to search for any systematic causes of the tension in either the direct or indirect measurements, or both [6–22] (for a review, see Refs. [2, 23]). Yet, the SH0ES team recently provided a comprehensive measurement of the H_0 parameter to 1.3% precision, with attempts at addressing these potential systematic errors, and concluded that there is “no indication that the discrepancy arises from measurement uncertainties or [over 70]

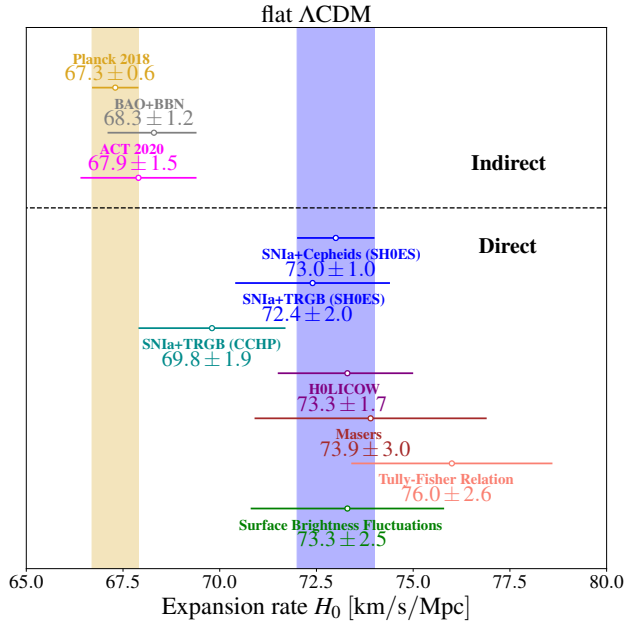


FIG. 1. A summary of a representative selection of the indirect and direct measurements of the current expansion rate H_0 , with errors below 3 km/s/Mpc, based on Ref. [24]. We refer to Ref. [2] for a complete compilation.

¹ Note that some high-accuracy “direct” measurements that find high H_0 also rely on the assumption of Λ CDM (*e.g.* the ‘H0LiCOW’ strongly lensed quasars [3]) but not on the early-universe calibration.

analysis variations considered to date” [5]. Moreover, the appearance of this discrepancy across an array of probes suggests that a single systematic effect is unlikely to be sufficient to resolve it.

Indeed, on the one hand there exists a variety of different techniques for calibrating Λ CDM at high-redshifts and subsequently inferring the value of H_0 , which do not involve *Planck* data. For instance, one can use alternative CMB data sets such as WMAP, ACT, or SPT, or even remove observations of the CMB altogether and combine measurements of BBN with data from BAO [8, 25], resulting in H_0 values in good agreement with *Planck*. On the other hand, alternative methods for measuring the local expansion rate have been proposed in the literature, in an attempt to remove any biases introduced from Cepheid and/or SN1a observations. The Chicago-Carnegie Hubble program (CCHP), which calibrates SNIa using the tip of the red giant branch (TRGB), obtained a value of $H_0 = (69.8 \pm 0.6 \text{ (stat)} \pm 1.6 \text{ (sys)}) \text{ km/s/Mpc}$ [15, 26], in between the *Planck* CMB prediction and the SH0ES calibration measurement, and a re-analysis of the CCHP data by Anand et al. yields $H_0 = 71.5 \pm 1.9 \text{ km/s/Mpc}$ [27]. The SH0ES team, using the parallax measurement of ω -Centauri from GAIA DR3 to calibrate the TRGB, obtained $H_0 = (72.1 \pm 2.0) \text{ km/s/Mpc}$ [28, 29]. Additional methods intended to calibrate SNIa at large distances include: surface brightness fluctuations of galaxies [30], MIRAS [31], or the Baryonic Tully Fisher relation [32]. Bypassing the SN1a altogether and relying on Cepheids alone, the SH0ES team recently obtained $H_0 = (73.1 \pm 2.5) \text{ km/s/Mpc}$ [17]. There also exists a variety of observations which do not rely on observations of SNIa – these include for e.g. time-delay of strongly-lensed quasars [3, 33, 34], maser distances [35], cosmic chronometers [36], the age of old stars [36–38] or gravitational waves as “standard sirens” [39]. A representative² summary of current determinations of the Hubble constant is provided in fig. 1, with errors less than 3 km/s/Mpc, following Ref. [23]. While not all measurements are in strong tension with *Planck*, these direct probes tend to yield values of H_0 systematically larger than the value inferred by *Planck*. Depending on how one chooses to combine the various measurements, the tension oscillates between the $4 - 6\sigma$ level [2, 5, 23].

Observational evidence for or against the Hubble tension is poised to change significantly within the next several years. The use of multi-messenger gravitational-wave measurements of binary systems (i.e., ‘standard sirens’) is projected to reach 2% error bars within the next five years [41], providing an independent check of the local value of H_0 . We are also only a few years away from significant improvements in our measurements of galaxy clustering (e.g., from DESI [42] and Euclid [43]) and in our measurements of CMB anisotropies (e.g., from Simons Observatory [44] and CMB Stage 4 [45]). These upcoming measurements will be decisive in determining if physics beyond Λ CDM is necessary to account for any discrepancy between the direct and indirect estimations of H_0 . This relatively short timeline provides a strong impetus to develop a range of possible extensions to Λ CDM which address the Hubble tension.

In the following, we review attempts involving dark energy in the pre-recombination universe, loosely named “Early Dark Energy” (EDE). We show in Fig. 2, a representative summary of the reconstructed maximum fractional contribution of EDE to the energy density of the universe taken from the literature, and the associated value of H_0 , when the models are fit to a combination of cosmological data involving *Planck*, a compilation of BAO data, and SN1a measurements calibrated using the SH0ES value. One can see that this data combination consistently yields EDE contribution around $\sim 10\%$ and values of H_0 that are within $\sim 2\sigma$ of the SH0ES measurement³. We also provide the $\Delta\chi^2 \equiv \chi^2(\text{EDE}) - \chi^2(\Lambda\text{CDM})$ of *Planck* and SH0ES data to gauge the relative success of the models in addressing the Hubble tension: compared to Λ CDM, most models can significantly improve the fit to SH0ES data, while providing a slightly better fit to *Planck* data. The rest of the review is organized as follows: after a brief introduction in Sec. II to the underlying general mechanism leading to high- H_0 in cosmology with EDE, we present the various models suggested in the literature in Sec. III. We discuss in details the phenomenology of EDE within CMB and LSS data (at linear order in perturbations) in Sec. IV, and present the results of analyses of EDE models in light of *Planck* data in Sec. V. We then review in Sec. VI the recent hints of EDE found when analyzing ACT data, and the impact of SPT data on the preference over Λ CDM. Sec. VII is devoted to discussing challenges to EDE cosmologies, including how probes of matter clustering at late-times (galaxy weak-lensing and clustering in particular) can constrain the EDE solution to the Hubble tension. We eventually summarize our discussion in Sec. VIII. We mention that another review was recently produced on the same topic [48], which covers part of the material presented here. While [48] presents in great detail the current status of the Hubble tension, the purpose of the present review is instead to dive deeper into details of the EDE phenomenology and the analysis results of the various models suggested in the literature, and therefore provide a complementary view on the very active topic of Early Dark Energy and the Hubble tension.

² Some notable measurements not represented here include the TDCOSMO results, which update the H0LiCOW results by constraining lens profiles from stellar kinematic data rather than assuming a specific parameterization. The latest analysis including spatially-resolved stellar kinematics by Ref. [34] finds $H_0 = 77.1^{+7.3}_{-7.1} \text{ km/s/Mpc}$, while earlier work that included data from a different sample of lenses to constrain the population of lens galaxies led to $H_0 = 67.4^{+4.1}_{-3.2} \text{ km/s/Mpc}$ [33]. Since the TDCOSMO collaboration concludes that their later results corroborate the methodology of time-delay cosmography, we choose to represent the “optimistic” number in this summary, but note that there is a level of subjectivity in this decision. The choice of including this optimistic measurement is further supported by Ref. [40], which disfavored the possibility that mass-modelling of strong lenses introduces an $O(10\%)$ bias in measurements of H_0 . This conclusion relies on the excellent agreement found when comparing distances measured with strong-lensing time delays to distance-redshift relations from both calibrated and uncalibrated supernovae, implying that residual systematics in either measurement of H_0 cannot account for the current level of tension with the CMB determination.

³ Note that one cannot directly compare the posterior of H_0 reconstructed in each model to that of SH0ES to assess the tension level, given that SH0ES is included in the analysis. This estimate of the tension level comes from computing a tension metric presented later.

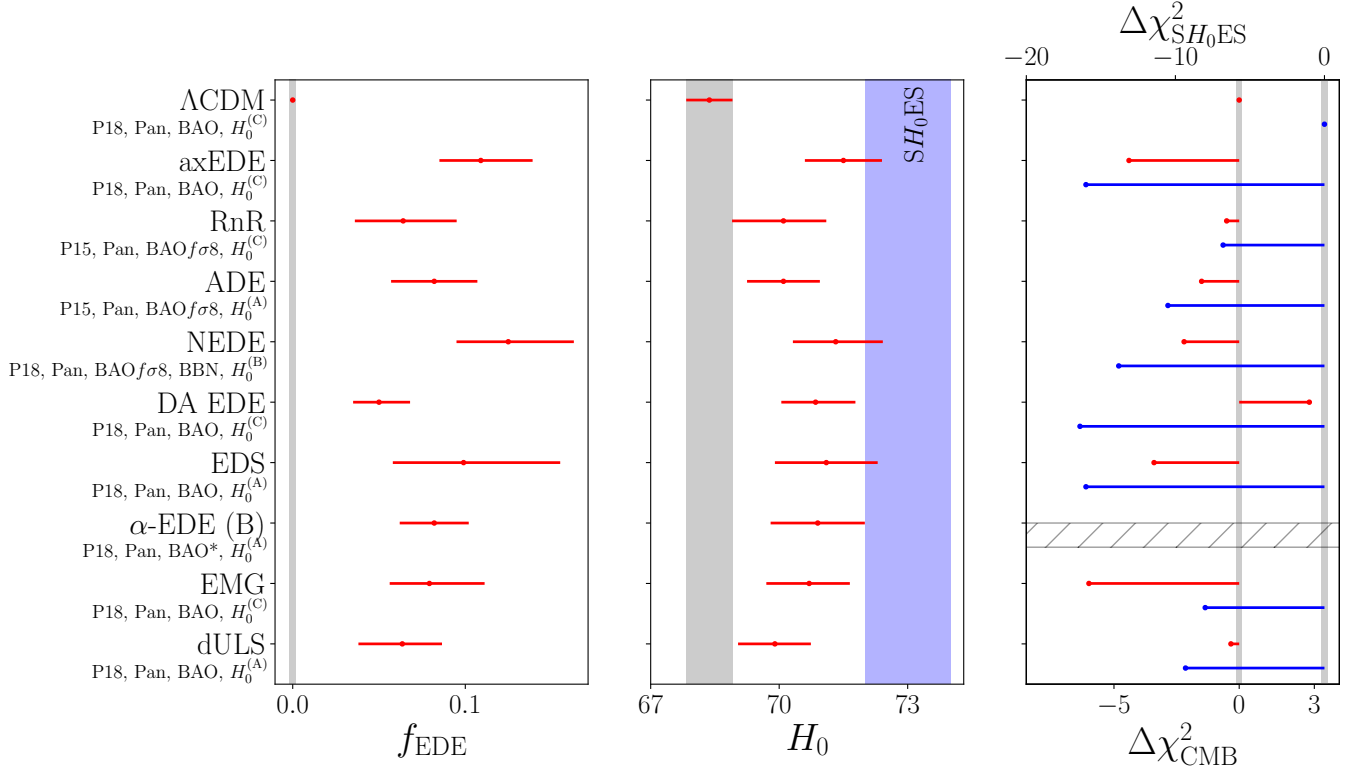


FIG. 2. Comparison of the reconstructed 1D posteriors of $\{f_{\text{EDE}}, H_0\}$ at 68% C.L. in a representative sample of EDE models suggested in the literature, compared with ΛCDM . Note that all models were not analyzed using the exact same datasets (see legends for details), but all analyses include (at least) *Planck* data (2015 or 2018), BOSS BAO DR12, Pantheon and SH0ES. The label $H_0^{(A)}$ refers to the value from Ref. [46], $H_0^{(B)}$ from Ref. [47] and $H_0^{(C)}$ from Ref. [5]. In the rightmost plot, we show $\Delta\chi^2_{\text{CMB}}$ in red and $\Delta\chi^2_{\text{SH}_0\text{ES}}$ in blue. We do not have access to the $\Delta\chi^2$ for the α -EDE model.

II. GENERAL CONSIDERATIONS FOR MODELS THAT ATTEMPT TO ADDRESS THE HUBBLE TENSION

The parameter that drives constraints on H_0 from observations of physics in the early universe is the angular scale of the sound horizon $\theta_s(z) \equiv r_s(z_*)/D_A(z)$, where $r_s(z_*)$ is the physical size of the sound horizon at the redshift z_* at which the oscillating material (i.e., photons and baryons) decouples (i.e., z_* refers to recombination or baryon drag), and $D_A(z)$ is the angular diameter distance to the observation (CMB or galaxy surveys):

$$r_s(z_*) = \int_{z_*}^{\infty} \frac{c_s(z')}{H(z')} dz', \quad (1)$$

$$D_A(z) = \int_0^z \frac{1}{H(z')} dz'. \quad (2)$$

Here $H(z) \equiv \dot{a}/a$ is the Hubble parameter, the sound speed of acoustic oscillations in the tightly coupled photon-baryon fluid is given by $c_s(z) \equiv c[3(1+R)]^{-1/2}$, $R \equiv 3\rho_b/(4\rho_\gamma)$, ρ_X is the energy density in baryons ($X = b$) and photons ($X = \gamma$). It is in this way that r_s provides a standardizable ruler: it is a fixed length scale which, when projected on our sky, can be used to measure distances ($D_A(z)$) in the Universe.

Resolutions to the Hubble tension can be split between *late-* and *early-*universe solutions. Late-universe solutions modify the $z \lesssim 2$ expansion history to raise the value of H_0 without changing the value of the angular diameter distance to last-scattering $D_A(z_*)$. As a result, these theories predict the same value of $r_s(z_*)$ as in ΛCDM . A strong constraint on these models comes from the fact that the SH0ES determination of H_0 is not a determination of the expansion rate at $z = 0$. Instead, it is an absolute calibration of SNIa, which can be used to turn the sample of SN1a measured at $0.001 \leq z \leq 2.26$ (Pantheon+ [49]) into a measurement of the luminosity distance (and therefore the expansion rate) between these redshifts. This constrains large deviations away from ΛCDM across these redshifts which would be necessary to explain the tension. In addition to this, the assumption of ΛCDM in the early universe

allows us to infer a value of $r_s(z_d)$ from observations of the CMB, calibrating measurements of the BAO which also extend to $z \simeq 2$ [50], and provide an independent measurements of the angular diameter distance (and therefore also of the expansion rate). A remarkable result is that, if one uses the measurements from SH0ES to calibrate SN1a on the one hand, and the value of $r_s(z_d)$ predicted in Λ CDM to calibrate BAO on the other hand, the reconstructed angular/luminosity distances are in tension with one another [51–55]. As a result, measurements of $H(z)$ along with $\theta_s(z)$ significantly constrain late-universe solutions⁴ [52, 54, 62].

Early-universe solutions reduce the size of the sound horizon (Eq. (1)) and change the CMB/BAO calibrator [51, 63], resulting in a larger range of allowed dynamics. Resolutions using EDE decrease the size of the sound horizon by proposing the existence of additional pre-recombination energy density which, in turn, increases the Hubble parameter around the time of photon decoupling. Since $H(z)$ is a decreasing function, both integrals in Eqs. (1) and (2) are dominated by their behaviors at their lower limits, so we can roughly write [H\(z\) derivation can be a starting point here](#)

$$\theta_s(z) = \frac{r_s(z_*)}{D_A(z)} \sim H_0 \frac{c_s(z_*)}{H(z_*)} F(\Omega_m; z) \Rightarrow H_0 \sim \theta_s(z) \frac{H(z_*)}{c_s(z_*)} F^{-1}(\Omega_m; z) \quad (3)$$

where $F(\Omega_m; z)$ asymptotes at high redshift to a redshift-independent function, $F(\Omega_m; z \gg 1) \simeq 2.8(1/\Omega_m - 1)^{1/3}/\sqrt{1 - \Omega_m}$.

The approximate expression on the right side of Eq. (3) helps us to quickly understand how EDE can address the Hubble tension. Measurements of the late-time expansion history (such as through SNeIa) provide tight constraints on Ω_m , and atomic physics (plus the CMB temperature today) gives tight constraints on z_* . In addition, assuming standard baryon/photon interactions, $c_s(z_*)$ is fixed from strong constraints on the baryon density obtained either through the CMB power spectra or through measurements of the abundances of light elements formed during BBN. Given that the CMB or BAO provide a precise measurement of θ_s , the role of EDE is to enhance $H(z_*)$ so as to increase the inferred value of H_0 [8, 25, 51, 63, 64]. We note that modifications to the physics of recombination can increase the indirect H_0 by increasing z_* (see, e.g., Refs. [65–69]) but a discussion of these models is beyond the scope of this review.

It is important to note that the larger value of H_0 from direct measurements predicts a larger physical matter density than is inferred from the CMB assuming Λ CDM. In a flat Λ CDM Universe, measurements of the expansion history from SNIa, BAO, and CMB provide a relatively tight constraint on $\Omega_m \equiv \rho_m/\rho_{\text{crit}}$, which, when combined with the SH0ES determination of H_0 gives a physical matter density $\omega_m \equiv \Omega_m h^2 = 0.1603 \pm 0.0063$, which is about 3σ larger than the value inferred from *Planck* assuming Λ CDM: $\omega_m = 0.14228^{+0.00079}_{-0.00091}$ [4]⁵. Remarkably, an increase in $H(z > z_*)$ naturally leads to an increase in ω_m . Indeed, at the background level, the increase in $H(z)$ leads to an increase in Hubble friction which slows the growth of the CDM density contrast. Within the EDE model, this is compensated for by increasing the DM density, leading to a larger ω_m .

An increase in $H(z_*)$ also leads to increased damping of the small scales of the CMB. When $H(z_*)$ increases, the angular scale of the sound horizon, $\theta_s(z_*)$, is kept fixed by increasing H_0 . The angular scale θ_D corresponding to damping roughly depends on

$$\theta_D(z_*) \sim \frac{H_0}{\sqrt{\dot{\tau}(z_*) H(z_*)}}, \quad (4)$$

where $\dot{\tau}(z_*) = n_e(z_*) x_e(z_*) \sigma_T / (1 + z_*)$, n_e is the electron density, x_e is the ionization fraction, and σ_T is the Thomson cross section. If the indirect H_0 increases by a fraction f , with $\theta_s(z_*)$ fixed, $\theta_D(z_*)$ increases by $f^{1/2}$. A larger $\theta_D(z_*)$ leads to greater suppression of power which must be compensated for by an increases in n_s and ω_m . This may have interesting consequences for models of cosmic inflation (see, e.g., Ref. [70]) as we discuss later on. With these general properties of early-universe solutions, we next detail several models of EDE proposed in the literature.

III. OVERVIEW OF EARLY DARK ENERGY MODELS

Broadly speaking, Early Dark Energy is any component of the Universe which was dynamically relevant at $z \gg 1$ and has equation of state $w \simeq -1$ at some point in its evolution. Typically (but not only), it takes the form of a cosmological scalar field which is initially frozen in its potential by Hubble friction. The possibility of the presence of dark energy before last-scattering has been studied for over a decade [71–73], but these models gained acute attention

⁴ It has been suggested that the Pantheon+ sample and strongly lensed QSOs may indicate that at high redshifts, the determination of Ω_m deviates from Λ CDM [56–60], although these deviations are still under the 2σ level [61].

⁵ where $\rho_{\text{crit}} \equiv 3H_0^2/(8\pi G)$ and $h \equiv H_0/(100 \text{ km/s/Mpc})$

in the context of the Hubble tension, starting with the work of Refs. [74, 75], followed by several variations on the underlying scalar field model by numerous authors [76–106].

EDE models typically postulate the existence of a scalar field whose background dynamics are driven by the homogeneous Klein-Gordon (KG) equation of motion

$$\ddot{\phi} + 3H\dot{\phi} + \frac{dV(\phi)}{d\phi} = 0. \quad (5)$$

For most EDE models, the dynamics can be summarized as follows: the field is frozen in its potential, such that the background energy density is constant. The fractional contribution of the field to the total energy density, $f_{\text{EDE}}(z) \equiv \rho_{\text{EDE}}(z)/\rho_{\text{tot}}(z)$, therefore increases over time, in a manner similar to that of DE. Eventually, some mechanism (e.g., Hubble friction dropping below a critical value, or a phase transition changing the shape of the potential) releases the scalar, at which point the field becomes dynamical and the background energy density dilutes away faster than matter. The contribution of EDE to the Hubble rate is hence localized in redshift, typically within the decade before recombination, and acts to reduce the size of the sound horizon as previously described. A successful solution usually requires a fractional contribution $f_{\text{EDE}} \sim 10\%$ that reaches a maximum at $z \sim 10^3 - 10^4$ and subsequently dilutes at a rate greater than or equal to that of radiation. The various proposed models can (broadly speaking) be characterised by (1) the shape of the scalar field potential, (2) the mechanism through which they become dynamical, and (3) whether or not the scalar field is minimally coupled.

With these characteristics, we describe several models in the literature, briefly discuss their theoretical motivation and delineate their parameters.

A. Axion-like Early Dark Energy

Axions ??
What's their
exact nature?

Model: The axion-like Early Dark Energy (axEDE) proposes a potential of the form

$$V(\theta) = m^2 f^2 [1 - \cos(\theta)]^n, \quad \begin{array}{l} \text{Potential of the field ??} \\ \text{what is theta?} \end{array} \quad (6)$$

where m represents the axion mass, f the axion decay constant, and $\theta \equiv \phi/f$ is a re-normalized field variable defined such that $-\pi \leq \theta \leq \pi$. The background field is held fixed at some initial value until $H \sim \partial_\theta^2 V(\theta)$, at which point the field becomes dynamical and oscillates about the minimum of its potential. A more detailed description of this model can be found in Refs. [75, 76]. It was implemented in a publicly available modified version of the CLASS code [107]⁶.

Motivation: Rather than being tied to a fundamental theory, this toy potential was introduced to provide a flexible EDE model with a rate of dilution set by the value of the exponent n . Taken at face-value, this potential may be generated by higher-order instanton corrections [108–110] that require fine-tuning to cancel the leading contributions [98, 103], or through the interaction of an axion and a dilaton [79] and is therefore non-generic [111]. Related constructions of this potential in the context of ‘Natural Inflation’ were also proposed in Refs. [112–114]. Interestingly, recent works have paved the way to embed this potential in a string-theory framework [98, 115], showing that the theory challenges for building an EDE with such a potential are not particularly different from that of other cosmological models, such as inflation, dark energy, or fuzzy dark matter [115]. The general behavior of this EDE component is well-described by cycle-averaging the evolution of the background and perturbative field dynamics [75, 116], as we describe in more detail in sec. IV.

Parameters: It is now conventional to trade the ‘theory parameters’, m and f , for ‘phenomenological parameters’, namely the critical redshift z_c at which the field becomes dynamical and the fractional energy density $f_{\text{EDE}}(z_c)$ contributed by the field at the critical redshift. Additionally, the parameter θ_i controls the effective sound speed c_s^2 and thus the dynamics of the perturbations (mostly). Moreover, it is assumed that the field always starts in slow-roll (as enforced by the very high value of the Hubble rate at early times), and without loss of generality one can restrict $0 \leq \theta_i \leq \pi$. Note that running MCMCs on the theory parameters can change the effective priors for the phenomenological parameters, and impacts constraints [117].

B. Rock 'n' Roll Early Dark Energy

Model: The Rock 'n' Roll Early Dark Energy model [77] (RnR EDE) refers to a rolling scalar field with a potential

⁶ <https://github.com/PoulinV/AxiCLASS>

of the form

$$V(\phi) = V_0 \left(\frac{\phi}{M_{\text{pl}}} \right)^{2n} + V_\Lambda, \quad (7)$$

where V_Λ is a constant. The behavior of this model is very similar to the axion-like early dark energy model, as the $(1 - \cos(\phi/f))^n$ term can be approximated by a $(\phi/f)^{2n}$ in the small ϕ/f limit. This EDE field also begins in slow-roll and eventually rolls down and oscillates in its potential with a time-averaged constant equation of state $w = (n-1)/(n+1)$ when the Hubble parameter drops below the effective mass $\partial_\phi^2 V(\phi)$.

Motivation: Such potentials naturally arise from the requirement of a constant equation of state, and have been studied in the context of axiverse-motivated models. However, they too suffer a similar tuning issue as the axion-like EDE model, as in realistic UV completions, terms with exponents $k < n$ are generated and impact the dynamics, and must therefore be made sub-dominant through fine-tuned cancellations.

Parameters: Similar to the axion-like EDE, one can trade the two theory parameters, the initial field value ϕ_i and V_0 , for phenomenological parameters $f_{\text{EDE}}(z_c)$ and $1+z_c$. The power-law exponent n can be fixed or be free to vary, with data favoring $n \simeq 2$. We again note that RnR EDE is identical to axEDE in the limit $\theta_i \ll 1$.

C. Acoustic Early Dark Energy

Model: Acoustic Early Dark Energy (ADE) is a phenomenological fluid description of EDE suggested in Ref. [78]. It is characterized by its background equation of state $w_{\text{ADE}} = p_{\text{ADE}}/\rho_{\text{ADE}}$ and rest-frame sound speed c_s^2 , which in general may be different from the adiabatic sound speed $\dot{p}_{\text{ADE}}/\dot{\rho}_{\text{ADE}}$. The ADE equation of state is parameterized as

$$1 + w_{\text{ADE}}(a) = \frac{1 + w_f}{[1 + (a_c/a)^{3(1+w_f)/p}]^p}, \quad (8)$$

where a_c controls the scale factor at which the equation of state transitions from $w_{\text{ADE}} = -1$ to $w_{\text{ADE}} = w_f$ and p controls the rapidity of the transition. The case $p = 1$ approximates the behavior of the axion-like EDE model.

Motivation: Scalar-field EDE models with oscillating potentials require a level of fine-tuning that is unsatisfactory from a theoretical perspective. Additionally, they represent somewhat ad-hoc choices of modelling. This phenomenological approach generalizes the modeling (at least at the background level) attempting to optimize the success of the EDE model. It also has the advantage of being realized in the K-essence class of dark energy models, where the dark component is a perfect fluid represented by a minimally-coupled scalar field ϕ with a general kinetic term and a constant sound speed c_s^2 , as given by the Lagrangian density

$$P(X, \phi) = \left(\frac{X}{A} \right)^{\frac{1-c_s^2}{2c_s^2}} X - V(\phi), \quad (9)$$

where $X = -\nabla^2 \phi/2$ and A is a constant density scale. In this category of models, $w_{\text{ADE}} \rightarrow c_s^2$ if the kinetic term dominates, whereas $w_{\text{ADE}} \rightarrow -1$ if the potential $V(\phi)$ dominates.

Parameters: In this model, the parameters are: the ADE maximum fractional energy density contribution $f_{\text{EDE}}(a_c)$; the critical scale factor a_c at which the maximum is reached, similar to other EDE models; the equation of state at late-times w_f ; the sound speed c_s^2 ; and the exponent p which quantifies the rapidity of the transition. In practice, the number of parameters is reduced by setting $p = 1/2$, and data seem to favor $w_f = c_s^2$. The case of a canonical scalar field corresponds to setting $w_f = c_s^2 = 1$. While data have a slight preference for $c_s^2 = w_f = 0.8$, the case $w_f = c_s^2 = 1$ is perfectly compatible, and in the following we will quote results for this minimal model.

D. New Early Dark Energy

Model: The new Early Dark Energy (NEDE) model introduced in Refs. [82, 83] proposes two cosmological scalar fields, the NEDE field ψ of mass M and the ‘trigger’ (sub-dominant) field ϕ of mass m , whose potential is written as (with canonically normalized kinetic terms):

$$V(\psi, \phi) = \frac{\lambda}{4} \psi^4 + \frac{1}{2} \beta M^2 \psi^2 - \frac{1}{3} \alpha M \psi^3 + \frac{1}{2} m^2 \phi^2 + \frac{1}{2} \gamma \phi^2 \psi^2. \quad (10)$$

where $\lambda, \beta, \alpha, \gamma$ are dimensionless couplings. When $H \lesssim m$, ϕ rolls down its potential, eventually dropping below a threshold value for which the field configuration with $\psi = 0$ becomes unstable. At this point, a quantum tunneling to

a true vacuum occurs and the energy density contained in the NEDE field rapidly dilutes. A modified CLASS version presented in Ref. [83] is publicly available⁷.

Motivation: The NEDE proposal in a first-order phase-transition that can naturally be triggered in two-scalar-field models, and may therefore be more theoretically appealing than the original axEDE model. The trigger field has two functions: at the background level, it ensures that the percolation phase is short on cosmological time scales, preventing the emergence of large anisotropies. At the perturbation level, adiabatic perturbations of the trigger field set the initial conditions for the decaying NEDE fluid. In addition, recently Ref. [118] suggested a modification to the model, dubbed ‘hot’ NEDE, where the temperature of a (subdominant) dark sector radiation fluid plays the role of the trigger, thereby removing the need for an additional scalar field. In addition, NEDE naturally introduces interactions between the dark sector radiation fluid and NEDE or DM (with potential implications for the S8 tension), and can connect the phase-transition to the origin of neutrino masses. However a test of the latter model against data has yet to appear in the literature.

Parameters: The NEDE model is specified by the fraction of NEDE before the decay $f_{\text{NEDE}}(z_*) \equiv \bar{\rho}_{\text{NEDE}}(z_*)/\bar{\rho}_{\text{tot}}(z_*)$ (where z_* is given by the redshift at which $H = 0.2m$), the mass m_ϕ of the trigger field⁸ which controls the redshift z_* of the decay, and the equation of state w_{NEDE} after the decay. In Ref. [83], the effective sound speed c_s^2 in the NEDE fluid is set equal to the equation of state after the decay, i.e. $c_s^2 = w_{\text{NEDE}}$.

E. Dissipative Axion Early Dark Energy

Model: Thermal friction is a mechanism that gives rise to warm inflation, a class of inflationary models in which the Universe maintains a finite temperature through continuous particle production, but has also been applied to EDE in Refs. [86, 119]. In this scenario a scalar field ϕ couples to light degrees of freedom that self-thermalize and make up dark radiation. It experiences friction Υ through this interaction, which acts to extract energy density from the scalar field into the dark radiation bath. This is similar to a drag force acting on an object moving through a fluid - the object slows and loses kinetic energy while the fluid heats up and gains thermal energy. The system evolves as

$$\ddot{\phi} + (3H + \Upsilon)\dot{\phi} + V_\phi = 0 \quad (11)$$

$$\dot{\rho}_{dr} + 4H\rho_{dr} = \Upsilon\dot{\phi}^2. \quad (12)$$

The dark radiation has strong self-interactions and rapidly thermalizes. The cumulative effect of this coupled system resembles EDE with the frozen scalar field making up the pre- z_c segment, and the dark radiation redshifting as $(1+z)^4$ making up the post- z_c segment.

Motivation: This model was proposed to resolve the fine-tuning of the scalar potential of EDE. Under thermal friction EDE (or dissipative axion EDE as it is called in [86, 119]), the impact and constraints of the model are completely independent of the chosen scalar potential. An additional benefit is that dark radiation in the form of extra relativistic degrees of freedom can also alleviate the LSS tension, making it desirable to incorporate into an EDE model. A very similar mechanism was also studied in Ref. [120].

Parameters: The parameters of the model are the initial position ϕ_i of the scalar, the friction Υ that couples it to dark radiation and a parameter controlling the potential, assumed to be the mass m of the scalar in [86, 119] which employed a quadratic potential. Posteriors of this model favour the region of parameter space in which DA EDE asymptotes to an ever-present dark radiation with very high z_c , instead of an injection close to matter-radiation equality associated with most EDE models. Although DA EDE improves the fit to data over simply varying N_{eff} due to additional degrees of freedom, the improvement in total χ^2 under this model stems exclusively from fitting a higher H_0 . Hence, while this model attempts to address important challenges to EDE, ultimately, it is disfavoured by data - DA EDE cannot increase the Hubble parameter while maintaining the excellent fit to the CMB provided by ΛCDM .

F. Early Dark Energy Coupled to Dark Matter

Model: One can introduce a conformal coupling $A(\phi)$ between an EDE scalar field and dark matter [94, 95]. The impact of the coupling is a modification of the potential $V(\phi)$ of the scalar to an effective potential V_{eff} that includes dark matter contributions

$$V_{\text{eff}}(\phi, a) = V(\phi) + \rho_{\text{DM}}(a), \quad (13)$$

⁷ <https://github.com/flo1984/TriggerCLASS>

⁸ In the following, we will use the simpler notation $m_{\text{NEDE}} \equiv m_\phi \times \text{Mpc}$.

and a modulation of the particle mass of dark matter

$$m_{\text{DM}}(\phi) = m_0 A(\phi), \quad (14)$$

where m_0 is its mass at $z = 0$, and Eq. 14 modifies the dark matter energy density ρ_{DM} . Specifically for the choice of an exponential coupling $A(\phi) = e^{c_\theta \phi / M_{\text{Pl}}}$ between EDE and dark matter, this phenomenology can arise from considering the predictions of the Swampland distance conjecture. In this case, axion dark matter is sensitive to super-Planckian field excursions of the EDE scalar field through an exponential coupling, leading to an ‘early dark sector’ (EDS) [95]. Other coupling can arise from chameleon models, as usually postulated for late-time dark energy [94, 121, 122].

Motivation: While EDE offers a flexible solution to the Hubble tension, it also raises certain fundamental questions, including a new ‘why then’ problem relating to the injection redshift of EDE, akin to the ‘why now’ problem of late-time dark energy. In these models, the dynamics of EDE are triggered by the onset of matter domination, when dark matter becomes the dominant energy component in the Universe. Another benefit of such a coupling is that it modifies the evolution of dark matter perturbations, with possible implications for the emergent tension in measurements of the growth of structure.

Parameters: Within this scenario, various forms of the conformal coupling and the potential of the scalar field may be explored. EDS [95, 123] explores an exponential coupling and the original axEDE potential [75, 76, 116]. The parameters of this model are the three axEDE parameters with the addition of a coupling constant c_θ .

G. α -attractors EDE

Model: The framework of α -attractors corresponds to an EDE scalar field in which the potential is given by

$$V(\phi) = \Lambda + V_0 \frac{(1 + \beta)^{2n} \tanh(\phi/\sqrt{6\alpha}M_{\text{Pl}})^{2p}}{[1 + \beta \tanh(\phi/\sqrt{6\alpha}M_{\text{Pl}})]^{2n}}, \quad (15)$$

where V_0, p, n, α, β are constants. The normalization factor $(1 + \beta)^{2n}$ ensures the same normalization of the plateau at large ϕ regardless of the choice of (p, n) . The role of (p, n) is to give flexibility to the form of the potential to reproduce various shapes of the energy injection. Authors of Ref. [88] have studied three specific choices $(p, n) = \{(2, 0), (2, 4), (4, 2)\}$, chosen to imitate the dynamics of the R’n’R, axion-like EDE and cADE models respectively.

Motivation: Such potentials can naturally arise through a field re-definition that turns a non-canonical kinetic pole-like term into a canonical one [88]. These α -attractor models have been studied in the context of inflation, and lead to predictions for the spectral index n_s and tensor-to-scalar ratio r , that are largely independent of the specific functional form of $V(\phi)$, leading to the name of “attractors”. They have also been studied in the context of dark energy [124–126], and invoked to connect dark energy and inflation [127, 128] naturally leading to their application for EDEs as well⁹.

Parameters: Besides (p, n) and β which are fixed, the models has three free parameters which are chosen to be the usual maximum fraction of EDE $f_{\text{EDE}}(z_c)$, the critical redshift z_c and the initial field value $\theta_i \equiv \phi_i / (\sqrt{6\alpha}M_{\text{Pl}})$. In the following, we will report results for the case $(p, n) = (2, 4)$ and $\beta = 1$, as it leads to the best potential resolution of the tension [88].

H. Early Modified Gravity

Model: Modified gravity (MG) models which deviate from General Relativity at early times have shown promise in explaining the H_0 tension [88, 130–136]. In particular the early modified gravity (EMG) model from Ref. [137] postulates the existence of a scalar field σ with non-minimal coupling ξ to the Ricci scalar of the form $f(\sigma) = (M_{\text{Pl}} + \xi\sigma^2)R/2$, on top of a simple quartic potential $\lambda\phi^4/4$. In the limit where $\xi \rightarrow 0$ this model reduces to the R’n’R model, while in the limit $\lambda \rightarrow 0$ it reduces to the case of a non-minimally coupled massless scalar field considered in Refs. [132, 133].

Motivation: Non-minimally coupled scalar fields were first suggested to circumvent strong constraints on the variation of Newton’s constant in laboratory and solar-system experiments. The value of G_{eff} measured in the

⁹ Recently, an alternative, exponential potential was suggested in Ref. [129], arguably simpler than the one presented in Eq. 15, introduced to connect early and late dark energies for suitable choices of parameters in the context of α -attractors (with model extensions that can connect with inflation). A dedicated analysis in light of cosmological data is still lacking, though arguments at the background-level suggest that the parameter space might be viable.

laboratory by Cavendish-type experiments for a nearly massless scalar tensor theory of gravity is given by

$$G_{\text{eff}} \equiv \frac{1}{8\pi F} \frac{2F + 4F_\sigma^2}{2F + 3F_\sigma^2} \quad (16)$$

where F_σ refers to the first derivative of $F(\sigma)$, and deviations away from the locally measured value tend to zero as the scalar field settles into its minimum today. In addition, the non-minimal coupling introduces a new degree of freedom to control the gravitational strength at early times that improves over the result of the standard R'n'R model [137].

Parameters: This model consists of three extra free parameters, two describing the field, namely σ_i the initial field value and V_0 which sets the amplitude of the potential and is related to λ through

$$\lambda = 10^{2V_0} / (3.156 \times 10^{109}), \quad (17)$$

where 3.156×10^{109} is the numerical value of M_{Pl}^4 in units of eV⁴, while the third one describes the strength of the non-minimal coupling ξ . To ease comparison with other EDE models, along with ξ , we will report $f_{\text{EDE}}(z_c)$ and $\text{Log}_{10}(z_c)$, derived parameters in the analyses performed in Refs. [69, 137], that are defined as the peak of the EDE contribution and the redshift at which it is reached, respectively.

I. Decaying Ultralight Scalar

Model: The decaying ultralight scalar (dULS) model uses a ‘standard’ axion potential, $V = m^2 f^2 (1 - \cos \phi/f)$, coupled to dark radiation. As the axion oscillates, resonant effects pump energy into the dark radiation, leading to an axion energy density that dilutes faster than matter.

Motivation: Ref. [120] introduced this model in order to address some of the theoretical issues found in the axion-like EDE models. The axion-like EDE potential ($V \sim (1 - \cos \phi/f)^3$) phenomenologically leads to a resolution of the Hubble tension since, in large part, the scalar field energy density dilutes faster than matter. However, this form of the potential is also highly fine-tuned since the potential does not have quadratic and quartic contributions (see Sec. VII for a discussion). The dULS model addresses these issues, allowing a non-minimally coupled scalar field with a standard axion potential to dilute faster than matter.

Parameters: Ref. [120] analyzed this model using a fluid approximation tuned to the exact dynamics. The equation of state evolves as

$$w_s = -1 + \frac{1}{1 + (a_c/a)^3} + \frac{1/3}{1 + (g_d a_c/a)^4}, \quad (18)$$

where $g_d = 1.1$. The dULS background energy density is then specified by a_c and Ω_{dULS} . The perturbative dynamics are modeled using the sound speed

$$c_s^2 = 1 - \frac{1}{1 + (a_c/a)^3} + \frac{1/3}{1 + (g_d a_c/a)^4}. \quad (19)$$

Note that the perturbative dynamics implied by this choice of sound speed may be quite different from the actual perturbative dynamics in the full theory. For example, it is well known that the effective sound speed of an oscillating scalar field varies in both time and scale as described in detail in Sec. IV [116, 138]. We note that Ref. [?] showed the gravitational wave production that accompanies the scalar field decay is ruled out by current CMB observations.

J. Other models

Finally, we mention a selection of other models that have been suggested in the literature but have not directly confronted cosmological data, or are disfavored by the data. These include the model of Refs. [80, 139], which attempt to explain the injection redshift of EDE (*i.e.*, the EDE mass must overcome the Hubble friction right around matter-radiation equality to be successful) by introducing a conformal coupling between EDE and neutrinos. This leads to a modified KG equation, that now counts an additional source term proportional to the trace of the neutrino energy-momentum tensor. The effect of the neutrino coupling is to kick the scalar out of its minimum and up its potential right when the neutrinos become non-relativistic, $T_\nu \sim m_\nu$, independently of the value of the scalar field mass and its initial condition. Although elegant, this mechanism requires neutrinos with individual masses of $\mathcal{O}(0.1 - 0.5)$

eV, testable with current and near-future CMB and LSS observations, with current bounds on the sum of neutrino masses $\sum m_\nu \lesssim 0.1$ eV (e.g. Refs. [4, 140, 141]) that can be relaxed in scenarios with exotic neutrino interactions (e.g. Refs. [142, 143]). While a dedicated analysis including the conformal coupling is still lacking, we mention that Refs. [144, 145] performed analyses of EDE while simultaneously allowing the sum of neutrino masses to vary and did not find any significant relaxation of the neutrino masses constraint.

Another example is the ‘chain EDE’ model of Ref. [87], where the Universe undergoes a series of first-order phase transitions, starting at a high-energy vacuum in a potential, and tunneling down through a chain of lower-energy metastable minima. In general, a single phase transition occurring around matter-radiation equality (as favored to resolve the Hubble tension), and characterized by a constant tunneling rate per volume Γ , is excluded by CMB and LSS observations due to the non-observation of anisotropies induced by the presence of bubbles of false vacuum on large scales. One way out of this constraint is a time-dependent tunneling rate Γ , e.g. due to an additional trigger field as in the NEDE proposal (an idea originally introduced in the context of double-field inflation [146, 147]). Authors of Ref. [87] suggest a different way to evade the CMB constraints. They invoke tunneling along a chain of false vacua with decreasing energy at a constant tunneling rate and, using simple scaling arguments, find that a solution to the Hubble tension requires $N > 600$ phase transitions to avoid very large anisotropies. A specific example of Chain EDE is given, featuring a scalar field in a tilted cosine potential, that authors argue to be ubiquitous in axion physics and have strong theoretical motivation. However, a dedicated analysis of this promising model against cosmological data is still lacking.

A variant of RnR EDE is AdS-EDE, originally studied in Ref. [85]. It consists of a scalar field with a quartic potential ($V \propto \phi^4$) which is modified so that the field goes through an Anti-De Sitter (AdS) (i.e., $V < 0$) phase. Constraints on this model in the literature are, at best, incomplete due to the use of a theory prior that appears to enforce a non-zero lower bound on the EDE fraction¹⁰. Yet, in Ref. [85], when fixing the depth of the AdS phase, the model is shown to have a better χ^2 when including the SH0ES prior than RnR, which is encouraging regarding the potential of this model.

Our final example is the model of assisted quintessence studied in Ref. [89] (see also Ref. [149] for a similar phenomenological model). This model, originally introduced two decades ago to resolve the ‘cosmic coincidence’ problem [150, 151], introduces a scalar-field that exhibits tracking behavior, such that its energy density is a fixed fraction of the dominant background species. As a result of the transition from radiation- to matter-domination, an era of early dark energy occurring around matter-radiation equality is inevitable. Nevertheless, authors of Ref. [89] show that this field leads to an irreducible contribution to DM after the transition, that prevents a resolution of the tension (in fact it slightly exacerbates it). Indeed, as mentioned in the text above, EDE must vanish faster than matter to alleviate the Hubble tension. An additional energy component in the early universe that dilutes like matter worsens the tension as shown in [116].

IV. PHENOMENOLOGY OF EARLY DARK ENERGY

The basic physics of a minimally-coupled EDE can be captured through the ‘generalized dark matter’ formalism first presented in Ref. [152] (see also Ref. [116]). The dynamics of any cosmological material can be described by specifying an equation of state $w(a)$, an effective sound-speed $c_s^2(k, a)$ (defined in the material’s local rest-frame), and the anisotropic stress $\sigma(k, a)$. For scalar fields, the anisotropic stress is zero; for the following discussion we will take $\sigma = 0$ (see Ref. [90] for a discussion of the phenomenology when the anisotropic stress is non-zero).

A. Background and perturbations evolution

For an EDE with an equation of state $w_{\text{EDE}}(a)$, the continuity equation immediately gives the evolution of the energy density,

$$\rho_{\text{EDE}}(a) = \rho_{\text{EDE},0} e^{3 \int_a^1 [1+w_{\text{EDE}}(a)] da/a}. \quad (20)$$

The basic background dynamics of EDEs we review here have $w_{\text{EDE}} \rightarrow -1$ at some point in the past, which then transitions to $0 < w_{\text{EDE}} < 1$ at some critical scale factor a_c . Specifically for a scalar field with a potential of the

¹⁰ Evidence for this can be found by noting that in Ref. [148] the AdS-EDE f_{EDE} is non-zero at the 17σ level but the overall χ^2 is *degraded* by 3.

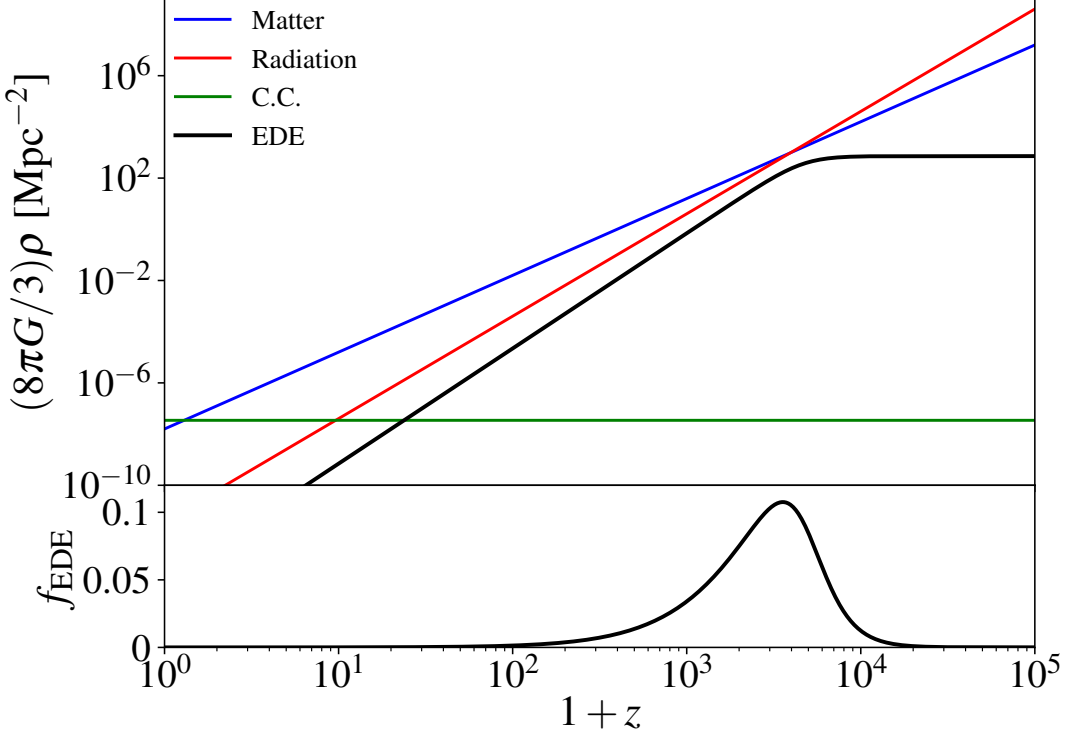


FIG. 3. *Top panel:* Evolution of the energy densities of the various components of the Universe, including an early dark energy active before recombination. *Bottom panel:* Fractional contribution $f_{\text{EDE}} \equiv \rho_{\text{EDE}}/\rho_{\text{tot}}$ of EDE. As a representative example, we chose a model where the maximum contribution $f_{\text{EDE}}(z_c) = 0.1$ is reached at the critical redshift $z_c \simeq 3500$ subsequently diluting with an equation of state $w = 1/2$ afterwards.

form $V \propto \phi^{2n}$ around its minimum, we have $w_f = (n-1)/(n+1)$ [116, 153]. We can parameterize this through the function

$$w_{\text{EDE}}(a) = \frac{1+w_f}{1+(a_c/a)^{3(1+w_f)}} - 1, \quad (21)$$

which describes a fluid that does not dilute with cosmic expansion when $a \ll a_c$, but dilutes as $a^{-3(1+w_f)}$ for $a \gg a_c$. This parameterization also describes the ADE model when $p = 1$ as discussed in the previous section.

For such an equation of state, the background evolution of $\rho_{\text{EDE}}(a)$ is shown in Fig. 3, and is summarized by $f_{\text{EDE}} \equiv \rho_{\text{EDE}}/\rho_{\text{tot}}$, which shows that the contribution of EDE is localized around the time when the field becomes dynamical (denoted by the ‘critical’ redshift, z_c).

Perturbations on the other hand evolve according to the continuity and Euler equations [152, 154]:

$$\frac{d}{d\eta} \left(\frac{\delta_{\text{EDE}}}{1+w_{\text{EDE}}} \right) = -(\theta_{\text{EDE}} + h'_\delta) - 3\frac{a'}{a}(c_s^2 - c_a^2) \left(\frac{\delta_{\text{EDE}}}{1+w_{\text{EDE}}} + 3\frac{a'}{a}\frac{\theta_{\text{EDE}}}{k^2} \right) \quad (22)$$

$$\theta'_{\text{EDE}} = -\frac{a'}{a}(1-3c_s^2)\theta_{\text{EDE}} + c_s^2 k^2 \frac{\delta_{\text{EDE}}}{1+w_{\text{EDE}}} + k^2 h_v, \quad (23)$$

where primes denote derivatives with respect to conformal time η , the gravitational potentials are $h_\delta = h_s/6$ and $h_v = 0$ in synchronous gauge, and $h_\delta = \phi_N$ and $h_v = \psi_N$ in conformal Newtonian gauge [154],

$$c_a^2 = \frac{\rho'_{\text{EDE}}}{P'_{\text{EDE}}} = w_{\text{EDE}} - \frac{1}{3} \frac{dw_{\text{EDE}}/d\ln a}{1+w_{\text{EDE}}}, \quad (24)$$

and c_s^2 is the EDE’s effective sound speed, defined in its local rest-frame [152]. Note that the choice of $w_{\text{EDE}}(a)$ given by Eq. 21 gives $c_a^2(a \ll a_c) = -(2+w_f)$ and $c_a^2(a \gg a_c) = w_f$, which approximates the time variation of the adiabatic sound speed in scalar-field EDE models [116].

The choice of c_s^2 is more complicated, since in general it depends on both k and a . In scalar-field models with a potential of the form $V \propto \phi^{2n}$ [116],

$$c_s^2(k, a) = \frac{2a^2(n-1)\varpi^2 + k^2}{2a^2(n+1)\varpi^2 + k^2}, \quad (25)$$

where ϖ is the angular frequency of the oscillating background field and is well-approximated by [76, 116, 155]

$$\begin{aligned} \varpi(a) &\simeq m \frac{\sqrt{\pi}\Gamma(\frac{1+n}{2n})}{\Gamma(1+\frac{1}{2n})} 2^{-(1+n)/2} \theta_{\text{env}}^{n-1}(a), \\ &\simeq 3H(z_c) \frac{\sqrt{\pi}\Gamma(\frac{1+n}{2n})}{\Gamma(1+\frac{1}{2n})} 2^{-(1+n)/2} \frac{\theta_{\text{env}}^{n-1}(a)}{\sqrt{|E_{n,\theta\theta}(\theta_i)|}}, \end{aligned} \quad (26)$$

where $\Gamma(x)$ is the Euler Gamma function and the envelope of the background field ($\theta_{\text{env}} \equiv \phi_{\text{env}}/f$) once it is oscillating is roughly

$$\phi_{\text{env}}(a) = \phi_c \left(\frac{a_c}{a} \right)^{3/(n+1)}, \quad (27)$$

and we have written the scalar field potential as $V_n(\phi) = m^2 f^2 E_n(\theta = \phi/f)$. We recall that m and f are the axion mass and decay constant respectively.

The angular frequency ϖ defines a scale that governs the sound speed affecting a given mode: For $a \gg a_c$, $\varpi = 0$, so that $c_s^2 = 1$; when $a \ll a_c$ and $k \ll a\varpi$, $c_{s,\text{eff}}^2 = (n-1)/(n+1) = w$; when $a \ll a_c$ and $k \gg a\varpi$, $c_s^2 = 1$. Note that this approximate sound speed only applies when $\varpi/H \gg 1$ —i.e. when the field oscillates several times per Hubble time. For simplicity in what follows, we will take the effective sound speed to be constant in time and scale. Since, in all cases, c_s^2 is of order unity, our choice of $c_s^2 = \text{constant}$ will give a good sense of how the perturbative dynamics impact observables. This approximation also matches the dynamics in the ADE model. We discuss the axion-like case later on.

B. Understanding the dynamics of EDE

We now turn to describing the evolution of EDE density perturbations δ_{EDE} . The initial conditions are easiest to derive in synchronous gauge (it is straightforward to derive the corresponding initial conditions in conformal Newtonian gauge through the standard gauge transformation [154]). Adiabatic perturbations are generated dynamically since the gravitational potential, h_S , is initially non-zero. Specifically we have $h_S = (k\eta)^2/2$ [154], leading to the initial behavior when $w_{\text{EDE}} \simeq -1$, on superhorizon scales, and during radiation-domination for the EDE fluid variables¹¹

$$\frac{\delta_{\text{EDE}}}{1+w_{\text{EDE}}} = -\frac{(4-3c_s^2)/2}{32+6c_s^2+12w_f}(k\eta)^2, \quad (28)$$

$$\theta_{\text{EDE}} = -\frac{c_s^2/2}{32+6c_s^2+12w_f}k(k\eta)^3, \quad (29)$$

where η is the conformal time, and w_f appears because the adiabatic sound speed at $a \gg a_c$ is $c_a^2(a \ll a_c) \simeq -(2+w_f)$. The initial conditions show that on superhorizon scales the density perturbation is suppressed for $a < a_c$ since $\delta_{\text{EDE}} \propto (1+w_{\text{EDE}})$, with $w_{\text{EDE}} \rightarrow -1$. This statement is also true in conformal Newtonian gauge since the gauge transformation is proportional to $\rho'_{\text{EDE}}/\rho_{\text{EDE}} \propto (1+w_{\text{EDE}})$.

On subhorizon scales where matter perturbations dominate, one has

$$\frac{d^2}{d\eta^2} \left(\frac{\delta_{\text{EDE}}}{1+w_{\text{EDE}}} \right) = -k^2 \left(c_s^2 \frac{\delta_{\text{EDE}}}{1+w_{\text{EDE}}} + \psi_N \right) - (1-3c_a^2) \frac{a'}{a} \frac{d}{d\eta} \left(\frac{\delta_{\text{EDE}}}{1+w_{\text{EDE}}} \right), \quad (30)$$

where we have written the fluid equation in conformal Newtonian gauge, since this gauge can help us build intuition for the mode dynamics on subhorizon scales.

The redshift evolution of δ_{EDE} (and the fractional contribution $\delta\rho_{\text{EDE}}/\delta\rho_{\text{tot}}$) in a model with $f_{\text{EDE}}(a_c) = 0.1$, $a_c = 10^{-3.5}$ and $w = 1/2$ is shown in the left panels of Fig. 4 for three different modes $k = 0.001, 0.01, 0.1 \text{ Mpc}^{-1}$,

¹¹ When $w_{\text{EDE}} \simeq -1$, the EDE makes a negligible contribution to the total energy density and so does not affect h_S at this time.

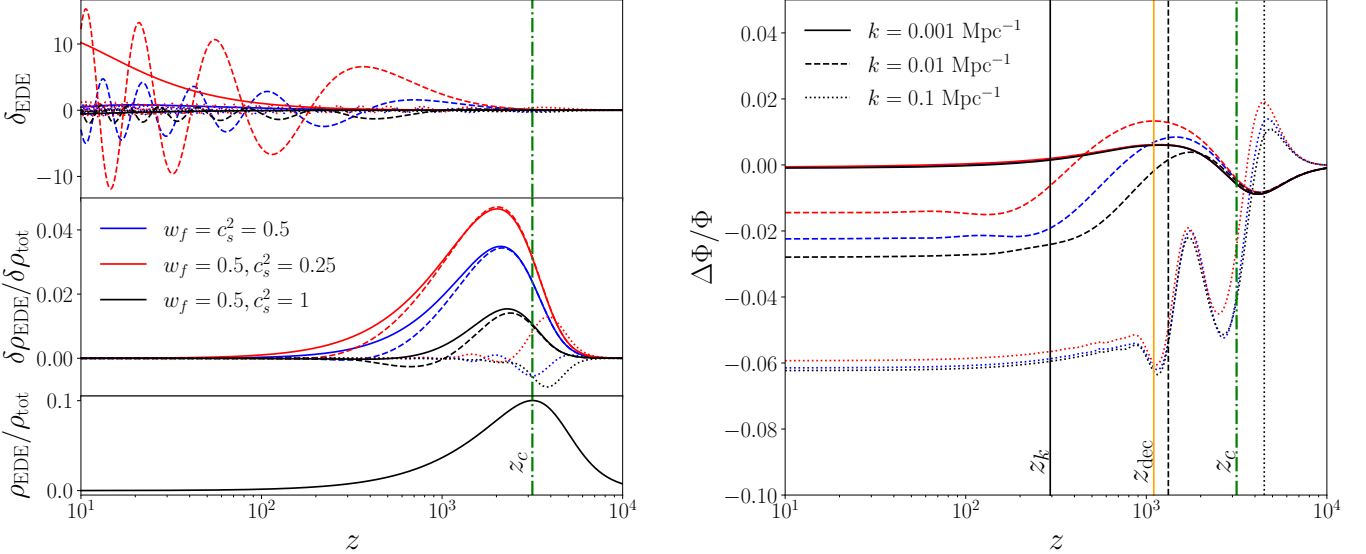


FIG. 4. *Left panel:* The evolution of EDE perturbations in the phenomenological fluid model for different values of the effective sound speed. In each panel, we show the evolution of the background (bottom) and perturbed EDE (top and middle) energy density for three different wavenumbers. *Right panel:* The difference in the evolution of the Weyl potential, relative to ΛCDM with the same values of $\{h, \omega_{\text{cdm}}, \omega_b, A_s, n_s, \tau_{\text{reio}}\}$. We also show the redshift of horizon entry for each mode (black), the critical redshift of the EDE (dot-dashed green) and the redshift of decoupling (solid orange).

and three different sound speeds $c_s^2 = 0.25, 0.5, 1$. These wavenumbers are chosen to demonstrate the impact of EDE and the key role played by c_s^2 (and the interplay with w) on modes entering the horizon after, close to and before the EDE critical redshift, respectively. In addition, we show the effect of varying the equation of state w compared to varying c_s^2 for the mode $k = 0.01 \text{ Mpc}^{-1}$ in Fig. 5. The modes evolve as follows:

- First, one can see from Eq. 30 that with a non-zero sound speed c_s^2 , the fluid has significant pressure support, leading to oscillations whose frequency is set by c_s^2 . The greater c_s^2 is, the more effective the pressure gradients are in preventing the EDE density contrast from collapsing. Accordingly, smaller c_s^2 lead to a larger contribution to the overall density perturbation, as shown in the middle panel of the left graphic in Fig. 4.
- Second, the friction term ($\propto \delta_{\text{EDE}}$) can cause the oscillation amplitude to either decrease or increase, depending on the sign of $(1 - 3c_a^2)$. For the case shown here with $w_f = 1/2$ at $a > a_c$, $1 - 3c_a^2 = 1 - 3w_f = -1/2$, leading to an *enhancement* of the oscillation amplitude as the universe expands.
- Third, at the perturbation level, the competition between the effects of pressure inside the horizon (controlled by c_s^2) and the growth of EDE modes outside the horizon ($\delta_{\text{EDE}} \propto (1 + w_{\text{EDE}})$) leads to a positive correlation between c_s^2 and w_f . This can be seen in Fig. 5, where we show that reduced pressure support (i.e., $c_s^2 = 1/4$) can partially mimic an increase in the final equation of state to $w_f = 2/3$, and consequently, a larger w_{EDE} can partly compensate for the impact of greater pressure support c_s^2 [78].

C. Impact of EDE perturbations on the Weyl potential

In the case where the EDE is minimally coupled, the effects of its perturbations are only communicated through changes in the gravitational potentials. In conformal Newtonian gauge, changes to the photon perturbations are governed by the Weyl potential, $\Phi \equiv (\phi_N + \psi_N)/2$, which is sourced by

$$\Phi = -\frac{3}{4k^2} \left(\frac{a'}{a} \right)^2 \left(2\delta + \sum_i [1 + w_i] [6(a'/a)\theta_i/k^2 + 3\sigma_i] \right), \quad (31)$$

where the sums are over all cosmological species and σ_i is the anisotropic stress. The right panel of Fig. 4 shows the fractional change to the Weyl potential in the phenomenological EDE model. The changes shown there can be split into the effects due to modifications to the background and due to EDE perturbative dynamics. At the background

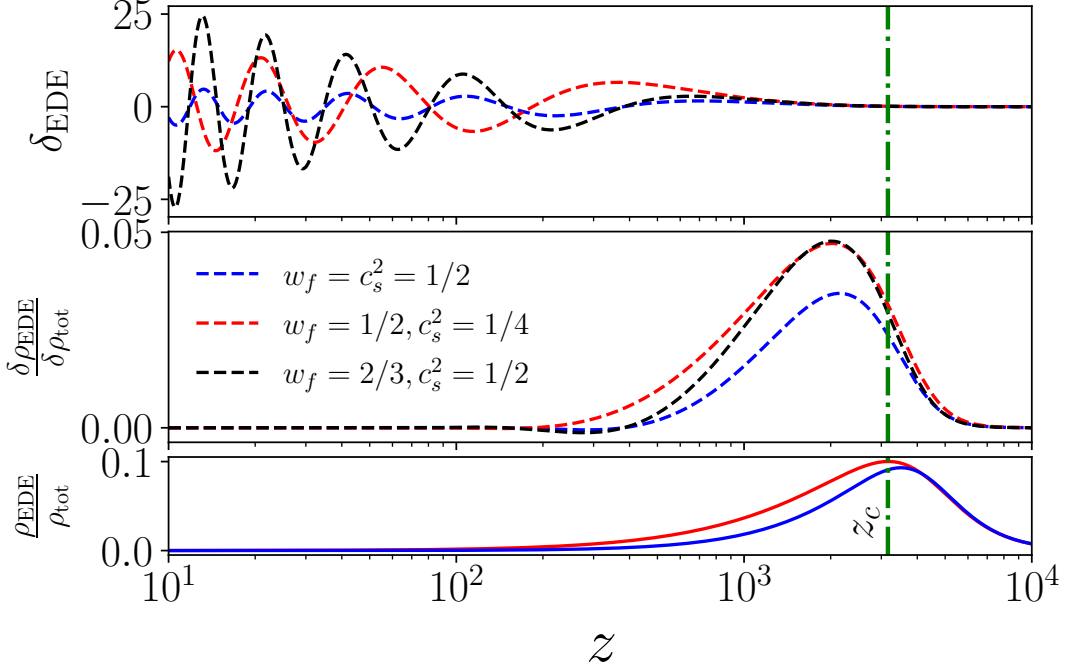


FIG. 5. The evolution of EDE perturbations with $k = 0.1h/\text{Mpc}$ in the phenomenological fluid model for different values of c_s^2 and w_f . The middle panel shows that the amplitude of the first compression in $\delta\rho_{\text{EDE}}/\delta\rho_{\text{tot}}$ can be increased by either decreasing c_s^2 or increasing w .

level, the story is simple: the presence of EDE causes the Hubble parameter to increase around $a \sim a_c$, leading to an increase in the Hubble friction experienced by the CDM modes that are within the horizon at a_c . This explains the dominant effect visible in the right panel of Fig. 4: a reduction of the amplitude of the Weyl potential, stronger for larger k modes, that spend a longer time in the horizon while the EDE contributes significantly to the energy budget.

At the perturbation level, the story is more complex. Indeed, one important aspect of the left panel of Fig. 4 is that the dynamics of a given EDE mode and its impact on observables are tied to whether the mode enters the horizon (i.e. when it satisfies $k = a_k H(a_k)$) around the time when the EDE fluid becomes dynamical a_c . This can be understood as follows:

- All modes begin outside the horizon, where the density perturbation $\delta_{\text{EDE}} \propto 1 + w_{\text{EDE}}$. As a result, modes which enter the horizon before a_c , when $w_{\text{EDE}} \simeq -1$ (satisfying $a_k \ll a_c$ with $k = a_k H(a_k)$), will be stabilized by pressure gradients with an overall amplitude suppressed by $\sim 1 + w_{\text{EDE}}(a_k)$, relative to modes that enter the horizon later. This explains why in the left panel of Fig. 4, the mode $k = 0.1 \text{ Mpc}^{-1}$ has a smaller amplitude (and overall contribution to $\delta\rho_{\text{tot}}$) than other modes which enter when $w_{\text{EDE}} > -1$. Due to this suppression, the Weyl potential is basically insensitive to the c_s^2 -dependent details of the evolution of these early EDE modes in this phenomenological model.
- In principle, the EDE velocity perturbations also contribute to the gravitational potentials through the resulting heat-flux $(\rho_{\text{EDE}} + P_{\text{EDE}})\theta_{\text{EDE}} \propto (1 + w_{\text{EDE}})\theta_{\text{EDE}}$, but are also suppressed when $w_{\text{EDE}} \simeq -1$.
- Taking the other limit $a_k \gg a_c$ (see for example the mode with $k = 0.001 \text{ Mpc}^{-1}$), one may expect that modes entering the horizon later will strongly impact the Weyl potential dynamics, because of their enhanced growth on super-horizon scales. However, their impact turns out to be minimal because once they enter the horizon (around $z \sim 300$ for this mode), the physical perturbations are suppressed by $\rho_{\text{EDE}}/\rho_{\text{tot}} \ll 1$, and one can see on the right panel that the Weyl potential with $k = 0.001 \text{ Mpc}^{-1}$ is largely unaffected by EDE.

In summary, details of the EDE perturbative dynamics are imprinted on cosmological observables only for modes

that enter the horizon around a_c . We can clearly see this in the fractional change to the Weyl potential for each mode in the right panel of Fig. 4: the only mode with an appreciable dependence on the value of c_s^2 is $k = 0.01 \text{ Mpc}^{-1}$, which is entering the horizon slightly after $a_c = 10^{-3.5}$. This is particularly important in determining where the support for specific EDE dynamics (beyond the background evolution) comes from within the data, and shows that one can hope to precisely measure *when* and *how* the EDE contribution occurred.

D. Impact on the CMB and matter power spectra

The impact of EDE $f_{\text{EDE}}(a_c) = 0.1$, $a_c = 10^{-3.5}$ and $w = 1/2$ on the CMB and matter power spectra for three different values of $c_s^2 = 0.25, 0.5, 1$ is shown in Fig. 6. We show the relative difference with respect to ΛCDM with the same values of $\{h, \omega_{\text{cdm}}, \omega_b, A_s, n_s, \tau_{\text{reio}}\}$. We focus on illustrating the impact of c_s^2 , as the dominant effects of changing f_{EDE} , a_c and w_f are fairly straightforward, since they (mostly) come from the changes due to background dynamics. For a discussion on the roles of f_{EDE} , a_c and w_f , we refer to App. A.

First, as discussed in the introduction, the purely background effect of EDE (at fixed h) is to increase the early-universe expansion rate, thereby decreasing the angular sound horizon and damping scales, which lead to residual wiggles and a higher amplitude at large ℓ in TT and EE that is common to all models, regardless of the value of c_s^2 . The effect of perturbations on the other hand, is localized and tied to the dynamics of modes which enter the horizon right around z_c , as discussed previously. Using $k_c(\eta_0 - \eta_c) \simeq l_c$ and $k_c \eta_c = 1$, we see that the perturbative dynamics will impact CMB observations around $l_c \simeq \eta_0/\eta_c \simeq 100$ for $a_c = 10^{-3.5}$, with a width extending about a factor of 10 in redshift, corresponding to a $\delta\ell \simeq 100$. This is clearly seen in Fig. 6, where all models lead to the same dynamics at $\ell \gtrsim 1000$, but deviate below this scale.

The more subtle effects induced by modifying the sound speed are detailed in the previous section, closely following their first presentation in Ref. [78] (see also Ref. [52] for a related discussion). To further explore the role of EDE perturbations, we show the fractional change to the individual contributions to the CMB TT power spectra, namely the Sachs-Wolfe, (early) integrated Sachs-Wolfe (eISW), and Doppler terms for $c_s^2 = 0.25$ and 0.5 in the bottom panel of Fig. 7. The top panel of Fig. 7 shows the fractional difference of the phenomenological EDE *at fixed* $c_s^2 = 0.5$ and ΛCDM . We remove the dominant background effect that is highly correlated with h from these plots by fixing θ_s instead of h . The solid curves show the fractional differences at fixed physical CDM density (at $\omega_{\text{cdm}} = 0.12$), giving $h = 0.67$ and $\Omega_m = 0.31$ in ΛCDM , while the phenomenological EDE model has $h = 0.80$ and $\Omega_m = 0.22$. The dotted curves show what happens when Ω_m is held fixed (at $\Omega_m = 0.31$), giving $\omega_{\text{cdm}} = 0.14$ and $h = 0.723$ in the EDE model. The effect of EDE perturbations can then be understood as follows:

- Changes to the Weyl potential due to EDE perturbations affect the “acoustic driving” of the CMB photon perturbations - the decay of gravitational potentials can boost the amplitude of acoustic oscillations in the baryon-photon fluid. Acoustic driving impacts the Sachs-Wolfe term in the line-of-sight integral which determines the overall CMB power spectra, and this is primarily responsible for the differences in the CMB power spectra between EDE models with different perturbative dynamics. Concretely, we have seen in the previous section that a larger c_s^2 (i.e. greater pressure support) leads to a smaller amplitude of EDE perturbations and therefore a faster decay of the Weyl potential, affecting the driving force acting on CMB perturbations. This means that larger c_s^2 will show a larger SW amplitude than smaller c_s^2 (and vice versa), leading to the small differences between the EDE models seen in the bottom panel of Fig. 7. This effect dominates constraints on c_s^2 [156].
- In addition, differences in the time-dependence of the gravitational potential around recombination affect the amplitude of the eISW term, which is strongly impacted by the presence of EDE [157]. This is most clearly visible in the top panel of Fig. 7, where we show the fractional difference of the phenomenological EDE (at fixed $c_s^2 = 0.5$) and ΛCDM , with a large eISW contribution around $\ell \sim 100$. In fact, as we have adjusted h to match θ_s , one can see that the dominant impact of EDE at $\ell \sim 100$ is through the eISW term, rather than the SW term. The additional time variation in the gravitational potentials in EDE is due to the small residual EDE contribution to the background energy density after recombination. The dotted curve shows that when we fix Ω_m , thereby increasing ω_{cdm} , the eISW difference is reduced. This feature is particularly important to understand the correlation in parameters that comes out of the MCMC analysis, specifically a (perhaps surprising) increase in ω_{cdm} .
- The top panel of Fig. 7 shows an increase in the SW contribution at low multipoles. This is due to the effect of the time-varying total equation of state while the EDE is a sizable fraction of the total energy density. The

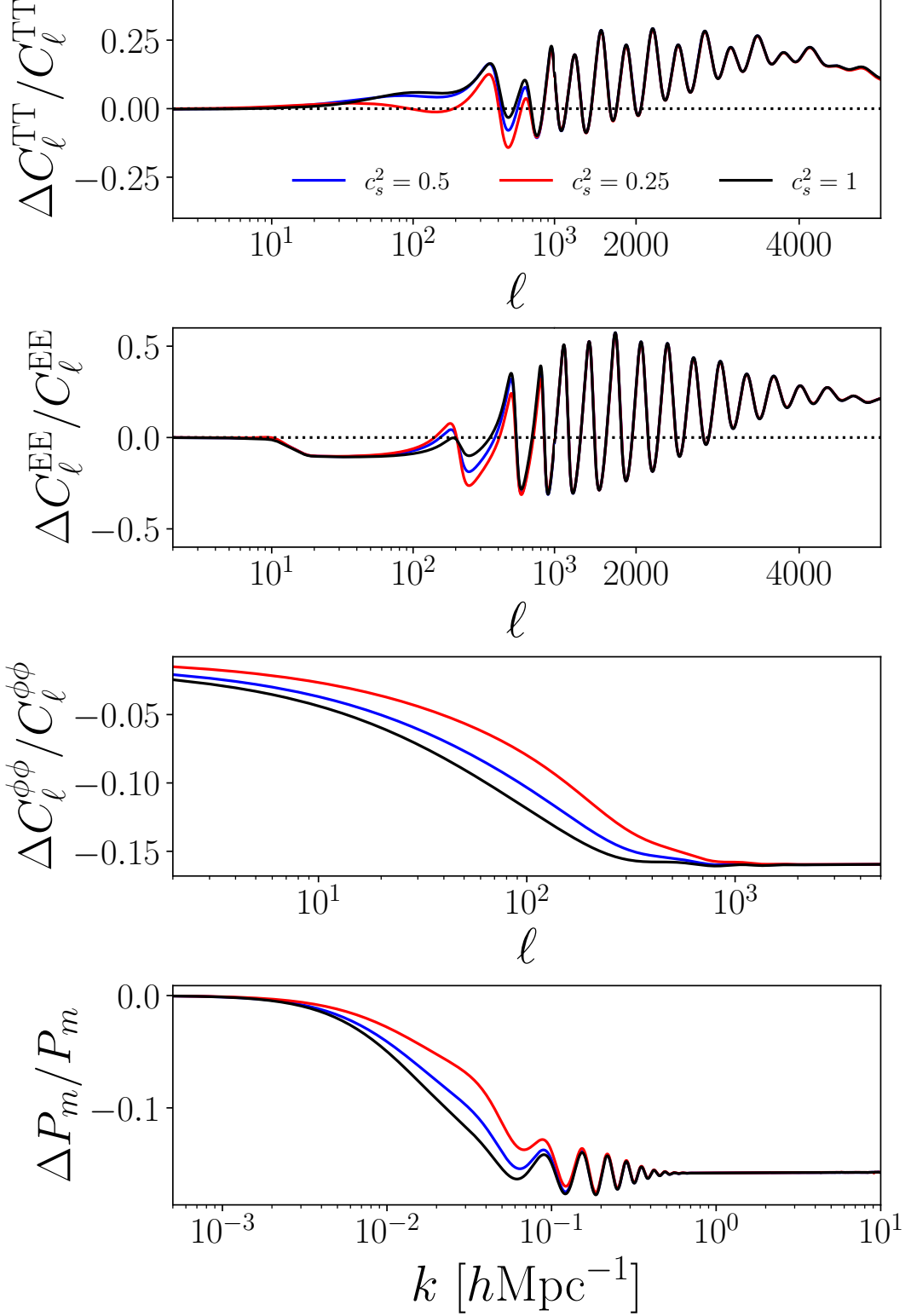


FIG. 6. The impact of EDE $f_{\text{EDE}}(a_c) = 0.1$, $a_c = 10^{-3.5}$ and $w = 1/2$ on the CMB and matter power spectra for three different values of $c_s^2 = 0.25, 0.5, 1$. We show the relative difference with respect to ΛCDM with the same values of $\{h, \omega_{\text{cdm}}, \omega_b, A_s, n_s, \tau_{\text{reio}}\}$.

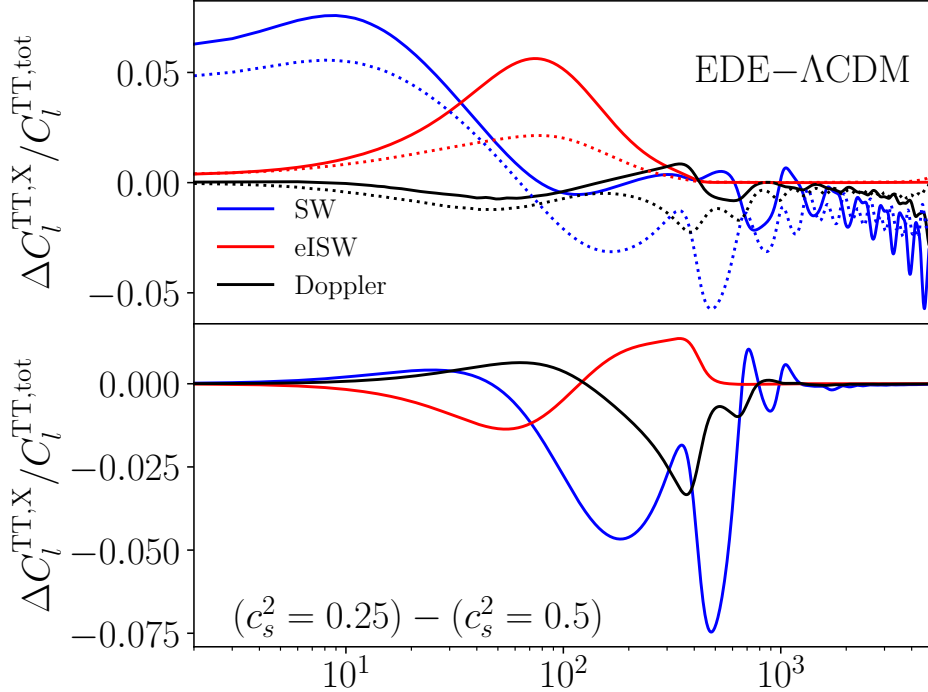


FIG. 7. The fractional change to the Sachs Wolfe (SW), early ($z > 50$) integrated Sachs Wolfe (early ISW) and Doppler terms in the line-of-sight integral that determines the CMB temperature power spectrum. The top panel shows the fractional change between the phenomenological EDE and Λ CDM model. The bottom panel shows the fractional change between EDE models with different values of c_s^2 . Here, unlike in previous figures in this section, we have fixed the angular size of the sound horizon at photon decoupling to $100\theta_s = 1.04$ to remove the dominant background effect induced by EDE. In the top panel the solid curves show the differences at fixed physical CDM density, and in this case the EDE model has $h = 0.80$ and $\Omega_m = 0.225$ while the Λ CDM model has $h = 0.67$ and $\Omega_m = 0.31$. The dashed curves show the differences when Ω_m is held fixed (at 0.31) and in this case EDE model has $h = 0.723$ and $\omega_{\text{cdm}} = 0.14$ while the Λ CDM model has $\omega_{\text{cdm}} = 0.12$.

SW term for modes that are superhorizon before recombination is shown in Fig. 8. This evolution— a slight decrement followed by an enhancement— is also seen in the Weyl potential (see the right panel of Fig. 4). Note that the enhancement of the SW contribution is partially canceled by an anticorrelation with the early ISW term. The cancellation is nearly exact when comparing EDE and Λ CDM models with the same h and ω_{cdm} and is only partial when fixing θ_s . This can be seen in the low- ℓ differences shown in the figures in Appendix A.

Finally, the dynamics of EDE at the background level largely explain the changes to the matter and lensing spectra seen in Fig. 6: modes with larger k are suppressed due to the increased Hubble friction induced by the presence of EDE around a_c . This choice of a_c implies a suppression of the matter power spectrum for modes $k \gtrsim 0.01 \text{ hMpc}^{-1}$, while the amount of suppression at $z = 0$ increases with f_{EDE} , and decreases as w_f increases, since a larger w_f leads to a shorter period of time where the EDE is dynamically relevant. We stress that both *how much* and *how long* EDE contributes to $H(z)$ matter in setting the overall amplitude of the suppression. Yet, one can see that the shape of the suppression strongly depends on c_s^2 for the reasons discussed extensively above: one can partly compensate the effect of the Hubble friction by reducing the pressure support of EDE perturbations. As a result, the model with smaller c_s^2 shows a shallower suppression around k_c than that with larger c_s^2 . The CMB lensing potential power spectrum has a similar dependence, with the rough mapping $\ell \sim 10^3 - 10^4 k$, and the important difference that its large-scale amplitude is set by the matter power spectrum around $k_{\text{eq}} \simeq 0.02 \text{ hMpc}^{-1}$ [158].

E. Beyond the phenomenological model: the axion-EDE case

We now apply these insights to a more realistic case and study the results of data analyses. In Fig. 9, we show the same quantities as in Figs. 4 and 6 but for axEDE and RnR EDE. The only difference between these models is the value of the initial field displacement, θ_i : in axEDE the field has a relatively large displacement so that it starts

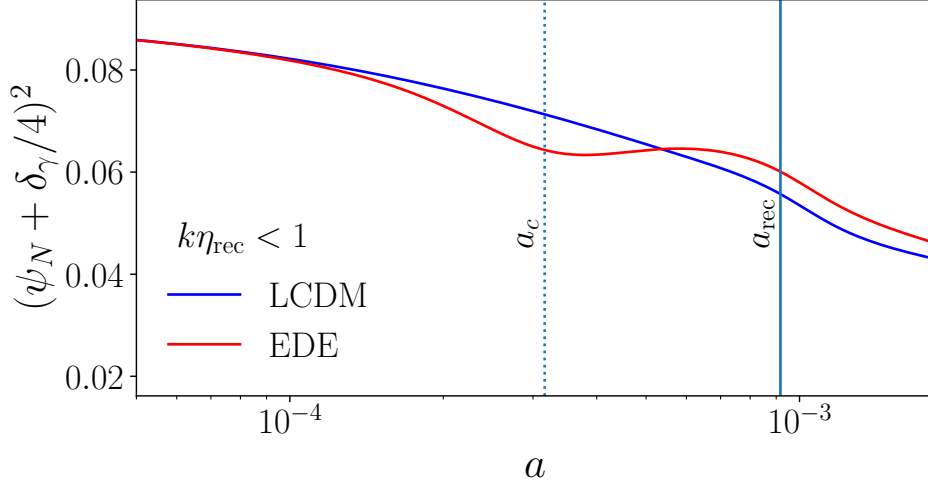


FIG. 8. The time evolution of SW Fourier modes which are superhorizon before recombination (i.e., $k\eta_{\text{rec}} < 1$) in Λ CDM and EDE. The presence of non-adiabatic pressure in the EDE causes a time variation in this mode around $a \simeq a_c$ which persists up to recombination, leading to an enhanced Sachs-Wolfe plateau at low multipoles.

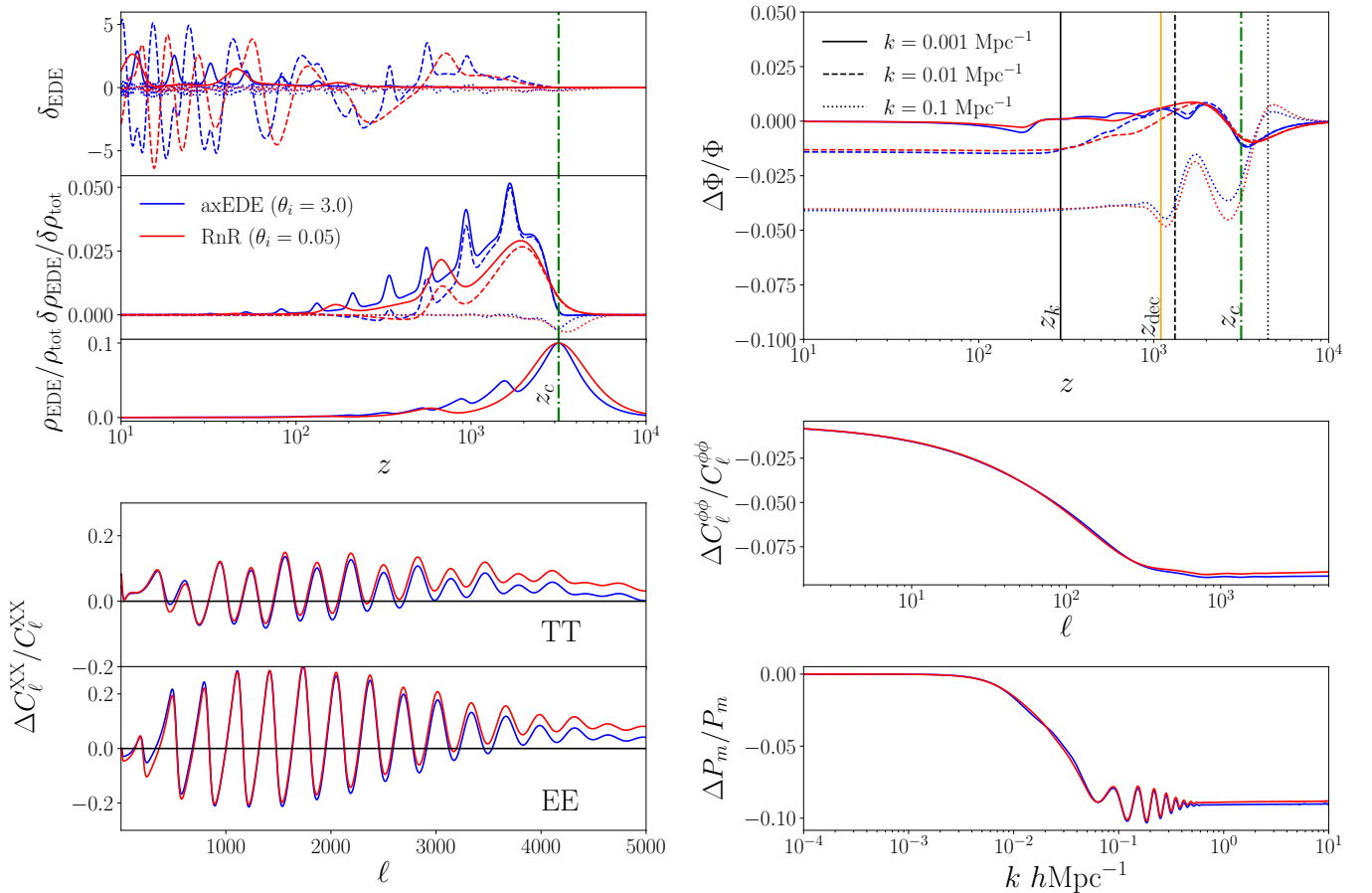


FIG. 9. The same as Figs. 4 and 6 but for axEDE and RnR EDE. For these, we fix $f_{\text{EDE}} = 0.1$, $\log_{10} z_c = 3.5$ and the Λ CDM parameters at the *Planck* best-fit values.

in a flatter region of the potential, whereas for RnR EDE the field has a relatively small displacement such that the potential can always be approximated as a power law (in this case $V \propto \phi^6$).

As discussed in detail in Ref. [76], and from Eq. 25, the choice of θ_i impacts the effective sound speed of the field, with a larger θ_i leading to a smaller effective sound-speed, and subsequently a decrease in pressure support. One can see this in the upper left panel of Fig. 9, with the fractional density perturbation for $\theta_i = 3$ reaching a higher maximum value than for $\theta_i = 0.05$. Note that the ‘spikes’ in the axEDE case are caused by the ‘driving force’ due to the background oscillations in the field. A similar feature is present in RnR, but with smoother spikes appearing at a lower frequency. The linear Klein-Gordon equation is sourced by the term $\phi' h_s'$, leading to a driving force that is 90° out of phase with respect to the oscillations of the background field, as can be seen in a comparison between the middle and lowest panels in the top left of Fig. 9.

The difference in the pressure support for modes entering the horizon around a_c has a similar impact on the CMB as previously described for the phenomenological case. However, unlike the comparisons shown in Fig. 4, the change in θ_i not only affects the perturbations but also impacts the background evolution of the EDE. The fractional contribution of the EDE to the background energy density is larger in RnR EDE at high redshift than axEDE, leading to a larger increase in the damping scale, $r_d^{\text{RnR}} = 44.50$ Mpc vs. $r_d^{\text{axEDE}} = 44.28$ Mpc, and to RnR EDE having more power compared to axEDE at small angular scales. Both differences in the perturbative and background evolution between the two models lead to axEDE being preferred over RnR EDE when fit to data that includes the SH0ES value of H_0 .

V. EARLY DARK ENERGY IN LIGHT OF PLANCK DATA

We now turn to the results of analyses of the EDE models presented in Sec. III in light of up-to-date cosmological data, and in particular the *Planck* CMB power spectra. Most EDE models, when fit to *Planck*, produce posterior distributions that show similar degeneracies in the various parameters. In Sec. V B, we first discuss the phenomenological EDE model, also called the ADE model [78], and draw generic conclusions about the background and perturbation dynamics preferred by the data. In Sec. V C, we turn to the the axion-like EDE model, since it has been studied in depth in the recent literature and is a representative toy-model for EDE scalar fields. We discuss and compare results for other models in sec. V G.

The baseline analysis includes the full *Planck* 2018 TT,TE,EE and lensing power spectra [4], BAO measurements from BOSS DR12 at $z = 0.38, 0.51, 0.61$ [159], SDSS DR7 at $z = 0.15$ [160] and 6dFGS at $z = 0.106$ [161], and a compilation of uncalibrated luminosity distances to SN1a from Pantheon [162]. The SH0ES measurement¹² is included through a Gaussian prior on the Hubble parameter H_0 . The exact value of the prior may vary depending on the analysis considered, as the measurement has been updated regularly over the last three years.

These analyses use the *Planck* conventions for the treatment of neutrinos: two massless and one massive species are included with $m_\nu = 0.06$ eV [4]. In addition, large flat priors are imposed on the dimensionless baryon energy density ω_b , the dimensionless cold dark matter energy density ω_{cdm} , the Hubble parameter today H_0 , the logarithm of the variance $\ln(10^{10} \mathcal{A}_s)$ of curvature perturbations centered around the pivot scale $k_p = 0.05 \text{ Mpc}^{-1}$ (according to the *Planck* convention), the scalar spectral index n_s , and the re-ionization optical depth τ_{reio} .

A. What does it mean to resolve a tension?

Before presenting results, let us briefly clarify what we mean by an extension of Λ CDM ‘resolves’ the Hubble tension (here EDE), as there has been some debate on this topic in the recent literature. On the one hand, one may consider that resolving the tension involves analysing a given model in light of a full compilation of datasets that *do not* include local measurements of H_0 , and finding that the model predicts a higher value of H_0 , in statistical agreement with the SH0ES (and other direct) determination. On the other hand, a more modest approach seeks to establish whether a model can provide a good fit to *all* the data (i.e. including SH0ES) and be favored over Λ CDM (by some measure of preference). As we discuss in the following, EDE models typically manage to achieve the latter definition of “success”, but fail according the former. The current situation with EDE may appear unsatisfactory, leading to the conclusion that, as of yet, no proper resolution has been put forth.

It has been argued that EDE’s inability to predict a larger H_0 without including constraints from direct measurements is tied to the fact that EDE models introduce several new parameters, only one of which (f_{EDE}) strongly

¹² Recently, the SH0ES and Pantheon+ teams have provided updated data with a new likelihood that takes into account the co-variance between the different measurements. Dedicated EDE analyses in light of these data are still lacking for most models, but we anticipate the impact of the more refined likelihood to be fairly minor since the EDE models studied here do not predict large deviations in the shape of $H(z)$ at late-times. For a first application of this data to the specific “axion EDE” model, see Ref. [163].

correlated with H_0 , while the others are undefined when $f_{\text{EDE}} \rightarrow 0$. If the data (other than SH0ES) do not statistically significantly favor non-zero f_{EDE} by themselves, a fit to these data may be affected by ‘prior volume’ effects: the auxiliary parameters will have no effect on the data, thus artificially increasing the ΛCDM -like volume, and leading to marginalized posteriors that ostensibly place strong upper limits on the presence of EDE, without being tied to a true degradation of the fit to the data (i.e. a decrease in the likelihood, or conversely a increase in the effective χ^2). On the other hand, once a direct determination of H_0 is included in the analysis, it can unveil regions of parameter space which both increases the indirect value of H_0 and provides a good fit to all data. One way to mitigate (or at least test) the impact of prior volume effects on a model is to perform “profile likelihood” analyses [164–167].

In this review, we present results of analyses that both include and exclude direct measurements of H_0 , in order to compare and contrast the conclusions that can be drawn from both approaches. In addition, we present recent results from likelihood profile analyses that show very different results from the standard Bayesian analyses in the absence of information from SH0ES. Let us note that it is generally recognized that this debate will become moot once near-future CMB and large-scale structure data, whose sensitivity to EDE models will be exquisite, become available.

B. Preliminary study: results for a phenomenological EDE model

To gain some insight into the results for specific models of EDE, we begin by discussing results for the phenomenological EDE model (also dubbed ”Acoustic Early Dark Energy (ADE)”, see Sec. III), whose dynamics were presented in the Sec. IV. We recall that this model is specified by the fraction $f_{\text{EDE}}(z_c)$ of EDE, the critical redshift z_c after which the field dilutes, the equation of state specified in Eq. 21, or more precisely by the exponent n entering in the definition of w_f , and the effective sound speed c_s^2 of the EDE fluid. The first questions we address with this preliminary study are: *i*) what background dynamics can resolve the tension, i.e., what value of $f_{\text{EDE}}(z_c)$, z_c and n (or equivalently w_f) are favored by *all* the data (including SH0ES), and *ii*) what are the constraints on the field perturbations and how do they correlate with the background dynamics. A similar analysis was first presented in Ref. [78].

We show in Fig. 10 the 2D posterior distributions of H_0 along with the four EDE parameters of the model $\{f_{\text{EDE}}(z_c), z_c, w_f, c_s^2\}$, reconstructed from analyzing the combination *Planck*+BAO+Pantheon+SH0ES data. We follow Ref. [78] and impose the priors $c_s^2 \in [0, 1.5]$ and $w_f \in [0.3, 6]$. Values of w_f and $c_s^2 > 1$ can be achieved with a non-canonical kinetic term [78].

One can see that data favors $f_{\text{EDE}}(z_c) = 0.094^{+0.023}_{-0.035}$, with $\log_{10}(z_c) = -3.59^{+0.13}_{-0.11}$ and $w_f = 1.46^{+0.33}_{-0.99}$. Consequently, models where the EDE fluid dilutes like matter ($n = 1$, $w_f = 0$) such as the standard axion are excluded at more than 2σ . The rate of dilution correlates with $\log_{10}(z_c)$ and $f_{\text{EDE}}(z_c)$, as later dilution (i.e. lower $\log_{10}(z_c)$) requires faster dilution (higher w_f) and a larger EDE contribution at the peak (larger $f_{\text{EDE}}(z_c)$). Hence data requires a fine balance in EDE parameters for the EDE phase to last long enough to impact the value of the sound horizon, without strongly affecting modes that enter the horizon around z_c . In addition, perturbations are tightly constrained, with $c_s^2 = 0.97^{+0.15}_{-0.28}$, and correlate with the background equation of state along the degeneracy line $c_s^2 = 0.54 + 0.25 \times w$ (shown with a black dashed line), with a mild preference for $c_s^2 \lesssim 1$. As we have discussed in Sec. IV, this is because the effect on the Weyl potential (and consequently on the acoustic driving of CMB perturbation) of faster rates of dilution can be compensated for by greater pressure support (larger c_s^2). These results update those presented originally in Ref. [78].

The features exhibited by this phenomenological analysis are also present (broadly speaking) in more involved EDE modeling, as we discuss below.

C. Axion-like EDE in light of *Planck* and SH0ES data

We now turn to the well-studied axion-like EDE model, for which (in addition to the standard ΛCDM parameters) a logarithmic prior on z_c , and flat priors for $f_{\text{EDE}}(z_c)$ and θ_i are considered as:

$$\begin{aligned} 3 &\leq \log_{10}(z_c) \leq 4, \\ 0 &\leq f_{\text{EDE}}(z_c) \leq 0.5, \\ 0 &\leq \theta_i \leq \pi. \end{aligned}$$

Note that, in principle, the exponent n (or equivalently the equation of state once the field rolls $w_f = (n-1)/(n+1)$) could be considered as an extra free parameter of the model. We find that the combination of *Planck*+BAO+Pantheon+SH0ES data yields $n = 3.37^{+0.41}_{-0.99}$, updating the original result from Ref. [76], and simply fixing the value of n to a number chosen within this interval has very little impact on the model’s performance

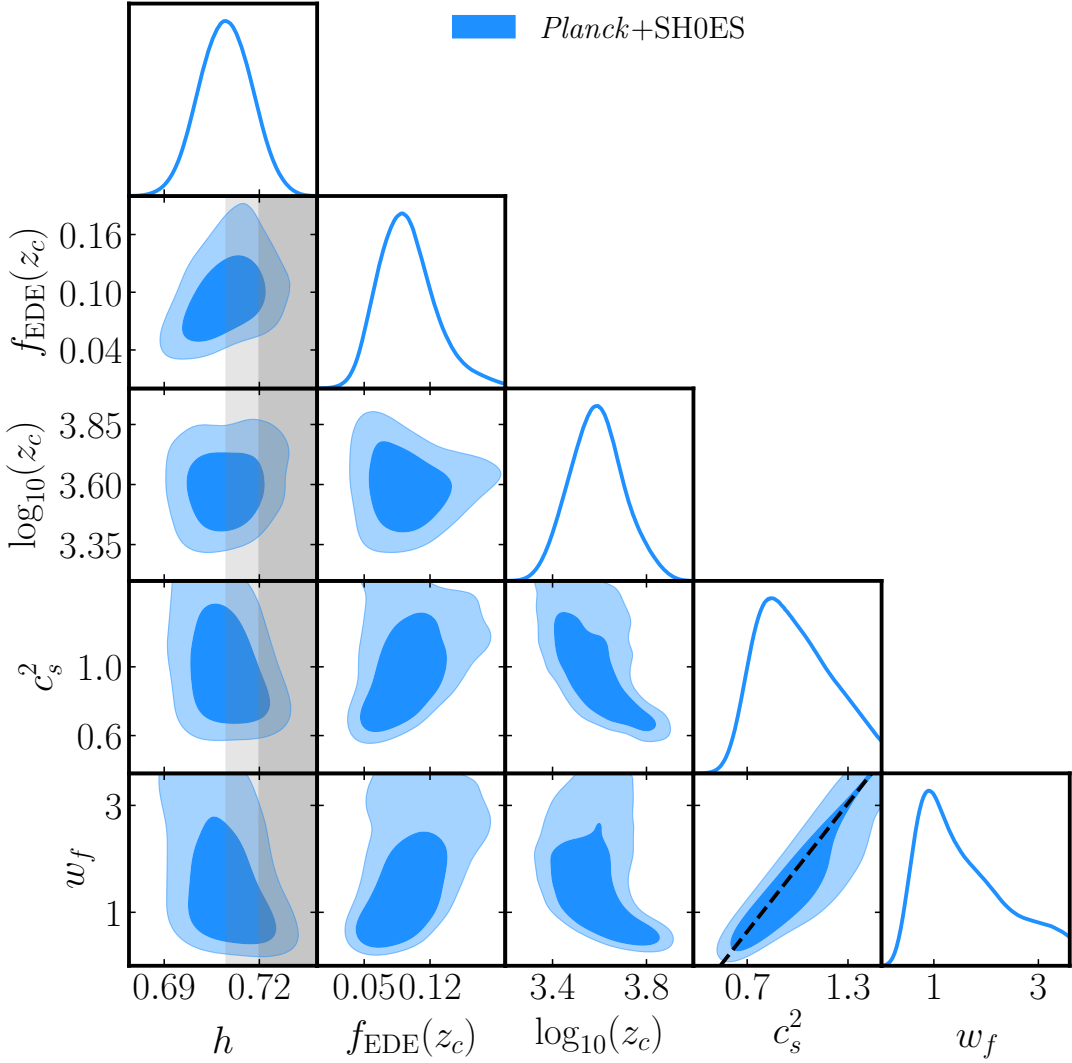


FIG. 10. 2D posterior distributions of $\{h, f_{\text{EDE}}(z_c), z_c, w_f, c_s^2\}$ reconstructed from analyzing *Planck*+BAO+Pantheon+SH0ES data.

at resolving the tension (see also Ref. [77] for a similar analysis in the RnR model). In the following, we present constraints setting $n = 3$, as is the conventional choice in the literature. For results with the explicit choice¹³ $n = 2$, we refer to the Appendix of Ref. [76].

We show in Fig. 11 the 2D reconstructed posteriors for the parameters

$$f_{\text{EDE}}(z_c) \text{ vs } \{h, \log_{10}(z_c), \theta_i, n_s, \omega_{\text{cdm}}, S_8\}$$

when analyzing *PlanckTTTEEE*+BAO+Pantheon with and without the SH0ES prior ($H_0 = 73.04 \pm 1.04$ [5]), taken from Ref. [163]. See also Refs. [76, 117, 144] for similar analyses with older datasets. In the absence of a prior on H_0 , the EDE model is not favored by the data in the Bayesian framework, and the combination *PlanckTTTEEE*+BAO+Pantheon simply provides an upper limit on the EDE contribution $f_{\text{EDE}}(z_c) < 0.091$, with $h = 0.688^{+0.006}_{-0.011}$.

However, as pointed out in various articles [69, 144, 167, 168], posteriors are highly non-Gaussian with long tails towards high- H_0 . These constraints should hence be interpreted with some degree of caution, and not naively scaled

¹³ It is worth stressing that the $n = 2$ case leads to similar posteriors for $\{f_{\text{EDE}}, H_0, z_c\}$, with only slightly worse χ^2 . The main difference lies in the reconstructed initial field value $\theta_i = 1.53^{+0.84}_{-0.37}$, which as we have argued before, controls the effective sound speed c_s^2 and the shape of the energy injection.

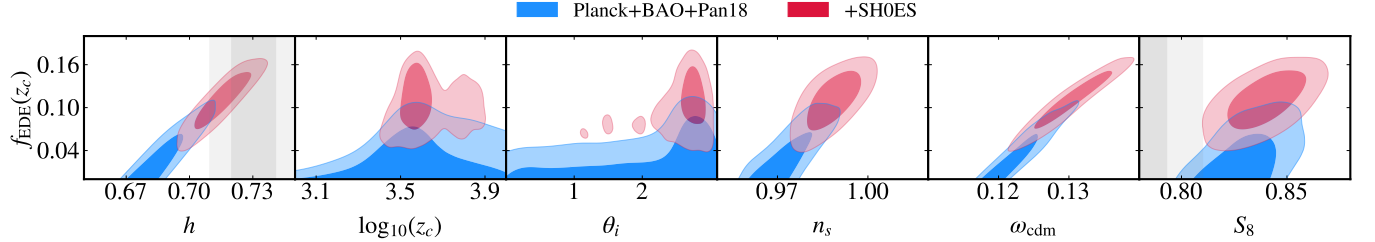


FIG. 11. 2D posteriors for $f_{\text{EDE}}(z_c)$ vs $\{h, \log_{10}(z_c), \theta_i, n_s, \omega_{\text{cdm}}, S_8\}$ when analyzing *Planck*TTTEEE+BAO+Pantheon with and without the SH0ES prior ($H_0 = 73.04 \pm 1.04$ [5]), as analyzed in Ref. [163].

using an intuitive Gaussian law. This is further supported by the fact that the best-fit point lies at the 2σ limit of the reported constraints ($f_{\text{EDE}}^{\text{b.f.}}(z_c) = 0.088$ and $h^{\text{b.f.}} = 0.706$).

Once the SH0ES prior is included in the analysis, one reconstructs $f_{\text{EDE}}(z_c) = 0.109^{+0.030}_{-0.024}$, at $\log_{10}(z_c) = 3.599(3.568)^{+0.029}_{-0.081}$ with $h = 0.715 \pm 0.009$, which at face value is in tension with the results that do not include SH0ES. This is tied to the effect discussed in previous sections and the non-Gaussianity of the posterior (without SH0ES). To measure the level of tension with SH0ES, the following tension metric is suggested [69, 169]

$$Q_{\text{DMAP}} \equiv \sqrt{\chi^2(\text{w/ SH0ES}) - \chi^2(\text{w/o SH0ES})}, \quad (32)$$

which agrees with the usual Gaussian-metric tension for Gaussian posteriors, but can better capture any non-Gaussianity in the posterior. This metric can easily be interpreted from the rule-of-thumb stating that for a single additional data point (SH0ES here), the χ^2 value of a “good” model should not degrade by more than ~ 1 (for a rigorous discussion, see Ref. [169]). Applying this to EDE, one finds the tension metric $Q_{\text{DMAP}} = 1.9\sigma$, while the metric gives 4.8σ in ΛCDM . Additionally, in the combined analysis, one finds $\Delta\chi^2 \equiv \chi^2_{\text{EDE}} - \chi^2_{\Lambda\text{CDM}} = -23.7$ with SH0ES and therefore a strong preference in favor of the EDE model (a simple estimate gives $\sim 4\sigma$ preference, assuming $\Delta\chi^2$ is χ^2 -distributed with 3 degrees of freedom). Therefore, the EDE model is able to accommodate large values of H_0 , while providing a good fit to *Planck*+BAO+SN1a. It is in this sense that *EDE can resolve the Hubble tension*.

Although *Planck*+BAO+SN1a data alone do not favor EDE and predict large H_0 to claim of the discovery of new physics, it turns out that this is not unexpected. Mock analyses of *Planck* data alone that include an EDE signal have shown that they *cannot* detect even a 10% contribution of EDE at $z_c \sim 3500$ and only lead to upper limits. Fortunately, an experiment like CMB-S4 would unambiguously detect such a signal [76].

Let us also highlight that data provide a strong constraint on the initial field value θ_i (in units of f , the axion decay constant). As shown in Sec. IV, θ_i has two main impacts on the EDE model - its dominant impact is setting the effective sound speed at the perturbation level, and a secondary effect is modifying the shape of the energy injection at the background level. We recall that for an oscillating EDE, the sound speed can be both time- and scale-dependent (see Eq. 25). In fact, the data prefer an EDE for which modes inside the horizon around z_c have effective sound-speed $\lesssim 0.9$ [76], consistent with phenomenological ADE results in the previous section which favor $c_s^2 < 1$ for $w_f \sim 1/2$. This can be achieved if the potential is flat around the initial field value θ_i such that the term $\theta_i^{n-1}/\sqrt{E_{n,\theta\theta}(\theta_i)} \gg 1$ in Eq. 25. Since the range of k -modes within the horizon is a sharp function of the initial field value θ_i , data provide a fairly strong constraint on $\theta_i \sim \pi$ (see Fig. 11). We recall that in addition, θ_i also contributes to the shape of the energy injection, see Fig. 9, that in turns affects the sound horizon and damping scales. These constraints on the dynamics, and as a result on the shape of the potential, explain why simpler power-law potentials (as in the Rock'n'Roll model) fair less favorably in resolving the tension.

Finally, translating the phenomenological parameters back into the theory parameters, the axEDE model suggests the existence of an axion-like field with mass $m \simeq 10^6 H_0$, decay constant $f \simeq 0.15 M_{\text{Pl}}$, and initial field value $\phi_i/f \sim \pi$. This prompted studies to understand whether the near-Planckian values of the decay constant and field excursion can lead to additional phenomenology (as in the EDS model [95, 123]) and constraints, as it might violate the axion weak gravity conjecture [103, 111].

D. Profile likelihood analysis of axEDE

A question often arises about the inclusion of SH0ES data for EDE constraints and for comparison to ΛCDM : as discussed earlier, ideally, the proposed model when analyzed with CMB data alone should predict a higher H_0 , improve the χ^2 more than the additional degrees of freedom and be preferred over ΛCDM . While the best-fit EDE

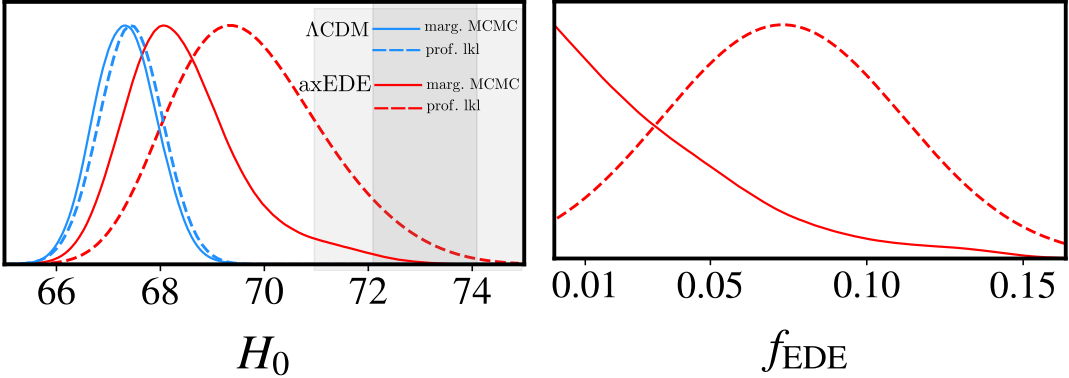


FIG. 12. Posteriors obtained from a profile likelihood (dashed) and MCMC methods (solid) are shown for Λ CDM (blue) and axEDE (red) for H_0 and f_{EDE} , for *Planck* 2018 CMB TTTEEE data. For the profile likelihoods, we plot the normalised curves of $e^{-\chi^2/2}$. While the posterior and profile likelihood match under Λ CDM, the profile likelihood indicates both a higher H_0 and f_{EDE} under the axEDE model. Note that although the location and width of the dashed curves will differ for different EDE models, this upward trend remains as they all are affected by prior-volume effects. Most notably, while the MCMC 1D posterior for f_{EDE} shows consistency with $f_{\text{EDE}} = 0$, the profile likelihood shows preference for EDE at $\gtrsim 2\sigma$.

with CMB data alone does exhibit the first two features, the MCMC posteriors are broad and show no H_0 solution, nor a preference for EDE. In fact, they ostensibly exclude the amount of EDE favored by the analysis that includes SH0ES. This signals the influence of ‘prior-volume effects’.

Indeed, a common feature of all EDE models is that, as the amount of EDE $f_{\text{EDE}} \rightarrow 0$, the other EDE parameters (e.g., z_c , θ_i , etc) become unconstrained. In the literature, it has been argued that this leads to a large prior volume at $f_{\text{EDE}} \simeq 0$, impacting results from MCMCs and skewing them towards $f_{\text{EDE}} \rightarrow 0$ [144, 167, 168]. These posteriors however do not trace the true data likelihood at each point in the extended Λ CDM+EDE parameter space¹⁴. While the literature largely concentrates on employing Bayesian techniques like MCMCs to constrain EDEs, alternate methods like likelihood profiles provide additional insight into the data response to these new models.

Constraints derived with a profile likelihood approach (e.g. [145, 167, 172, 173]) can lead to confidence intervals that are very different from the Bayesian credible intervals¹⁵. Profile likelihoods, rooted in the “frequentist” framework, trace the 1D data likelihood along a parameter direction - they optimise the χ^2 over all other parameters while holding the parameter of interest fixed. Constraints for that parameter can then be extracted directly from this χ^2 curve, with $\Delta\chi^2 \simeq 1$ giving the 1σ region in the case of a Gaussian profile when far from the prior boundaries on the parameter [174]¹⁶. For parameter spaces such as Λ CDM analysed using CMB data, where the profile is Gaussian and overwhelmingly dominates the prior contribution, constraints from profile likelihoods match those from MCMCs [176]. However for EDE, affected by prior-volume effects, these deviate [167, 172].

While profile likelihoods were already suggested as a check of potential prior-volume effects [164, 165]¹⁷, they have received much attention recently in the context of EDE constraints. In Fig. 12, we compare the MCMC 1D posteriors for H_0 and f_{EDE} in Λ CDM and axEDE to the profile likelihoods of the same parameters for *Planck* 2018 CMB TTTEEE data. There is little difference between posteriors and likelihood profiles of Λ CDM from the two approaches [176]. On the axEDE front however, there is stark contrast - tracing the true data likelihood leads to wider constraints on both H_0 and f_{EDE} . Moreover, data show preference for higher H_0 and f_{EDE} . As a result the (frequentist) confidence and (Bayesian) credible intervals extracted from the two strongly differ. While an MCMC analysis concludes that f_{EDE} is consistent with 0, a profile likelihood shows preference for $f_{\text{EDE}} > 0$ at over 2σ without a SH0ES H_0 prior.

This preference is already hinted at in the vast EDE literature that does not utilise profile likelihoods, by simply quoting the best-fit point (which by definition corresponds to the peak of the profile likelihood). Consistently, the best-fit point in EDEs does not coincide with the maximum of the MCMC posterior when an H_0 prior is excluded - that is, the greatest density of posterior-sampled points is not co-located with the best-fit point or the maximum

¹⁴ For further discussion about the mitigation of projection and prior volume effect, see Refs. [170, 171].

¹⁵ Strictly speaking, there are several ways to define credible intervals from a posterior distribution. For instance, one may choose to have the same fraction of samples at both ends of the distribution, or require that the value of the marginalized probability be the same at each limit.

¹⁶ In a more generic (non-Gaussian) case, one can use the Feldman-Cousins prescription to define confidence intervals [175]. For EDE, these match the simple Gaussian prescription [167].

¹⁷ These references suggest using the mean likelihood within a given bin to estimate the prior volume effect, a quantity that is simple to estimate directly from the MCMC sample, but that does not necessarily carry a well-defined statistical meaning.

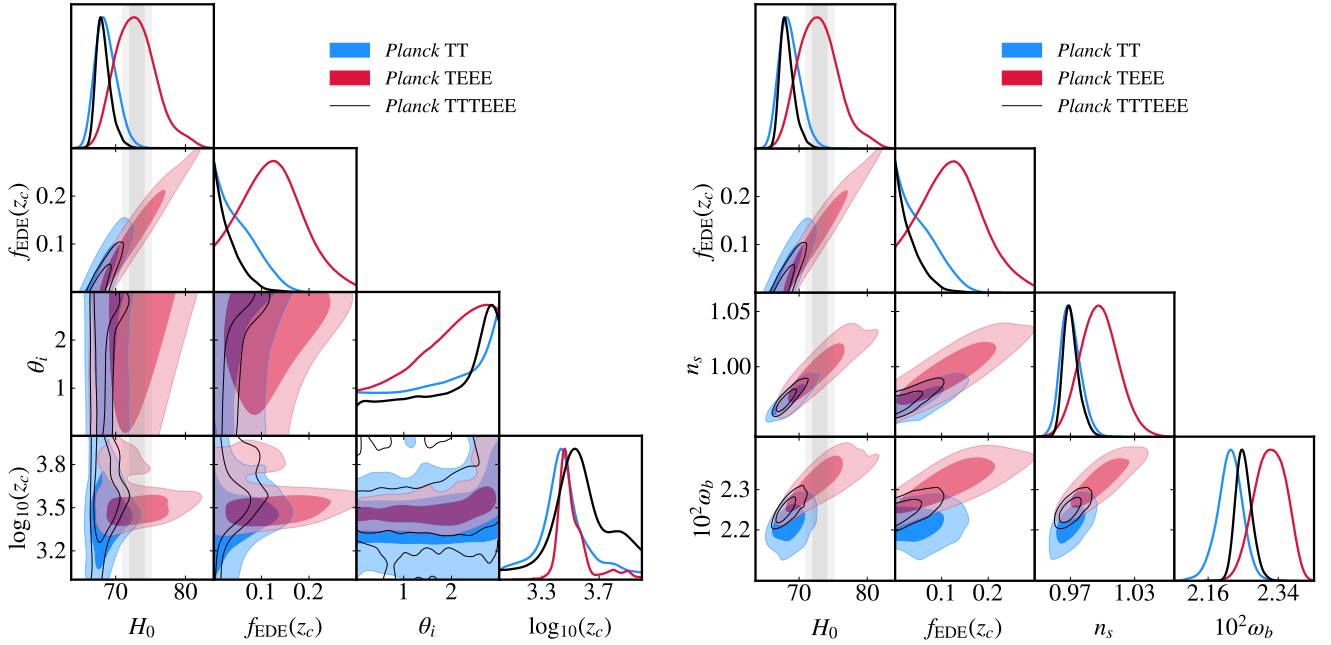


FIG. 13. Posterior distributions of $\{H_0, f_{\text{EDE}}(z_c), \theta_i, \log_{10}(z_c)\}$ (left panel) in the axEDE cosmology from analyzing *PlanckTT* and *PlanckTEEE*. The right panel replaces θ_i and $\log_{10}(z_c)$ with the posterior distributions of n_s and ω_b .

of the likelihood. In contrast, for ΛCDM , the best fit for any parameter is very close to the maximum of the 1D MCMC posterior. This raises the question of which is the most appropriate tool to use to constrain EDEs, or at least, suggests that both analyses methods should be performed to test the robustness of a constraint: when they diverge, care should be taken in strongly interpreting either result¹⁸.

As attention turns to profile likelihoods for EDE constraints, we note that for model-comparison purposes, one might still rely on Bayesian tools that account for the increase in parameter dimensions, using Bayesian evidence criteria, bearing in mind their dependence on the prior. Alternative methods have been suggested to overcome this limitation (e.g. Refs. [169, 177–182]). In principle, the Frequentist framework can also test whether the preference for a deviation from ΛCDM is statistically significant, given N number of additional degrees of freedom (taking into account the “look-elsewhere effect”). This can be done assuming the $\Delta\chi^2$ follows a χ^2 distribution with N degrees of freedom. In the case of EDE, because the parameters $\{z_c, \theta_i\}$ are unconstrained (i.e. have no effects on the likelihood) as $f_{\text{EDE}} \rightarrow 0$, this test statistic does not fully encapsulate the true significance, as required by Wilks’ theorem [183]. Still, it yields results more conservative than *local significance* tests which compute the preference at fixed $\{z_c, \theta_i\}$ with a single degree of freedom. More detailed analyses estimating the true significance, for instance following Refs. [184–186] or dedicated mock data analyses are still lacking.

E. Role of *Planck* polarization

To understand the origin of the preference for EDE from *Planck* alone, it is instructive to compare results from TT and TEEE separately. The reconstructed posterior distributions of $\{H_0, f_{\text{EDE}}(z_c), \theta_i, \log_{10}(z_c)\}$ are shown in the left panel of Fig. 13. Interestingly, one can see that *Planck TEEE* favors non-zero $f_{\text{EDE}}(z_c)$, at the 2σ level, with z_c and H_0 values in good agreement with the results of analyses that include SH0ES. *PlanckTT* data on the other hand do not show preference for EDE, although when explored alone, the constraints on EDE are weak with $f_{\text{EDE}} \lesssim 0.15$ at 95% C.L.. It is intriguing that the combination of *PlanckTT* and *TEEE* data lead to significantly stronger constraints than what one may naively expect from the individual constraints. To better understand this, in the right panel of

¹⁸ We stress that we do not claim profile likelihoods are definitively better than the Bayesian approaches, as the latter analyses also carry an estimate of “Occam’s razor” by disfavoring models with unnecessary extra parameters, an aspect also known as the “look-elsewhere effect” in Frequentist terms and that is complicated to estimate in general. However, it can be problematic to exclude models based purely on their complexity when they, in fact, provide a quality fit to the data (and can, in this specific context, accommodate direct H_0 measurements).

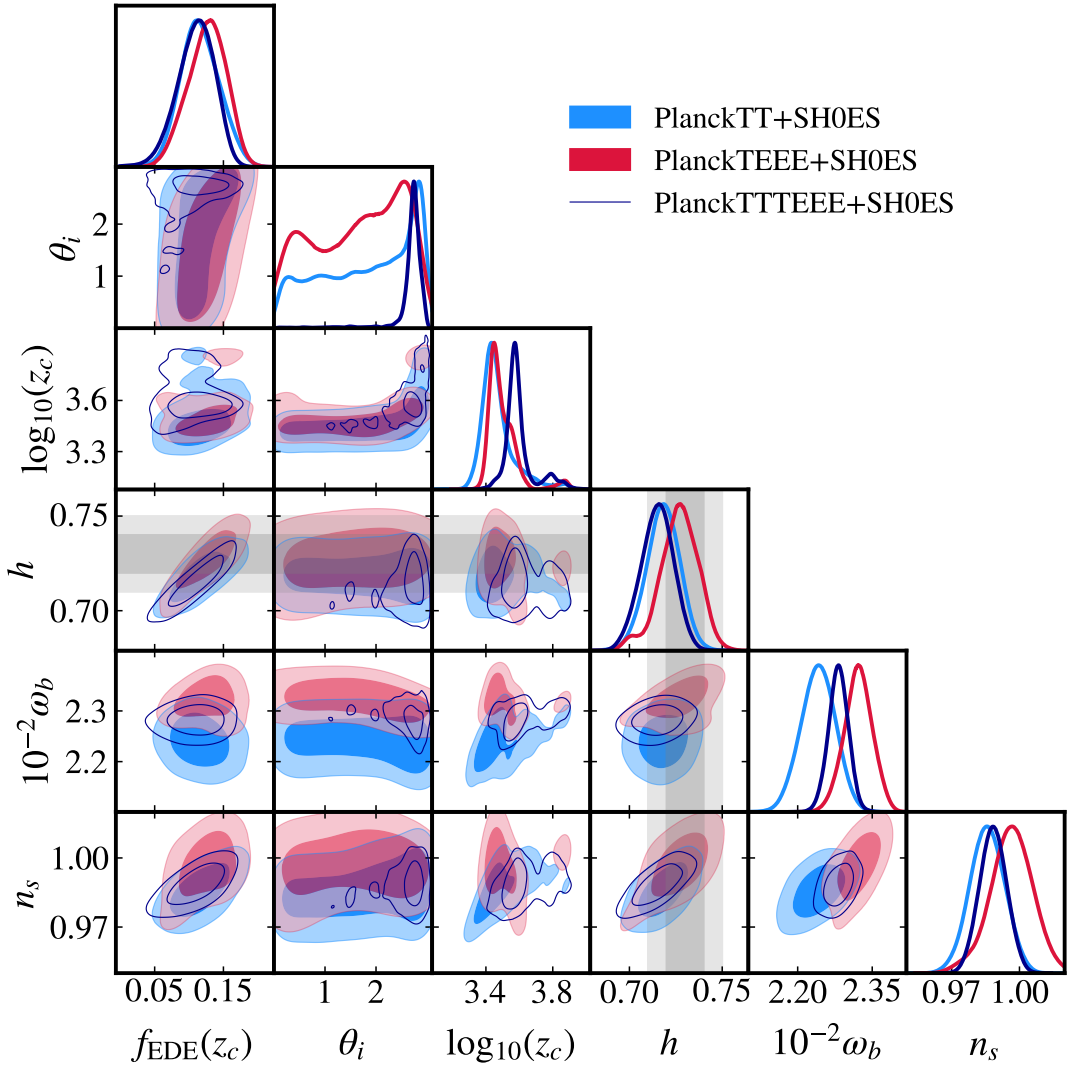


FIG. 14. 2D posteriors of $\{f_{\text{EDE}}(z_c), \log_{10}(z_c), \theta_i, h, \omega_b, n_s\}$ reconstructed from analyzing either *PlanckTT* or *TEEE* or the combination *TTTEE* data, along with the SH0ES prior. All analyses also include BAO and Pantheon data.

Fig. 13, we show the Λ CDM parameters that are most discrepant between TT and TEEE. The origin of these EDE constraints seems to be tied to the mild disagreement in the n_s and ω_b posteriors.

To contrast the role of TT and TEEE data in constraining EDE, and the importance of the mild ω_b mismatch between these data, it is also instructive to perform an analysis of TT and TEEE data separately, including the prior on H_0 . We show in Fig. 14 the reconstructed 2D posterior of $\{f_{\text{EDE}}(z_c), \log_{10}(z_c), \theta_i, h, \omega_b, n_s\}$ in these analyses. Evidently, both datasets individually allow for essentially any value of θ_i , and slightly favor lower values¹⁹ of z_c . It is only when they are combined that a very narrow range of θ_i values is favored, at the intersection of the posteriors at $\sim 1\sigma$ in the $\omega_b - \theta_i$ plane. Therefore, it is possible that high field values being favored by the data is driven by either small residual systematic errors in either TT or TEEE (or both), or by a statistical fluctuation that also drives the mismatch in ω_b . Since the preference for large θ_i indicates that pure power-law potentials are disfavored, this can be important from the model-building perspective, as pure power-law potentials may be more easily motivated than the axion-like cosine potential considered in this study.

Ref. [187] demonstrated that the preference in *PlanckTEEE* data is sensitive to assumptions in modeling the *PlanckTE* polarization efficiency (PE) calibration. There are two techniques for setting the TE PE parameters that

¹⁹ The combined analysis favors $\log_{10}(z_c) \sim 3.5$, while both separate analyses favor $\log_{10}(z_c) \sim 3.4$. Yet, values are compatible at 1σ and always roughly around z_{eq} . This seems to result from its correlation with θ_i visible in Fig. 14.

should give equivalent results, but in practice, estimates in *Planck* are slightly discrepant at the $\sim 2\sigma$ level (see Eqs. (45) - used as a baseline, and (47) of Ref. [4]). Ref. [187] found that the *Planck* preference for EDE decreases when the TE PE parameters are fixed to the non-standard values. Interestingly, the shift in this nuisance parameter goes in the same direction as results from the ACT collaboration, which found that a potential systematic error in their TE spectra can slightly reduce the preference for EDE within ACT DR4 data [188].

It has also been noted that the galactic-dust contamination amplitude is strongly correlated with the primordial tilt n_s . The fiducial analysis does not treat the galactic-dust contamination amplitude as a free parameter, but given the mild discrepancy seen in Fig. 13 in the determination of n_s , it is interesting to test how freeing these parameters can affect the preference for EDE. Ref. [187] showed that this only has a marginal effect on the preference for EDE (slightly increasing it).

F. Understanding the EDE- Λ CDM degeneracy in the CMB

Fig. 11 shows that incorporating EDE and a higher h also require readjusting other cosmological parameters to fit CMB data. We compare all six Λ CDM parameters in the concordance Λ CDM model when fit to *Planck*+BAO+Pantheon data to the axEDE model fit to *Planck*+BAO+Pantheon+SH0ES in Fig. 15.

One can see that (apart from h) ω_{cdm} and n_s are shifted the most between the Λ CDM and EDE cosmologies. To illustrate the degeneracy between EDE and these cosmological parameters, we show in Fig. 16 the evolution of the residual CMB TT and EE power spectra as cosmological parameters are adjusted to the best-fit EDE cosmology one by one. The best-fit Λ CDM model to *Planck* data is taken as reference.

When EDE is added to the Universe (orange curve), the most striking effect is a shift in the position of the peaks, as expected from the reduction of the size of the sound horizon induced by EDE and discussed in detail in Sec. IV. This effect is more strongly visible in the polarization spectra. The increase in h , from ~ 0.67 to ~ 0.72 partly compensates this shift, reducing the amplitude of oscillations (light red curve). In principle, h could be further increased to compensate the offset. However, the power at $\ell \sim 500$ is significantly larger than in Λ CDM. As discussed in Sec. IV, this corresponds to the multipole range where the effect of EDE perturbations on the acoustic driving of oscillations in the photon-baryon fluid and the time-dependence of the gravitational potential close to recombination (affecting the eISW term) is the most prominent. In particular, the gravitational potential tends to decay faster than in Λ CDM, leading to a notable increase of the eISW power at intermediate multipoles. In the EDE cosmology, this can be compensated for by increasing the CDM density, which stabilizes the potential decay and reduces the amplitude of the eISW effect (dark red curve) [157]. The effect of CDM on the angular diameter distance also compensates the reduced sound horizon, and the residual oscillation pattern further decreases. Note that, while the degeneracy with ω_{cdm} can balance the eISW effect introduced by EDE, it also limits the ability of the model to reach very high- H_0 due to the impact on the angular diameter distance.

Once h and ω_{cdm} have been adjusted, one can see that the spectrum shows a strong tilt, due to a different diffusion angular scale θ_d : the effect of EDE on the angular sound horizon is stronger than on the damping scale, and therefore the increase in h and ω_{cdm} cannot simultaneously keep θ_d and θ_s fixed. This effect is similar to that of an extra radiation species ΔN_{eff} , and can be compensated for by increasing n_s (brown curve). This is a remarkable consequence of the EDE cosmology: $n_s \sim 1$ is allowed at 2σ , impacting the viability of models of inflation and the evidence for a slow-roll phase of inflation in EDE cosmologies [189, 190]. In fact, such large values of n_s can be probed by future measurements of CMB spectral distortions, offering a way to test the EDE scenario [191]. The resulting residual shows an overall offset in amplitude, that can be compensated for by adjusting the combination $A_s \exp(-2\tau_{\text{reio}})$ (thin black curve). Finally, the remaining oscillations (particularly visible in polarization) are due to an offset in the ratio $\omega_b/\omega_{\text{cdm}}$ from increasing ω_{cdm} earlier. A slight increase in ω_b compensates for these.

The predictions for the residuals of the CMB TT and EE power spectra with respect to Λ CDM in the best-fit EDE cosmology are shown with the solid black line. To emphasize the irreducible effects imprinted by EDE in data (i.e. those that cannot be absorbed by a re-shuffling of Λ CDM parameters) that future surveys can target, we show in Fig. 17 the residuals of 100 samples randomly drawn from the MCMC chains, normalized to the Λ CDM best-fit to *Planck*. The color code indicates the value of H_0 in each sample. Note that we zoom in on the differences in the high- ℓ part of the plot.

First, the spectra show a bump-like feature around $\ell \sim 1500$ with increased power toward large ℓ in TT and EE that is present in essentially all the samples, and is due to larger n_s and ω_b (which affects the diffusion-damping scale besides the oscillations discussed earlier). This feature can be further probed with high-resolution ground-based measurements, such as ACT and SPT, and in the future, the Simons Observatory and CMB-S4. Multipoles $\ell \sim 100 - 500$ are particularly sensitive to details of the EDE dynamics as extensively discussed in Sec. IV, as these are the multipoles entering the horizon concurrently with the largest fractional contribution of the EDE energy density. Yet, the data require no strong departure from the Λ CDM prediction in that multipole range, and the samples oscillate

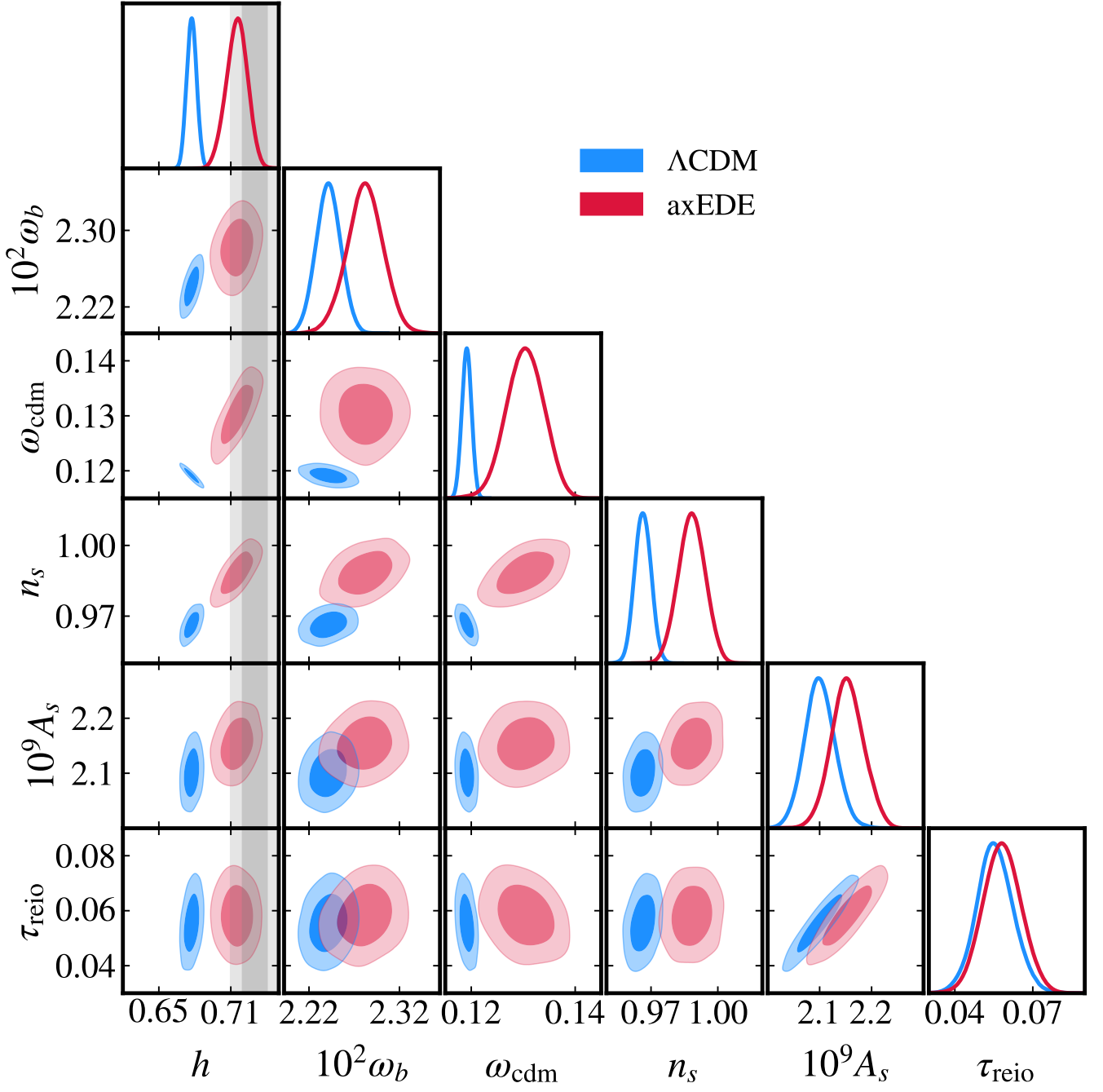


FIG. 15. 2D posteriors for the six Λ CDM parameters in the concordance Λ CDM and axEDE models fit to *Planck*+BAO+Pantheon data, illustrating how parameters reshuffle to accommodate the EDE contribution and a higher h .

around zero. Finally, one can also see large residual patterns at large angular scales ($\ell < 30$) in all three power spectra. The increased depth of the Sachs-Wolfe plateau in TT is (mostly) a consequence of slightly different values of A_s and n_s , and is common to all samples, albeit at different amplitudes. On the other hand, the large bump/dip in TE and EE, which is due to small differences in τ and ω_b , should not be over-interpreted, as the amplitudes of these vary greatly within the random samples of 100 points. It is therefore possible to easily adjust any forthcoming large-scale EE measurements with a slight shift in parameters and this signal is not a constraining feature for EDE. Note also that there is no strong correlation between the value of H_0 in each sample and the size of the residuals: it is possible to find samples of points with large H_0 values that show only small deviations from Λ CDM (and vice versa).

Finally, the modifications to the matter power spectrum and CMB lensing potentials once EDE is included are

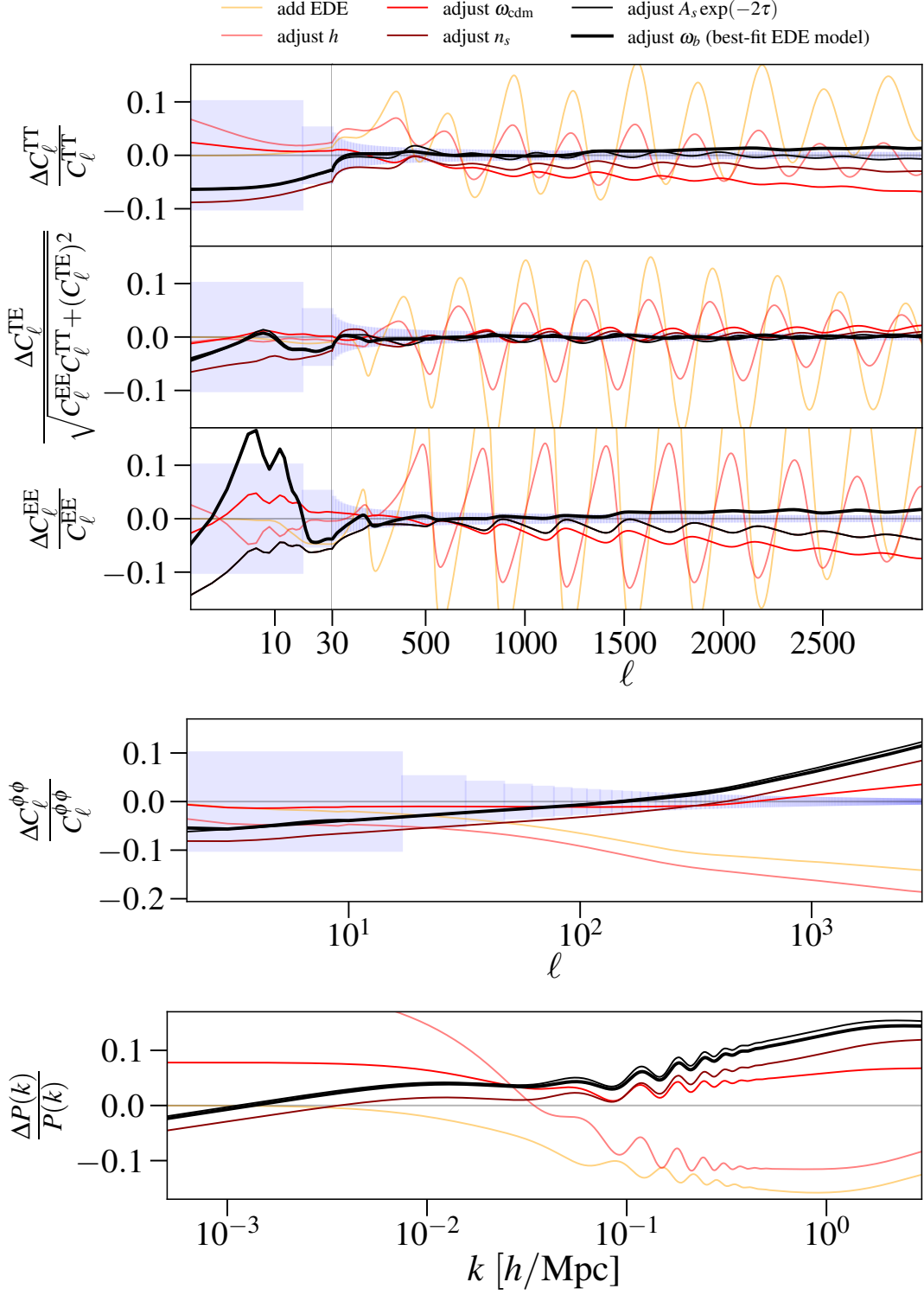


FIG. 16. From top to bottom: Evolution of the residual CMB TT, TE, EE, lensing $\phi\phi$ and linear matter power spectra as cosmological parameters are adjusted to the best-fit EDE cosmology one-by-one. The best-fit ΛCDM model to *Planck* data is taken as reference. Note that for TT, TE and EE we follow *Planck*'s convention and plot using a logarithmic scaling from $\ell = 2 - 30$ and a linear scaling from $\ell = 30 - 3000$. The fit to *Planck* TTTEEE data provided by the axEDE model is smaller by $\Delta\chi^2 = -6.4$ compared to that of ΛCDM .

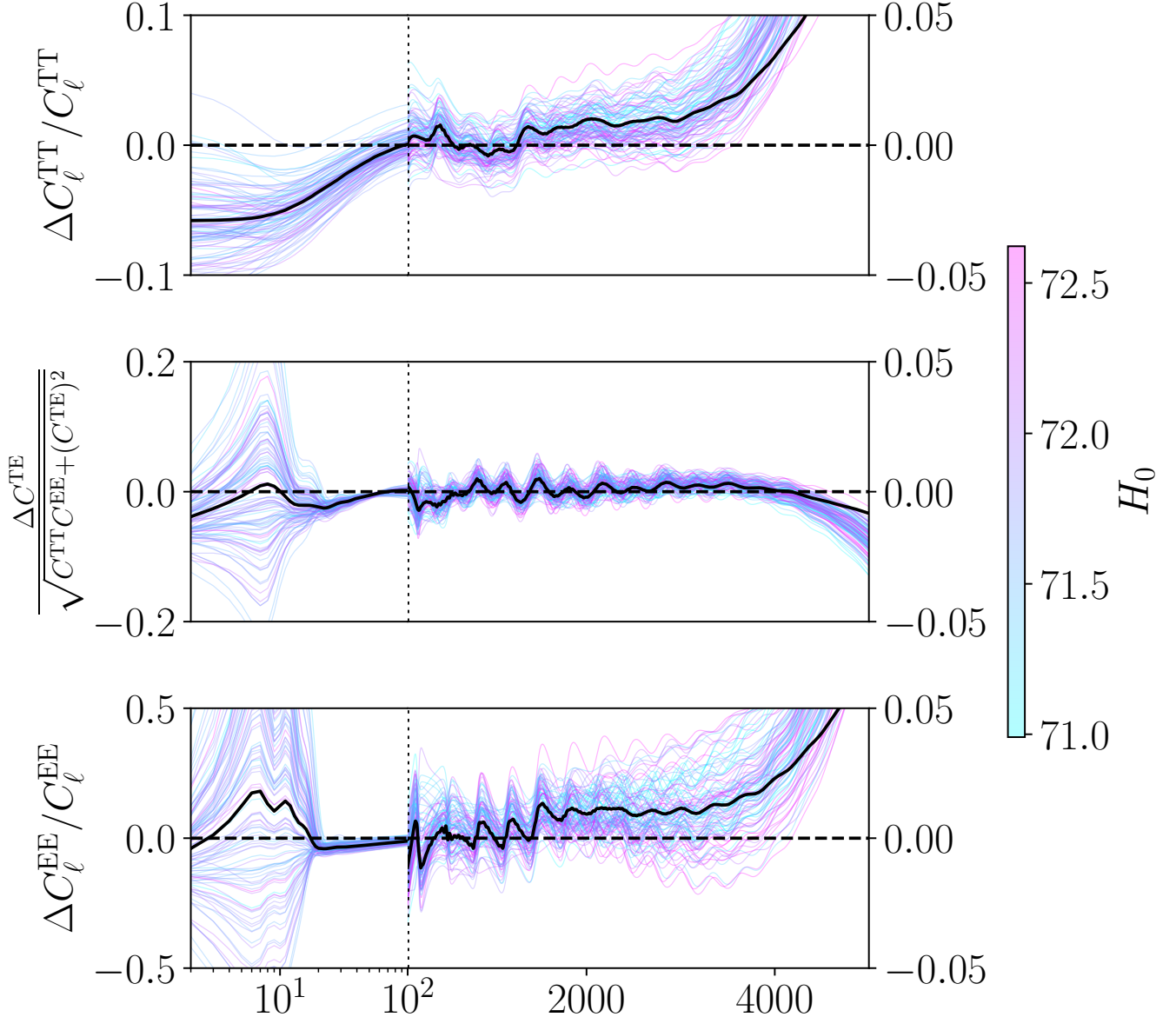


FIG. 17. Residuals of 100 samples randomly drawn from the MCMC chains in the axEDE model (fit to *Planck*+BAO+Pantheon+SH0ES), normalized to the Λ CDM best-fit to *Planck*. The color code indicates the value of H_0 in each sample.

primarily an overall power suppression, due to the fact that we added a non-clustering contribution to the energy density of the Universe. This clarifies that the increase in σ_8 is not due to the EDE *per se*, but in fact due to the reshuffling of Λ CDM parameters (in particular ω_{cdm}). Adjusting h has the effect of shifting the overall spectrum horizontally, and to increase the amplitude at large scales. This latter effect comes from keeping ω_{cdm} fixed at this stage, and the small- k branch is mostly controlled by $(g(a_0, \Omega_m)/\Omega_m)^2$ where $\Omega_m = \omega_{\text{cdm}}/h^2$ is more strongly decreased by the h increase than the effect on the growth rate $g(a_0, \Omega_m)$ due to the longer dark energy domination [192]. Increasing ω_{cdm} partly compensates this effect on large-scales, while also leading to earlier growth (z_{eq} is shifted to higher redshift) and therefore more power on small scales. Finally, adjusting A_s and n_s shifts up and blue-tilts the spectrum, while increasing ω_b slightly reduces the overall amplitude of the spectrum and leads to slightly more contrasted BAO oscillations. Very similar effects are visible in the lensing potential power spectrum (up to the BAO oscillations which are smoothed out).

<i>Planck+BAO+SN1a</i>			
Model	Parameters	w/o SH0ES	w/ SH0ES
axEDE [75, 76, 163] $n = 3$	h	$0.688(0.706)^{+0.006}_{-0.011}$	$0.715(0.719) \pm 0.009$
	f_{EDE}	$< 0.091(0.088)$	$0.109(0.122)^{+0.030}_{-0.024}$
	$\log_{10}(z_c)$	unconstrained (3.55)	$3.599(3.568)^{+0.029}_{-0.081}$
	θ_i	unconstrained (2.8)	$2.65(2.73)^{+0.22}_{-0.025}$ 1.9σ
RnR [77] $n = 2$	h	$0.6847(0.6788)^{+0.0057}_{-0.0083}$	$0.7033(0.7076)^{+0.0092}_{-0.0096}$
	f_{EDE}	$< 0.055(0.004)$	$0.067(0.0794) \pm 0.025$
	z_c	unconstrained (9950)	$3180(2907)^{+495}_{-604}$ 3.0σ
NEDE [82, 83]	h	$0.688(0.692)^{+0.0078}_{-0.013}$	$0.713(0.714)^{+0.011}_{-0.01}$
	f_{EDE}	$< 0.117(0.055)$	$0.125(0.130)^{+0.038}_{-0.03}$
	$\log_{10}(m_{\text{NEDE}})$	unconstrained (2.4)	$2.5(2.6)^{+0.2}_{-0.1}$
	$3w_{\text{NEDE}}$	unconstrained (2.06)	$2.11(2.06)^{+0.17}_{-0.21}$ 1.9σ
EMG [69, 137]	h	$0.6837(0.6853)^{+0.0049}_{-0.0055}$	$0.707(0.715)^{+0.0097}_{-0.01}$
	$f_{\text{EDE}}(z_c)$	$< 0.0346(0.024)$	$0.079(0.108)^{+0.032}_{-0.023}$
	$\log_{10}(z_c)$	unconstrained (3.59)	$3.612(3.626)^{+0.061}_{-0.058}$
	ξ	$< 0.86(0.017)$	$0.167(0.172)^{+0.065}_{-0.091}$ 1.9σ
ADE [78, 193] $w = c_s^2 = 1$	h		$0.706(0.7057) \pm 0.0085$
	f_{EDE}		$0.082(0.082) \pm 0.025$
	$\log_{10}(z_c)$		$-3.46(-3.45) \pm 0.06$
DA EDE [86, 119]	h		$0.7085(0.7143)^{+0.0093}_{-0.0080}$
	f_{EDE}		$0.050(0.063)^{+0.018}_{-0.015}$
	$\log_{10}(z_c)$		$4.79(4.96)^{+0.30}_{-0.20}$
	$\log_{10} \Upsilon [\text{Mpc}]^{-1}$		$8.01(7.47) \pm 0.76$
EDS [95]	h		$0.711(0.7252) \pm 0.012$
	f_{EDE}		$0.099(0.142)^{+0.056}_{-0.041}$
	$\log_{10}(z_c)$		$3.602(3.58)^{+0.071}_{-0.19}$
	θ_i		$< 3.14(2.72)$
α -EDE (B) [88]	h		$-0.0024(-0.0010)^{+0.0091}_{-0.015}$
	$f_{\text{EDE}}(z_c)$		0.709 ± 0.011
	$\log_{10}(1+z_c)$		0.082 ± 0.02
	Θ_i		$3.510^{+0.044}_{-0.05} < 0.184$
dULS [120]	h		$0.699^{+0.0084}_{-0.0086}$
	$f_{\text{EDE}}(z_p)$		$0.063^{+0.023}_{-0.025}$
	$\log_{10}(1+z_p)$		$3.880^{+0.033}_{-0.455}$

TABLE I. A summary of constraints on EDE parameters and the reconstructed Hubble parameter from analyzing *Planck+BAO+SN1a+SH0ES* with a Bayesian approach across various models suggested in the literature. Where possible, we quantify the residual tension with SH0ES using the tension metric $Q_{\text{DMAP}} \equiv \sqrt{\chi^2_{\text{min}}(\text{EDE}) - \chi^2_{\text{min}}(\Lambda\text{CDM})}$ introduced in Refs. [69, 169]. In the dULS model, there is a significant offset between what Ref. [120] calls ‘ z_c ’ and the redshift at the peak contribution of the EDE energy density. Here we report both f_{EDE} and z_c at the peak z_p . Since Ref. [120] does not report a value for f_{EDE} , we have estimated one using their reported constraint to Ω_{dULS} . Note that we do not report numbers for the ν EDE [80] and chain EDE models [87] as dedicated MCMC analyses are still lacking.

G. A summary of *Planck* constraints on the EDE dynamics

While our discussion was mostly focused on the axEDE model as the first (and a representative) candidate for EDE, other models have been subsequently studied in the literature in light of similar cosmological data. By comparing constraints from the various models, we can draw some generic conclusions about the dynamics required by the data to resolve the Hubble tension. We list in Tab. I and show in Fig. 18 the reconstructed 1D posteriors of the most relevant parameters in a representative sample of EDE models taken from the literature. We include results of analyses that all include (at least) *Planck* data (2015 or 2018), BOSS BAO DR12, Pantheon and SH0ES. Although this direct comparison should be taken with a grain of salt given that all models were not analyzed using the exact same data-sets, this simple exercise allows to draw some generic conclusions about the required EDE dynamics:

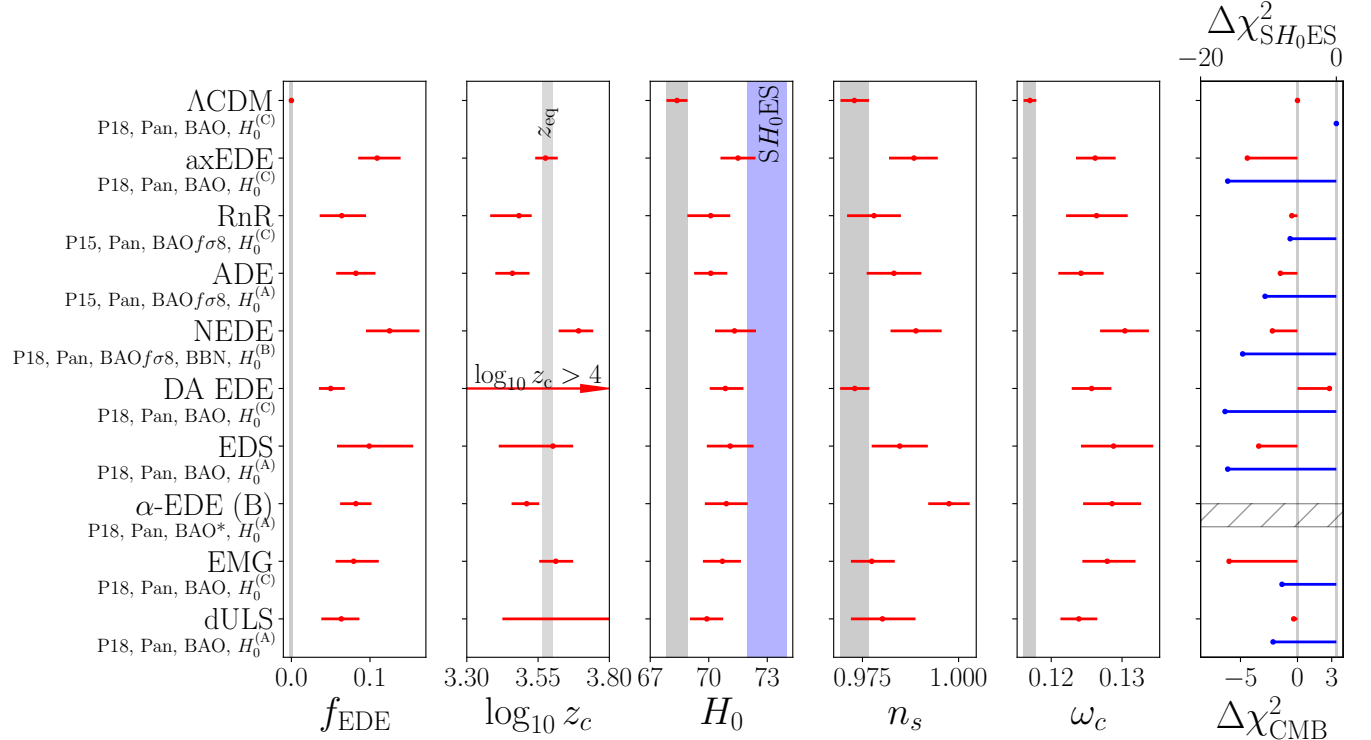


FIG. 18. Comparison of the reconstructed 1D posteriors of the most relevant parameters in a representative sample of EDE models suggested in the literature, compared with ΛCDM . Note that all models were not analyzed using the exact same datasets (see legends for details), but all analyses include (at least) *Planck* data (2015 or 2018), BOSS BAO DR12, Pantheon and SH0ES. The label $H_0^{(A)}$ refers to the value from Ref. [46], $H_0^{(B)}$ from Ref. [47] and $H_0^{(C)}$ from Ref. [5]. In the rightmost plot, we show $\Delta\chi^2_{\text{CMB}}$ in red and $\Delta\chi^2_{\text{SH0ES}}$ in blue. Note that for the dULS model, z_c is significantly larger than the redshift z_p at which the fractional EDE energy density peaks. Since z_p more closely corresponds to z_c in the other EDE models, here we report constraints on z_p . As Ref. [120] does not report a value for f_{EDE} , we have computed an approximate value using their constraint on Ω_{dULS} . We do not have access to the $\Delta\chi^2$ for the α -EDE model.

- all models indicate a maximum contribution $f_{\text{EDE}}(z_c) \simeq 5 - 12\%$ of EDE in the early universe;
- the maximum contribution is consistently found to be reached at $\log_{10}(z_c) \simeq 3.3 - 3.8$, i.e. around matter-radiation equality;
- all models lead to $H_0 \simeq 70 - 72 \text{ km/s/Mpc}$ (in fact no model can lead to values above $H_0 \sim 72.5 \text{ km/s/Mpc}$ at 1σ);
- all models have an increased primordial tilt of perturbations $n_s \simeq 0.98 - 1$ and an increased DM density $\omega_{\text{cdm}} \simeq 0.12 - 0.14$.

This demonstrates that the degeneracies discussed in the previous sections are generic, irrespective of the details of the EDE model. If EDE is responsible for the current Hubble tension, one generically expects a new $\sim 10\%$ DE-like contribution around matter-radiation equality accompanied with a higher DM density and primordial tilt. This shift in parameters has additional consequences on the growth of structure at late-times, and leads to a very different matter power spectrum than predicted in ΛCDM , that can further probe the model (see Secs. VII C and VII D). Furthermore, it may have important consequences for inflation, as the evidence for slow-roll behavior is currently tied to the detection of a small deviation from $n_s = 1$. In fact, it was argued that simple curvaton models (e.g. due to an axion-like particle reminiscent of the EDE field) would be favored over Starobinsky inflation [189, 190] if the Hubble tension, and the preference for EDE, stays.

To summarize, besides specifics of background dynamics, Sec. V B showed that data (in particular *Planck* polarization data) favor particular dynamics for the perturbations of the EDE field (as first shown by Ref. [78]), with the approximate relation $c_s^2 = 0.54 + 0.25 \times w$ where $w_f = (n-1)/(n+1)$. For an oscillating EDE with $n=3$, the data enforce dynamics in which modes inside the horizon around z_c have effective sound-speed of less than $\simeq 0.9$ [76]. This

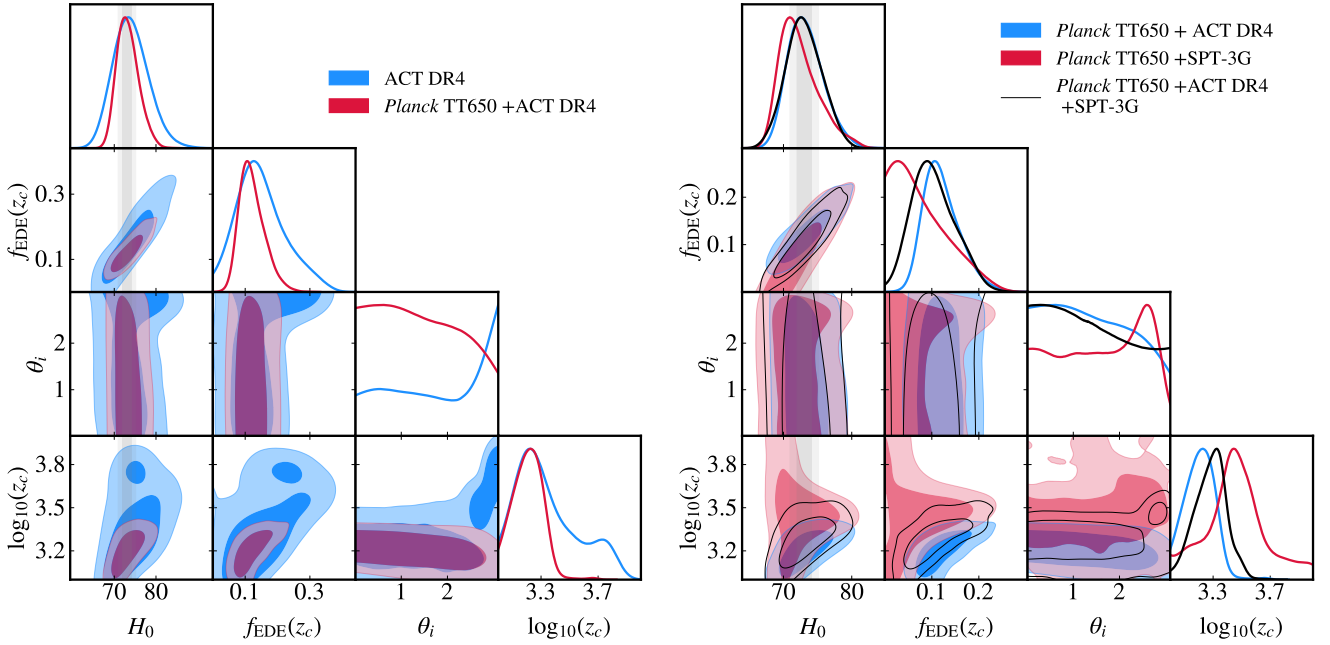


FIG. 19. Posterior distributions of $\{H_0, f_{\text{EDE}}(z_c), \theta_i, \log_{10}(z_c)\}$ reconstructed from various analyses. The left panel shows ACT data (with and without *Planck*TT data upto $\ell \leq 650$). The right panel shows a comparison between ACT and SPT, and their combination.

can be achieved if the potential is flat around the initial field value θ_i such that $\theta_i^{n-1}/V_n'' \gg 1$, which is realized in the axEDE model for $\theta_i \sim \pi$ (see Fig. 11). This explains why the RnR model, which matches the axEDE model in the limit $\theta \ll 1$, cannot attain as high an EDE contribution and therefore as good a resolution of the tension.

It is likewise interesting to compare the results of the RnR model with that of the EMG, given that their only difference is the addition of a non-minimal coupling to the Ricci scalar in the EMG model of the form $\xi\sigma^2 R/2$. As shown in Ref. [137], EMG models perform significantly better than the RnR model for $\xi > 0$, with data favoring $\xi \simeq 0.167_{-0.091}^{+0.065}$ once the SH0ES prior is included. The non-minimal coupling enhances the effect of the energy injection, while reducing the growth of CDM perturbations once the field starts to roll. In fact, this at least partly compensates for the effect of a larger ω_{cdm} on the linear matter power spectrum, and reduces the imprints of the EMG at late-times relative to the minimally-coupled EDE model, with potentially weaker constraints from galaxy surveys.

Similar results are obtained in the NEDE model which has very different micro-physical dynamics, as the NEDE fluid decays away through a phase-transition rather than coherent oscillations of the scalar field, showing that current data cannot yet characterize the transition from the DE phase to the dilution phase of EDEs. Note that in the results for the NEDE model presented here, we impose $c_s^2 = w$ when the fluid dilutes. However, even when c_s^2 is free to vary independently of w , the data enforce $c_s^2 \simeq 2/3$, i.e. to be very close to w [83]. Finally, in the α -EDE model, the balance between the shape of the energy injection at the background level and the dynamics of the perturbations leads instead to an upper-limit on θ_i [88], that is fairly tight given the choice of (p, n) and β (which dictates the shape of the potential, see Eq. 15).

This discussion highlights that while there are broad qualitative similarities between all the models, there are some quantitative differences that can help disentangle the exact EDE dynamics with CMB and LSS data.

In the following, we explore searches including additional data that can further distinguish the models.

VI. EARLY DARK ENERGY IN LIGHT OF ACT AND SPT DATA

Until now, we have limited our discussion to *Planck* CMB data (along with BAO and SN1a). Interestingly, recent literature has shown that the latest ACT data hints at a $2 - 3\sigma$ preference for EDE over Λ CDM, with H_0 values that are in good agreement with the SH0ES determination. We review these hints of EDE in light of the latest ACT and SPT data below.

A. Hints of EDE in ACT

When analyzing CMB data, one can test the robustness of results obtained with *Planck* by trading *Planck* data for a combination of WMAP, sensitive to $\ell \lesssim 800$ and a high-resolution ground based CMB telescopes, such as ACT [194] or SPT [195, 196]. For instance, ACT data cover multipoles $\sim 500 - 5000$ in TT and $\sim 350 - 5000$ in EE and TE, with exquisite precision such that the combination of WMAP+ACT was shown to constrain Λ CDM parameters at a precision similar (within a factor of 2) to that of *Planck*, and in agreement at $\sim 2\sigma$ [194]. Similar precision is attained by SPT [196], which covers the multipole range $\ell \sim 500 - 3000$.

We begin by presenting results with a similar baseline, where instead of WMAP, we make use of restricted *Planck* TT data at $\ell \leq 650$ which yield results in excellent agreement with WMAP and are therefore commonly used as a proxy for WMAP data [188]. The posterior distributions of $\{H_0, f_{\text{EDE}}(z_c), \theta_i, \log_{10}(z_c)\}$ are shown in Fig. 19 for various data combinations under an axEDE cosmology. One can see that ACT data favor a non-zero contribution of EDE at $\gtrsim 2\sigma$, with $f_{\text{EDE}}(z_c) = 0.152^{+0.055}_{-0.092}$ and $h = 0.742^{+0.036}_{-0.049}$, improving the $\Delta\chi^2 = -9.3$ with respect to Λ CDM. Very similar results were originally reported in Ref. [188] by the ACT collaboration with a different analysis pipeline. Once *Planck*TT650 is included, the preference for EDE increases to $\sim 3\sigma$, with $\Delta\chi^2 = -15.4$. Note that ACT+*Planck*TT650 favors a region of z_c below z_{eq} , and θ_i is essentially unconstrained, while *Planck*TTTEEE+SH0ES favored $z_c \sim z_{\text{eq}}$ with $\theta_i \sim \pi$. Ref. [188] established that the preference for EDE in ACT originates from a residual pattern at $\ell \sim 500$ in EE. This is visible in Fig. 20, left panel, where we show the residuals between EDE and the Λ CDM best-fit model to ACT DR4 data, with and without the inclusion of *Planck*TT650 data. The ~ 6 ACT DR4 data points in EE around $\ell \sim 500$ are significantly better fit by EDE than by Λ CDM. However, one can clearly see that there is also a large power excess at similar multipoles in TT in this model, which is not observed in *Planck* data. As a result, once large-scale *Planck*TT650 data are included, the residual features around $\ell \sim 500$ in EE and TT become less prominent. Instead, one can see a residual pattern of oscillations in all spectra that still yields a significantly better fit to ACT data, although the improvement now more equally arises from TT, TE and EE spectra.

B. Impact of SPT

Analyses with SPT 3G data have been presented in Refs. [187, 197] (for earlier works considering SPT Pol, see Refs. [198, 199]). On the right-hand side of Fig. 19, we show the results of analyzing *Planck*TT650+SPT 3G data compared to *Planck*TT650+ACT DR4, as well as the combination *Planck*TT650+ACT+SPT. One can see that SPT does not favor EDE, although error bars are large and not in particular tension with ACT. In combination with ACT, the preference for EDE is only slightly reduced compared to results with ACT alone. The most striking difference appears in $\log_{10}(z_c)$, with SPT 3G showing the usual degeneracy between $f_{\text{EDE}}(z_c)$ and H_0 for values of $\log_{10}(z_c)$, similar to the *Planck*TTTEEE+SH0ES analysis, while ACT DR4 favors lower values as mentioned previously. The difference between ACT and SPT data can be roughly understood from Fig. 20, left panel: around $\ell \sim 500$, where ACT data pull for an excess of power with respect to Λ CDM, SPT data prefer a small deficit.

Because of the small apparent differences between ACT and SPT, it is instructive to add *Planck* TEEE data to the analysis, which have a much larger signal to noise ratio at $\ell \sim 500$.

The right panel of Fig. 20 shows that all analyses with *Planck*TT650TEEE data consistently detect non-zero f_{EDE} . When *Planck* high- ℓ TT data are replaced by ACT DR4 data, the preference for EDE exceeds the 3σ level. The inclusion of SPT 3G TEEE data further increases the preference, and Ref. [200] reports $f_{\text{EDE}}(z_c) = 0.163(0.179)^{+0.047}_{-0.04}$ with $\log_{10}(z_c) = 3.526(3.528)^{+0.028}_{-0.024}$ and $\theta_i = 2.784(2.806)^{+0.098}_{-0.093}$, in good agreement with the EDE parameters reconstructed in the analysis of *Planck*+SH0ES presented earlier, with a $\Delta\chi^2 = -16.2$ (3.3σ preference) in favor of EDE over Λ CDM. In addition, the model predicts the value of $H_0 = 74.2^{+1.9}_{-2.1}$ km/s/Mpc, in good agreement with direct determinations. We now turn to discussing the impact of including *Planck* high- ℓ TT data on the analyses.

C. A new tension between ACT and *Planck* temperature data?

We show in Fig. 21 the reconstructed 1D posterior of $f_{\text{EDE}}(z_c)$ and H_0 as the range of multipoles (upto some ℓ_{max}) included in the *Planck* TT data is increased [187]. The results are unchanged until $\ell_{\text{max}} \simeq 1300$. Beyond that, the inclusion of small angular-scale data from the *Planck* temperature power spectrum decreases the preference of EDE to 2.3σ (in the absence of a H_0 prior). This is consistent with the fact that *Planck* high- ℓ TT data have most of their constraining power at those scales, and drive parameters very close to their Λ CDM values, limiting the ability to exploit degeneracies between Λ CDM and EDE parameters.

We show the results of analyses of *Planck*TTTEEE, *Planck*TT650TEEE+ACT+SPT and *Planck*TTTEEE+ACT+SPT in the right panel of Fig. 21. Notably, the reconstructions with *Planck*TTTEEE and *Planck*TT650TEEE+ACT+SPT

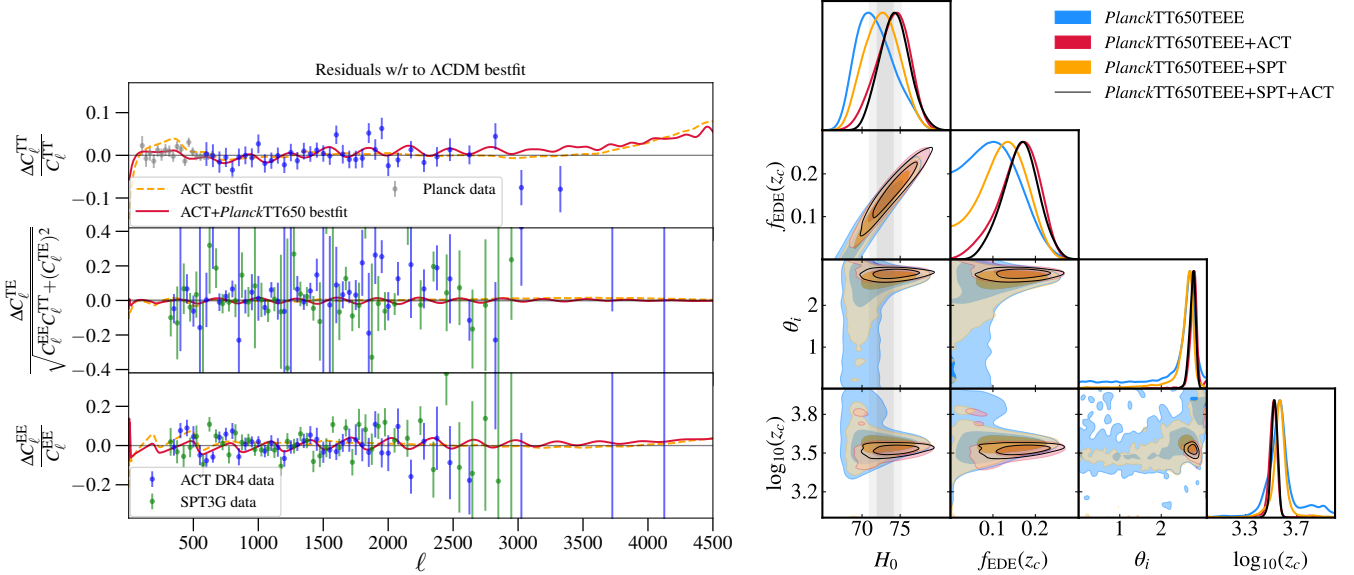


FIG. 20. *Left panel:* Residuals between EDE and Λ CDM when fit to ACT DR4 data alone and in combination with *Planck*TT650. We also show the residuals of ACT DR4, SPT3G and *Planck*TT650 in the Λ CDM model. *Right panel:* Comparison between the posterior distributions of $\{H_0, f_{\text{EDE}}(z_c), \theta_i, \log_{10}(z_c)\}$ reconstructed in the axEDE cosmology when analyzing ACT and SPT (and their combination) with *Planck*TT650TEEE. From Ref. [187].

appear to be in mild tension, and as a consequence, the combination *Planck*TTTEEE+ACT+SPT leads to the constraint $f_{\text{EDE}} < 0.128$, which is weaker than that obtained when analyzing *Planck*TTTEEE alone, $f_{\text{EDE}} < 0.091$.

It remains to be understood whether this mild tension between high- ℓ *Planck*TT data and ACT DR4 data is due to a statistical fluctuation or a sign of yet unknown systematic errors in either experiment. For further examination of the statistical agreement between these three CMB data sets, we refer the reader to Refs. [201, 202]. There have also been several studies looking into the consistency between the ‘low’ ($\ell \lesssim 1000$) and ‘high’ TT multipoles in *Planck* (see e.g. Refs. [4, 203, 204]). The high- ℓ TT power spectrum has a slight ($\sim 2\sigma$) preference for higher ω_{cdm} , higher amplitude ($A_s e^{-2\tau_{\text{reio}}}$), and lower H_0 . However, an exhaustive exploration of these shifts indicated that these are all consistent with expected statistical fluctuations [204]. Although there may be localized features in the high- ℓ TT power spectrum which are due to improperly-modeled foregrounds (see Sec. 6.1 in Ref. [4]), under the assumption of Λ CDM, there is no evidence that these data are broadly biased.

D. ACT and SPT constraints on other EDE models

Until now, our discussion has focused on results of analyses of the axion-like EDE model in light of ACT and SPT data, as a representative example. There have been, however, several notable analyses of other EDE models with these data, showing similar hints of a preference over Λ CDM.

First, the NEDE model was analyzed in Ref. [205] in light of ACT+WMAP data, finding that ACT supports the existence of two different “modes” corresponding to different trigger field masses (i.e. different transition redshifts). The high-mass mode has $\log_{10}(m_{\text{NEDE}}) = 2.916^{+0.13}_{-0.079}$ (corresponding to $z_* = 7870^{+1200}_{-900}$), with associated $f_{\text{NEDE}}(z_*) = 0.071^{+0.02}_{-0.024}$, and $H_0 = 70.3^{+0.89}_{-0.95}$ km/s/Mpc, while the low-mass mode has $\log_{10}(m_{\text{NEDE}}) = 1.687^{+0.22}_{-0.25}$ with $f_{\text{NEDE}}(z_*) = 0.12^{+0.03}_{-0.055}$ and $H_0 = 70.51^{+1.1}_{-2.2}$ km/s/Mpc. The high-mass mode represents an improvement with respect to Λ CDM of $\Delta\chi^2_{\min}(\text{NEDE}) = -17.6$, while the low-mass mode has $\Delta\chi^2_{\min}(\text{NEDE}) = -8.4$. Note that the high-mass mode – with a slightly lower H_0 – has a significantly lower χ^2 than the low-mass mode, and is thus favored over the mode that would fully resolve the Hubble tension.

When combining full *Planck* (instead of WMAP) with ACT, it was found that the NEDE model still improves the fit over Λ CDM by a small amount, $\Delta\chi^2_{\min}(\text{NEDE}) \simeq -5.7$, but $f_{\text{NEDE}}(z_*)$ is compatible with zero at 1σ . In addition, the 2σ constraint on the NEDE contribution significantly strengthens, from $f_{\text{NEDE}}(z_*) < 0.116$ (without ACT) to $f_{\text{NEDE}}(z_*) < 0.082$ (with ACT). This is in contrast with the results for axEDE (for which the combined constraint is weaker than *Planck* alone, see previous section), and indicates that the combination of *Planck* and ACT has the

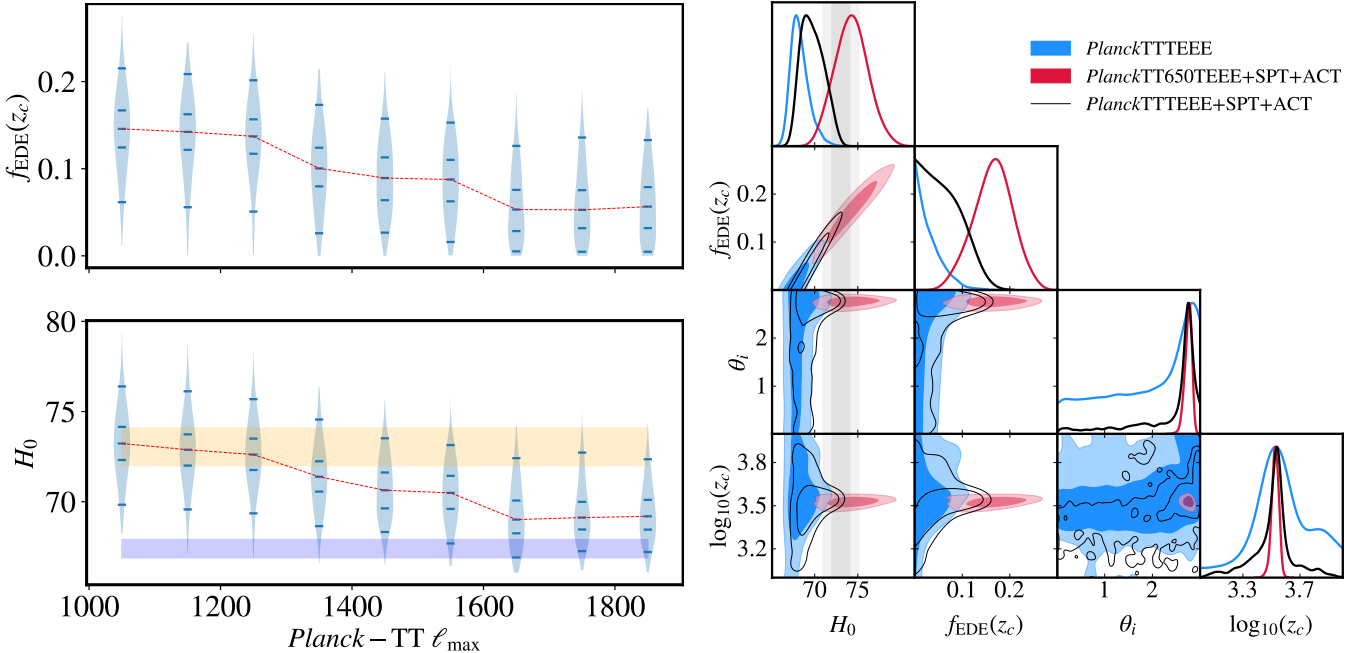


FIG. 21. The left panel shows the 1D posterior distribution of $f_{\text{EDE}}(z_c)$ and H_0 as the range of multipoles included in the *Planck* TT data is increased to ℓ_{\max} . The right panel shows $\{H_0, f_{\text{EDE}}(z_c), \theta_i, \log_{10}(z_c)\}$ reconstructed from *PlanckTTTEEE* compared to *PlanckTT650TEEE+ACT+SPT*, and the combination *PlanckTTTEE+ACT+SPT*. These figures are taken from Refs. [187].

potential to distinguish between different EDE cosmologies.

We illustrate the difference in the constraints on the NEDE and axEDE models from the combination of *Planck* and SH0ES, with and without ACT data (always including BAO and SNeIa data) in Fig. 22. One can see that once ACT data are added to the NEDE model, the preference for non-zero f_{EDE} and large H_0 decreases, while it increases in the axEDE model. To investigate the source of the difference, in Fig. 23, we show the difference in CMB TTTEE, lensing, and matter power spectra between the best-fit Λ CDM model and axEDE/NEDE when fit to *Planck* and SH0ES. Although both models provide qualitatively similar residuals in the CMB data, displaying the characteristic increase in power at small scales, and quantitatively similar fits to *Planck*, small differences between the models in the transition mechanism from the DE phase to the dilution phase can have important consequences with more accurate data.

This analysis was superseded by that performed in Ref. [190] which, in addition to ACT-DR4 data, also considered the impact of SPT-3G data on the NEDE model. They showed that prior-volume effects played a part in these constraints, as the constraint on $f_{\text{NEDE}}(z_*)$ significantly weakens when fixing the mass of the trigger field. Once the SH0ES prior is added, a non-zero value of $f_{\text{NEDE}}(z_*)$ is still strongly favored at 4.8σ (5.2σ without ACT), but the tension level with SH0ES remains $\sim 2.9\sigma$ (1.6σ without ACT). SPT data on the other hand have a relatively weak impact on the model, and although they do not favor a non-zero $f_{\text{NEDE}}(z_*)$ on their own, the preference over Λ CDM becomes 4.7σ when SH0ES is included in the analysis, with a tension level of 1.8σ .

The ADE model was studied in light of updated *Planck* and ACT data in Ref. [193], which highlighted the important role played by *Planck* TEEE data in the constraints: these restrict the ability of the ADE model to reach values larger than $H_0 \sim 71$ km/s/Mpc at 1σ , although the combination of *Planck*+ACT+BAO+Pantheon+SH0ES still favors ADE at $\sim 2.8\sigma$. On the other hand, ACT data do not play a significant role in favoring or disfavoring the ADE model, with ADE constraints barely affected by the inclusion of ACT data. These results are again in contrast with the axion EDE and NEDE models, and stress the considerable power of precision CMB data in distinguishing between different EDE dynamics.

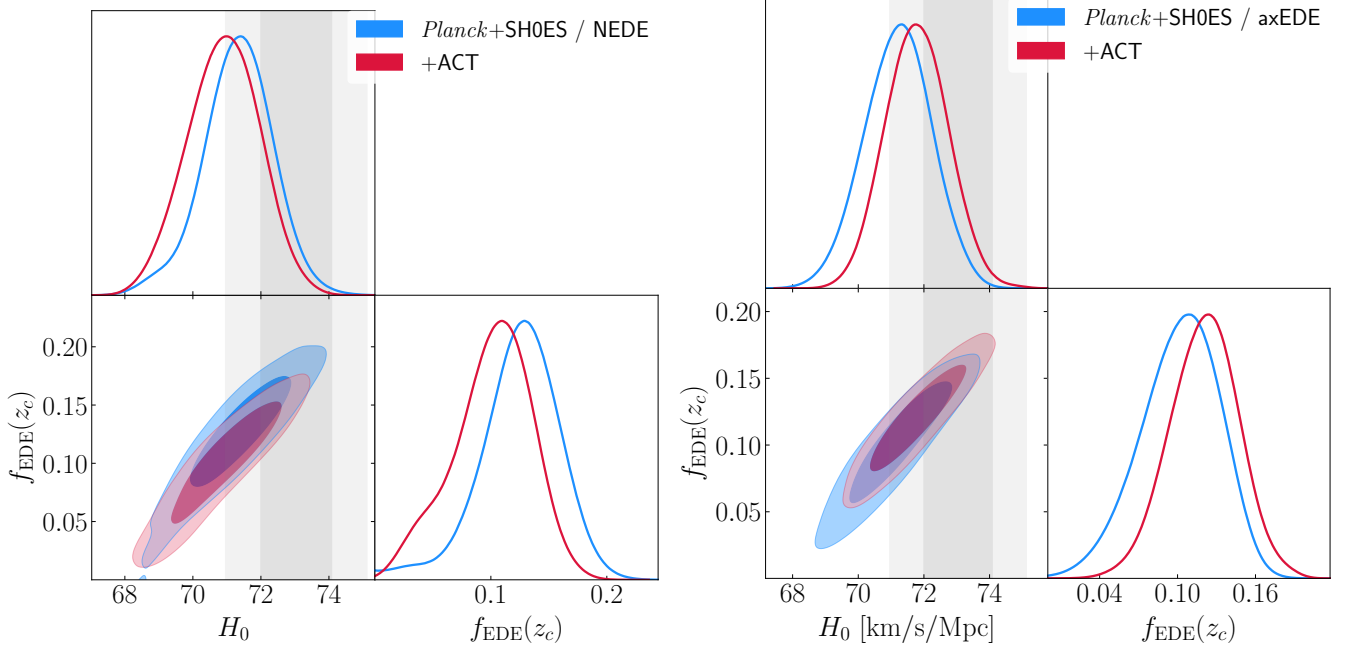


FIG. 22. The reconstructed H_0 - $f_{\text{EDE}}(z_c)$ posteriors in the NEDE and axEDE models, when considering either full *Planck* data or TT-restricted *Planck* data in combination with ACT.

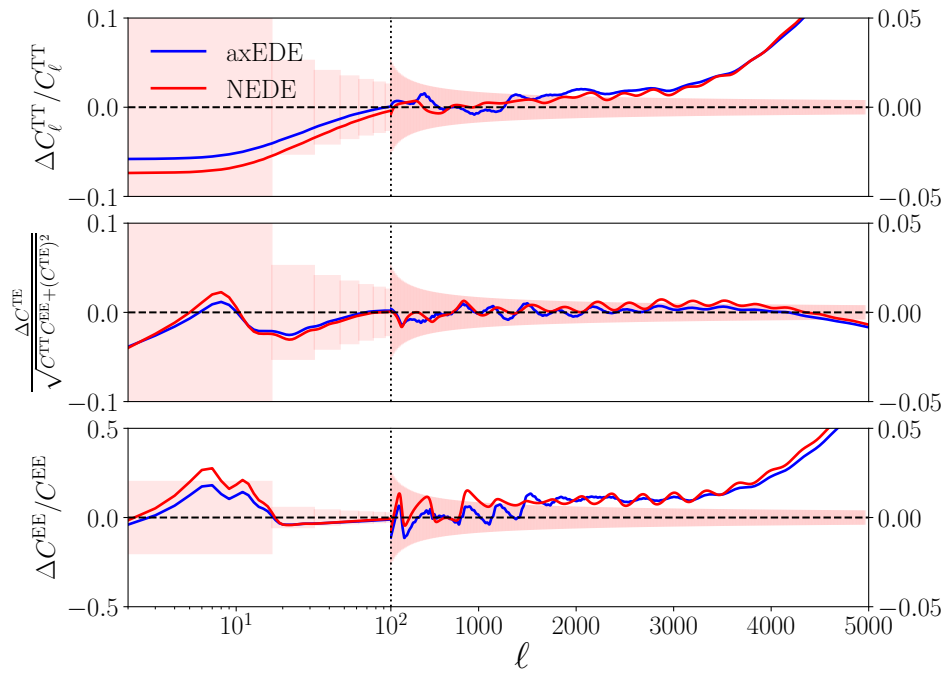


FIG. 23. The differences in residuals between the best-fit Λ CDM model and axEDE/NEDE. The models were fit to *Planck* CMB (TTTEEE+lensing) power spectra, BAO, SNeIa and SH0ES. Although they produce qualitatively similar signals, more accurate data at small angular scales are sensitive to the small quantitative differences between the models. The pink boxes give the cosmic variance uncertainty binned with a width of 15. Note that the linear part of these panels have a smaller y range in order to better compare the axEDE and NEDE models.

VII. CHALLENGES TO THE EDE MODELS

A. A second cosmic coincidence problem

An obvious question raised by EDE models is a coincidence or ‘why then’ problem – why does the EDE contribution become significant precisely close to matter-radiation equality, when it is most impactful on the CMB? This echoes the open question in cosmology regarding dark energy – the ‘why now’ or ‘cosmic coincidence’ problem that asks why the densities of dark energy and matter are similar today.

Models of ‘tracking dark energy’ [150, 206], in which the density of a scalar field is always a fixed fraction of the energy density of the dominant component may provide an interesting starting point for model-building, and connect various eras of accelerated expansion in the universe. A similar idea – assisted quintessence [151] was recently applied in the EDE context, but authors of Ref. [89] found that it could not alleviate the tension. Alternatively, chameleon EDE [94] and trigger EDS [123] connect the dynamics of the EDE model to the onset of DM domination by coupling the EDE scalar field to DM. These models trigger the dilution of EDE through their interaction with DM, tying z_c to matter-radiation equality and the DM mass to the EDE scalar field, with potential implications for the S_8 tension.

Yet, the answer to this coincidence question may be simple probability. As suggested in the “Axiverse” scenario [207], it is possible that there exist additional EDE-like fields in the Universe that may have been relevant (or not) at different eras, with a non-negligible probability that one such field becomes dynamical close to matter-radiation equality²⁰. In fact, in that context, it is plausible that the EDE field responsible for the Hubble tension is the first member of a family of such fields, that have yet to be detected (or second, if one counts late-DE) (see also Refs. [87, 206, 209–211]). It is also plausible that an EDE field acting around matter-radiation equality was detected first *precisely because* our cosmological data gains most of their sensitivity right around recombination. Fields acting at much earlier times would leave the CMB mostly unaffected [74, 116], while a field acting at much later times could play the role of dark energy. In any case, if the presence of an EDE-like field is confirmed with future data, the question of what if any connection exists between DE and EDE will become particularly relevant. Indeed, this new ‘why then’ problem may provide insight into the long-standing ‘why now’ problem.

B. Fine-tuning problems of some scalar-field EDE models

The “axion-like” potential given by Eq. 6 suffers from fine-tuning issues that makes it challenging to embed in a UV-complete theory. While one may generate such a potential from an instanton expansion, where the leading terms with order $n < 3$ (and higher order ones) have vanished due to a delicate balance in the controlled expansion, this is generically hard to achieve, as was pointed out in Refs. [98, 103, 120]. Attempts at realizing this potential in string theories have been discussed²¹ in Ref. [98, 115]. In addition, as mentioned earlier, the near-Planckian field excursions favored in the analysis may run into problems with the weak-gravity conjecture [103, 111]. Similarly, for models not protected by approximate shift-symmetries like the axion-like model, one expects that radiative corrections (arising from self-interactions or couplings to other fields) to the scalar-field mass will lead to additional lower-order contributions to the potential that scale as ϕ^2 . In both cases, these additional terms appear at energy scales that are connected to those of the higher-order terms, such that it may not possible to ignore lower-order terms in the analyses. When included, they may dominate the dynamics of the model, slowing the dilution of the field and leaving imprints on observables that are ruled out. For instance, if $m^2\phi^2$ terms dominate, the field dilutes like matter, spoiling the success of the EDE model [116].²²

Nonetheless, the axEDE model can offer insight into the background and perturbative phenomenological properties of EDE preferred by data that replacement, well-motivated EDE models can target to resolve the tension. For example, while DA EDE can emulate these properties at the background level, due to vastly different perturbation dynamics, it is unable to replicate the success of axEDE [119]. NEDE, α -attractors, and the dULS model, on the other hand, are theoretically better motivated and achieve results similar to axEDE, as they can reproduce both the required background and perturbative phenomenology to increase H_0 while also providing a good fit to CMB data.

Hence, two avenues of further research may be particularly interesting: exploring alternate, well-motivated scalar fields for EDE and directly reconstructing the EDE potential from data. Lower-order terms in the EDE scalar potential that address these fine-tuning issues, or the presence of multiple fields as in the NEDE model may have

²⁰ A similar ‘probabilistic’ scenario was introduced in Ref. [208], in order to solve the ‘why-now’ problem of late-time DE and leave observables unaffected.

²¹ Let us stress that the recent work presented in Ref. [115] concludes that EDE with a modified axion-like potential can be a viable cosmological model in a string-theory context, with model-building challenges similar to that of inflation, late DE and fuzzy dark matter.

²² If we include a quadratic term in the axEDE potential $V = m_b^2\phi^2/2 + m_a^2f^2(1 - \cos\phi/f)^3$, the resolution to the Hubble tension is unspoiled as long as $m_b/m_a \lesssim 10^{-4}$.

similar effects as additional ultra-light axions like in the ‘dark sector’ model, and may simultaneously alleviate the S_8 tension [98]. Alternatively, successful non-EDE scalar-field models have also been suggested [212–214] as Hubble tension solutions. On the other hand, abandoning parametric potentials altogether, one may directly reconstruct the EDE potential from data, as routinely done for the inflaton potential [215] and dark energy [216, 217]. Ref. [92] attempts to reconstruct EDE dynamics non-parametrically, but at the level of the fluid energy density, rather than the scalar-field potential. In any case, future high-accuracy CMB and clustering data will be crucial in distinguishing the various EDE models suggested so-far, and may shed light on the dynamics required to resolve the Hubble tension beyond a toy-model description.

C. The trouble with S_8

Besides the statistically-significant Hubble tension, another interesting tension is emerging in cosmology relating to the amplitude of density fluctuations on large scales, captured by estimations of the parameter $S_8 \equiv \sigma_8(\Omega_m/0.3)^{0.5}$. The amplitude σ_8 is the root-mean-squared of matter fluctuations on a $8h^{-1}\text{Mpc}$ scale and is defined through

$$\sigma_8^2 = \int \frac{k^3}{2\pi^2} P_m(k) W_8^2(k) d\ln k. \quad (33)$$

where $P_m(k, z=0)$ is the linear matter power spectrum today, $W(kR)$ is the top-hat window function in Fourier space, and $R = 8\text{Mpc}/h$ by convention. Inferences of S_8 from weak lensing surveys such as the CFHTLenS [218], KiDS, as well as from *Planck* SZ cluster abundances [4, 219] are about $2 - 3\sigma$ smaller than that from the CMB.

In fact, the combination of KiDS data with BOSS and 2dFLenS data leads to a 3σ lower value than *Planck*, and points to a σ_8 -tension rather than discrepancies in Ω_m [220]. However, some surveys such as DES [221] and HSC [222], while yielding S_8 lower than *Planck*, are statistically compatible with it at less than 2σ . More data are therefore awaited to firmly confirm this potential breakdown of the ΛCDM model (see Ref. [2] for a more complete review of measurements).

Unfortunately, a generic feature of early-universe models proposed to resolve the Hubble tension is to predict greater S_8 and *increase* this tension. For EDEs, this may appear surprising since, at fixed ΛCDM parameters, the impact of EDE is to decrease the amplitude of matter fluctuations. The subsequent increase in S_8 is due to the degeneracy with ω_{cdm} described in Sec. V F: the impact of the increased expansion rate on the time-evolution of potential wells (in particular the eISW effect), which manifests as an increase in the height of the first acoustic peak (see Sec. IV for details), is compensated for by increasing the DM density [75, 157]. As the DM density increases, the onset of DM domination and the formation of structure begin earlier, leading to larger σ_8 . In addition, a similar increase in the DM density is required to keep the angular scale of the BAO fixed, with the same consequences for S_8 . It has been suggested that it might simply be impossible to resolve both tensions simultaneously with a single new-physics mechanism [157, 223–225]. We show in Fig. 24 the linear (left) and non linear (right) matter power spectra in the EDE cosmology and in ΛCDM as computed in Ref. [226] for a fiducial analysis that includes *Planck*+BAO+Pantheon+SH0ES data. One can see a clear increase of power at scales $k \sim 0.1 h/\text{Mpc}$ and above, although the differences are smaller in the non-linear power spectrum.

Due to the impact on S_8 , it is possible to use low- S_8 measurements to constrain EDE. In particular, Ref. [117] showed that the combination of DES data, with priors on S_8 as measured by KiDS and HSC, leads to the constraint $f_{\text{EDE}}(z_c) < 0.06$ without SH0ES, and $f_{\text{EDE}}(z_c) = 0.062^{+0.032}_{-0.033}$ with SH0ES. At least part of this constraining power was found to originate from prior-volume effects, since once θ_i and z_c are fixed to their best-fit values, the constraints from a combined analysis with the KiDS/DES/HSC data relax substantially to $f_{\text{EDE}}(z_c) < 0.092$, and the inclusion of SH0ES leads to $f_{\text{EDE}}(z_c) = 0.087^{+0.029}_{-0.024}$ [144, 168]. However, it is clear that low- S_8 measurements cannot be explained by the presence of EDE [227], and that one can use LSS surveys to constrain the presence of EDE.

D. Is Early Dark Energy excluded by BOSS?

Beyond the mere value of S_8 , measurements of biased tracers of the matter power spectrum can be used to constrain EDE models. An example of such an observable is the galaxy power spectrum. Until now, we have reported analyses that only make use of compressed information from galaxy surveys done by BOSS, in the form of the BAO angles, and for some analyses, also use the redshift-space distortion information (quantified by $f\sigma_8$). The impact of including $f\sigma_8$ information for EDE is minor. For instance, in the latest analysis of the axEDE model which was presented above, the inclusion of $f\sigma_8$ from BOSS DR12 changes the constraints from $f_{\text{EDE}}(z_c) < 0.091$ without SH0ES ($f_{\text{EDE}}(z_c) = 0.109^{+0.030}_{-0.024}$ with SH0ES) to $f_{\text{EDE}}(z_c) < 0.088$ without SH0ES ($f_{\text{EDE}}(z_c) = 0.102^{+0.030}_{-0.024}$ with SH0ES) and the Q_{DMAP} metric still indicates a decrease of the tension with SH0ES to the 2σ level [163].

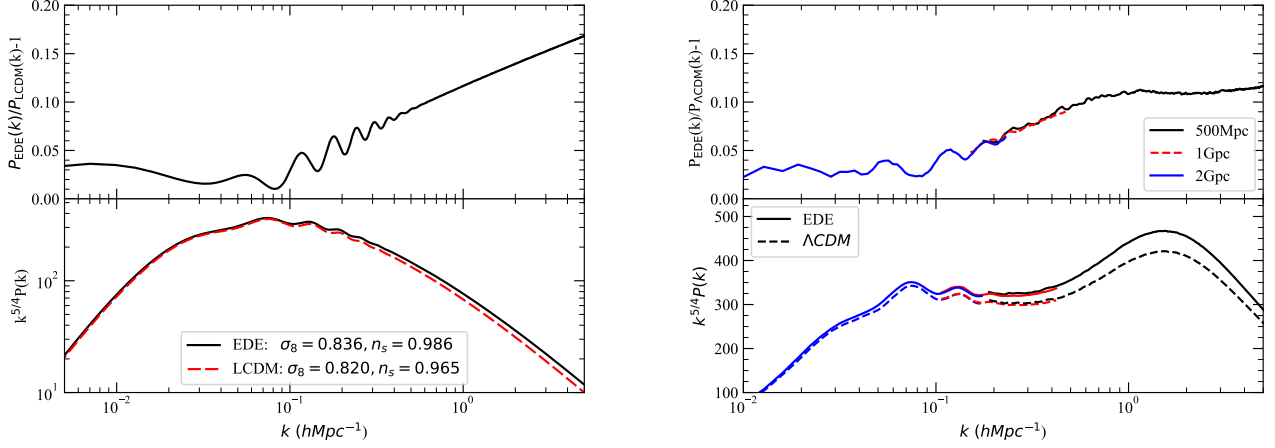


FIG. 24. The linear (left) and non linear (right) matter power spectra in an EDE cosmology and in Λ CDM. Taken from Ref. [226].

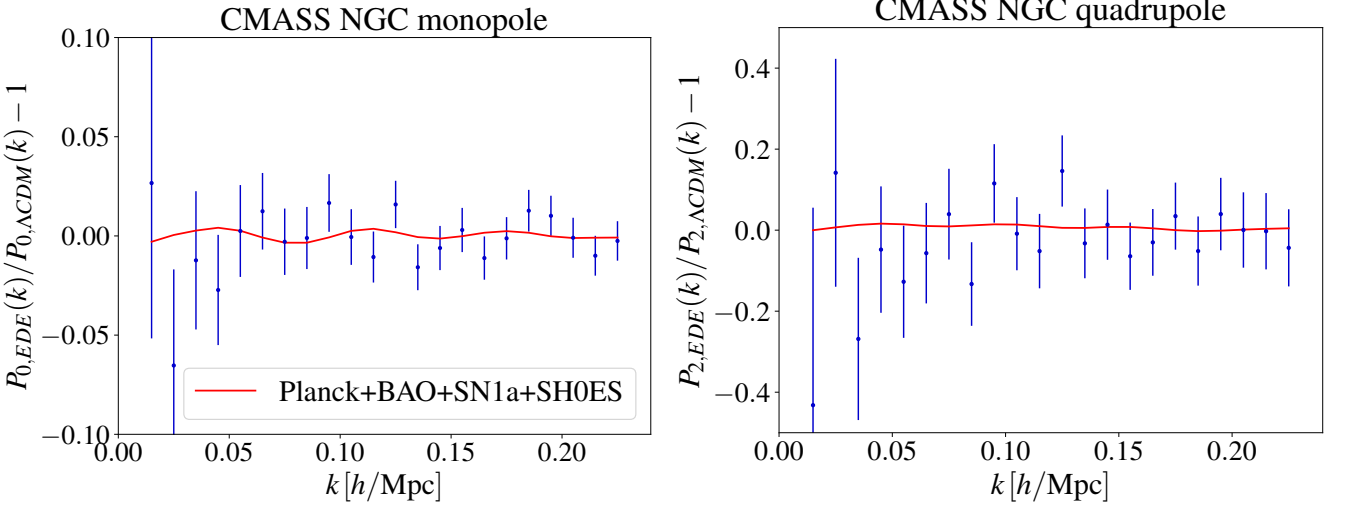


FIG. 25. Residuals of the monopole (left) and quadrupole (right) of the galaxy power spectrum calculated with the EFTofLSS between the EDE cosmology and Λ CDM.

Nevertheless, developments of the one-loop prediction of the galaxy power spectrum in redshift space from the Effective Field Theory of Large-Scale Structures²³ (EFTofLSS) [229–234] have made possible the determination of the Λ CDM parameters from the full-shape analysis of SDSS/BOSS data [235] at a precision higher than that from conventional analyses (i.e. using BAO/ $f\sigma_8$ information), and comparable to that of CMB experiments. This provides an important consistency test for the Λ CDM model, and leads to competitive constraints on models beyond Λ CDM (see e.g. Ref. [236–247]).

It has been argued that the full-shape analysis of the galaxy power spectrum of BOSS using the EFTofLSS (loosely named ‘EFTBOSS’ data) disfavors the EDE model [248, 249]. Indeed, fitting the BAO data in 2D and 3D at different comoving distances in a galaxy clustering survey (typically at $z \sim 0.1 - 1$) requires an increase in ω_{cdm} in the EDE cosmology [65, 75], which can affect the fit to the full shape [248, 249]. Thus, galaxy-clustering data offer a way to break the degeneracy introduced by EDE through the constraints they provide on ω_{cdm} and σ_8 . To gauge the constraining power of BOSS data, we show in Fig. 25 the residuals between an EDE cosmology and the Λ CDM prediction of the monopole and quadrupole of the galaxy power spectrum measured by BOSS in the north galactic cap (NGC)

²³ See also the introduction footnote in e.g. [228] for relevant related works on the EFTofLSS.

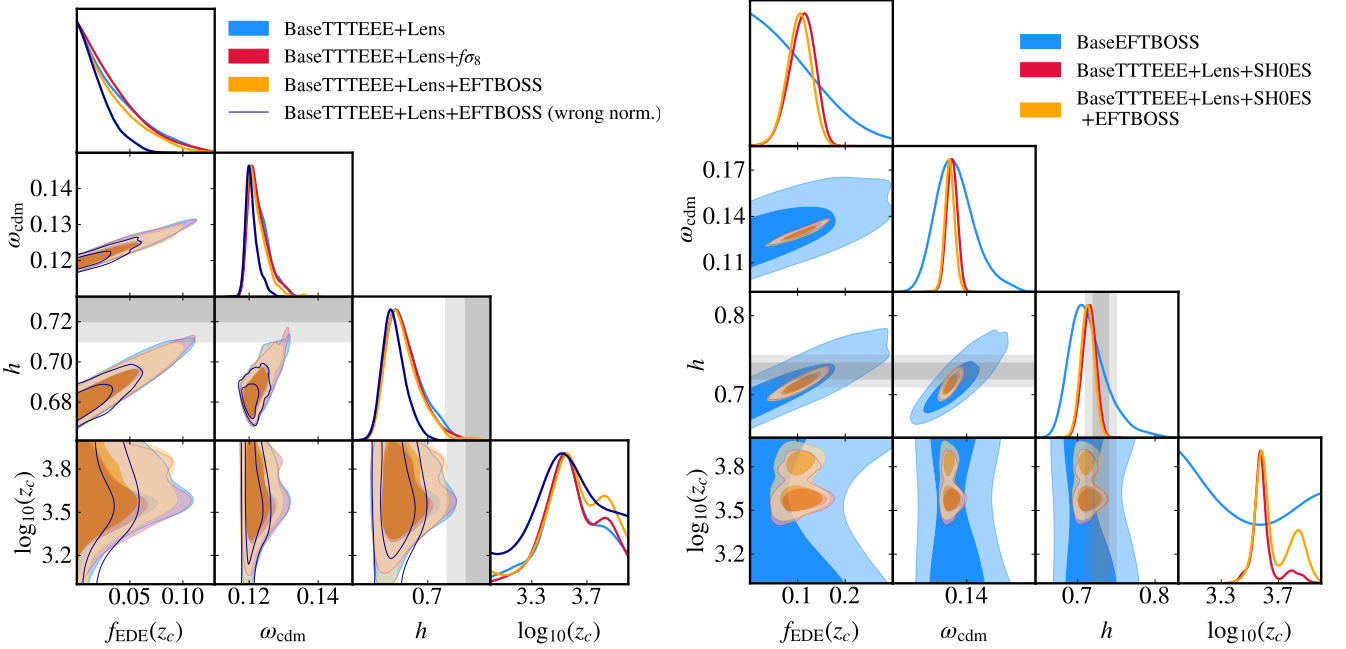


FIG. 26. *Left panel:* 2D posterior distributions from BaseTTTEEE+Lens, BaseTTTEEE+Lens+ $f\sigma_8$ and BaseTTTEEE+Lens+EFTBOSS. We also show the results from the EFTBOSS data with an incorrect normalization for comparison. *Right panel:* 2D posterior distributions from BaseEFTBOSS, and BaseTTTEEE+Lens+SH0ES, with and without EFTBOSS data. BaseTTTEEE refers to *Planck*TTTEE+BAO+Pan18, while BaseEFTBOSS refers to EFTBOSS+BBN+Lens+BAO+Pan18.

analyzed with the EFTofLSS. Here, we fix the cosmological parameters by fitting to *Planck*+BAO+Pantheon+SH0ES and then simply fit the EFT nuisance parameters to the data, to “predict” the signal to be searched for with BOSS data. One can see that the differences between EDE and Λ CDM are small compared to the data statistical errors, after marginalizing over the theoretical uncertainty, with a change in χ^2 of +1.1 in the EDE cosmology. Moreover, the p-value associated with the fit is acceptable ($\sim 16.7\%$) [163]. Yet, Refs. [248, 249] derived $f_{\text{EDE}}(z_c) < 0.08$ and $f_{\text{EDE}}(z_c) < 0.072$ respectively, with two different implementations of the EFT. The addition of S_8 measurements from KiDS/DES/HSC in Ref. [248] further tightens the constraint on $f_{\text{EDE}}(z_c) < 0.053$.

The original interpretation of the additional constraining power suggested in Refs. [248, 249] was disputed in Refs. [144, 167, 168]. As mentioned above regarding the constraints from S_8 data, the apparent constraining power from the BOSS full-shape analysis may be amplified by the impact of the prior volume artificially favoring Λ CDM in the Bayesian context. This was explicitly verified with a profile-likelihood approach [145, 167] which indicated that EDE is favored by the combination of *Planck*+BOSS at the $\sim 2\sigma$ level, with $f_{\text{EDE}}(z_c) = 0.072 \pm 0.036$ (see discussion in Sec. V D). This is similar to the value found in Refs. [144, 168] when fixing θ_i and z_c to their best-fit values. A similar argument was put forward in the case of the NEDE model, for which the inclusion of BOSS data has insignificant impact on the constraints [250].

Furthermore, Ref. [168] showed that the additional constraints from EFTBOSS come at least in part from a $\sim 20\%$ mismatch in the overall amplitude (typically parameterized by the primordial power spectrum amplitude A_s) between BOSS and *Planck*, rather than tighter constraints on ω_{cdm} . Recently, it was found that the original EFTBOSS data used in these analyses were affected by an inconsistency between the normalization of the survey window function and that of the data measurements, that led to a mismatch in A_s . Constraints obtained when combining *Planck* and EFTBOSS are shown in Fig. 26. After implementing the correction of the normalization of the window function, the combination of *Planck*TTTEEE+Lens+BAO+Pan18+EFTBOSS leads to $f_{\text{EDE}}(z_c) < 0.083$, which is a $\sim 10\%$ improvement over the constraints without BOSS data, and a $\sim 5\%$ improvement over the constraints with conventional BAO/ $f\sigma_8$ data [163]. The Hubble tension is reduced to the 2.1σ level in the EDE cosmology (1.9σ without EFTBOSS) compared to 4.8σ in the Λ CDM model, and one finds $f_{\text{EDE}}(z_c) = 0.103^{+0.027}_{-0.023}$ at $z_c = 3970^{+255}_{-205}$ when the SH0ES prior is included.

Nonetheless, EFTBOSS data can impact the recent hints of EDE observed in ACT DR4 data. Ref. [163] showed that they reduce the preference for EDE over Λ CDM seen when analyzing ACT DR4, alone or in combination with restricted *Planck* TT data. Constraints from combining ACT and EFTBOSS with *Planck* are shown in Fig. 27. The

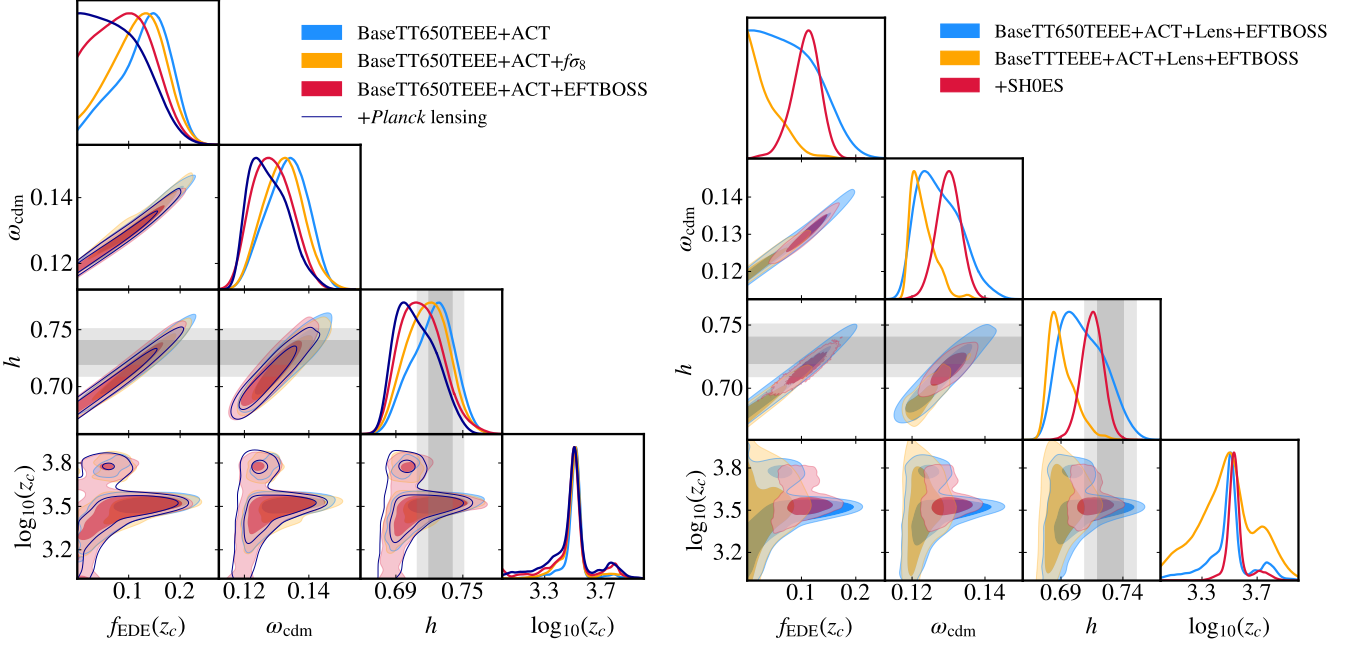


FIG. 27. *Left Panel:* 2D posterior distributions from BaseTT650TEEE+ACT in combination with $f\sigma_8$, EFTBOSS and *Planck* lensing. Note that BaseTT650TEEE refers to *Planck*TT650TEEE+BAO+Pan18 data. *Right Panel:* 2D posterior distributions from ACT+Lens+EFTBOSS in combination with either BaseTT650TEEE, or BaseTTTEEEE with and without SH0ES.

combination of *Planck*TT650TEEE+Lens+BAO+Pan18+ACT+EFTBOSS leads to a mild constraint on $f_{\text{EDE}}(z_c) < 0.172$ with $\Delta\chi^2(\text{EDE} - \Lambda\text{CDM}) = -11.1$, to be compared with $f_{\text{EDE}}(z_c) = 0.128^{+0.064}_{-0.039}$ without EFTBOSS, with $\Delta\chi^2(\text{EDE} - \Lambda\text{CDM}) = -14.6$. When full *Planck* data are included, the constraints narrow to $f_{\text{EDE}}(z_c) < 0.110$. Nevertheless, when all CMB data are included in combination with EFTBOSS, the Hubble tension is reduced to 1.5σ in the EDE model, to be compared with 4.7σ in ΛCDM . The inclusion of the SH0ES prior leads to $f_{\text{EDE}}(z_c) = 0.108^{+0.028}_{-0.021}$ at $z_c = 3565^{+220}_{-495}$. Therefore, EFTBOSS data do not rule out EDE as a resolution to the Hubble tension, although they do constrain very high EDE fractions, as seen from analyzing ACT DR4 data.

A novel way incorporating of EFTBOSS data was recently suggested in Refs. [251–253]. Their constraining power on h predominately comes from the BAO sensitivity to the sound horizon, and the same is true of measurements of the CMB. It is therefore of interest to develop new analysis methods that extract information about h from observations which are based on pre-recombination physics without relying on the value of the sound horizon. By marginalizing over the r_s -information within BOSS data and combining with constraints from light-element abundances, CMB lensing and Ω_m from the Pantheon+ Type Ia supernovae, Ref. [253] recently obtained the tight constraint $H_0 = 64.8^{+2.2}_{-2.5}\text{km s}^{-1}\text{Mpc}^{-1}$ within the ΛCDM model. As this determination does not depend on r_s , it has been suggested that it may constrain models that change the CMB prediction of H_0 by adjusting the sound horizon. In particular, any mismatch between the value of H_0 obtained from analyses that consider information from BAO, and those that marginalize over r_s would be a smoking-gun signal of the inconsistency of the model [252]. With current data however, Ref. [200] showed that the consistency tests based on comparing H_0 posteriors with and without r_s marginalization are currently inconclusive and in the r_s -marginalized analysis, EDE is not in significant tension with the SH0ES determination of H_0 . Finally, the galaxy power spectrum is not the only LSS observables affected by the presence of EDE. For instance, Ref. [226] has found that the predicted halo mass function is significantly different in the EDE model. The EDE model predicts more halos at any redshift, but the difference is small at $z = 0$, a 1 – 10% effect for very massive clusters. Interestingly, at larger redshifts, the number of halos in EDE is substantially larger than in ΛCDM . For example, the EDE model predicts about 50% more massive clusters of mass $M = (3 - 5) \times 10^{14} h^{-1} M_\odot$ at $z = 1$. Such differences will soon be tested by JWST observations [226, 254], and in fact, the first publicly available data are, in part, better fit by EDE than ΛCDM [255]. On the other hand, the recent work of Ref. [256] shows that Lyman- α data from eBOSS [257], the XQ-100 [258] and MIKE/HIRES [259] quasar samples are in tension with the EDE prediction, leading to the strongest constraints to date on f_{EDE} . In fact, even under ΛCDM , Lyman- α data favor significantly different value of the power spectrum tilt and amplitude at small scales, than reconstructed from analysis of CMB data, which (barring a simple statistical fluctuation) may indicate either a systematic effect, or some new physics is at play such as the running of the spectral tilt [260] or a new type of DM interactions [261].

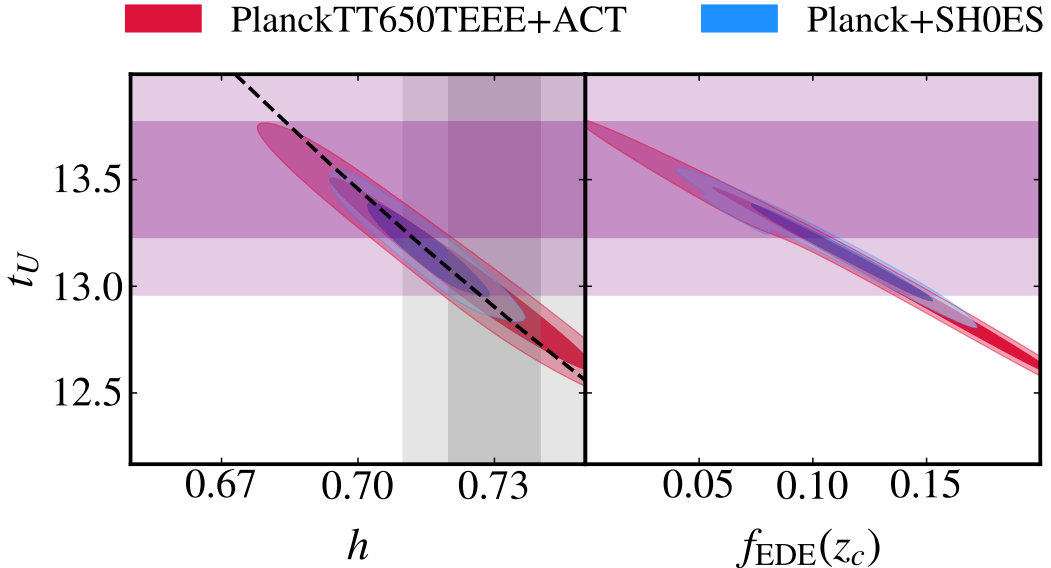


FIG. 28. The age of the universe t_U vs $\{h, f_{\text{EDE}}(z_c)\}$ in the axEDE cosmology. The purple bands mark the recent measurements from GCs, $t_U = 13.5 \pm 0.27$ Gyrs [263–265]. The dashed black line shows the prediction from Eq. 35, accounting for the small difference in Ω_m .

E. Age of the Universe tension

Another interesting consequence of the presence of Early Dark Energy in the early universe is that the age of the Universe is significantly smaller than Λ CDM. Given the definition of time t in an FLRW universe with scale factor a

$$t(a) = \int_0^a \frac{da}{aH(a)}, \quad (34)$$

one finds (assuming flat- Λ CDM and radiation is sub-dominant) that the age of the Universe today is approximately [262]

$$t_U \equiv t(a=1) \simeq t_{\text{pl}} \left(\frac{\Omega_m}{\Omega_{m,\text{pl}}} \right)^{-0.28} \left(\frac{h_{\text{pl}}}{h} \right). \quad (35)$$

As EDE reaches high H_0 without changing Ω_m significantly, one immediately sees that the higher h value measured by SH0ES leads to a universe $\sim 7.5\%$ younger than Λ CDM predicts. This is illustrated in Fig. 28.

This raises a potential issue in EDE cosmologies, and more generally, models that resolve the Hubble tension by adjusting the sound horizon, as it may lead to tensions with the measured ages of old objects such as globular clusters of stars (GCs) [262, 265, 266]. Recently, such measurements have been shown to be in slight tension with predictions from the axEDE cosmology fit to *Planck*+SH0ES, namely $t_U = 13.17^{+0.14}_{-0.16}$ Gyr [262, 265]. Here, we illustrate this potential tension in Fig. 28, for the axEDE model reconstructed from our *Planck*TT650TEEE+ACT and *Planck*+SH0ES analyses (two cosmologies for which the Hubble tension is resolved). The purple bands mark the recent measurements from GCs, $t_U = 13.5 \pm 0.27$ Gyrs [263–265] (see also Ref. [36, 38] for a discussion of other measurements). One can see that while the predicted age of the Universe is systematically lower than that measured from GCs, the differences are not yet statistically significant. The dashed black line shows the prediction from Eq. 35, accounting for the small difference in Ω_m . Any model that only modifies the early universe would follow a similar degeneracy line, and therefore can be tested with more accurate measurements of t_U .

Similar considerations apply to cosmic chronometers (e.g. Ref. [36, 267]) which are currently too imprecise to probe the EDE scenarios [69], but could provide interesting tests in the future. In fact, Eq. 34 indicates that the entire time-redshift relation is affected by the EDE model. Ref. [262] points out that it differs from the base Λ CDM model by at least $\sim 4\%$ at all z and t , and therefore this difference represents an important theoretical uncertainty on the connection between z and t . This can have significant implications for the era of reionization, that occurs at different times in the EDE and Λ CDM cosmologies. As a result, given the formation time of a typical globular cluster, such

objects may form *before* (in the EDE cosmology) or *after* (in Λ CDM) reionization. Yet, current uncertainties on the ages of such objects are too large to unambiguously constrain EDE. Given the constraints on Ω_m from BAO and Pantheon data, this potential issue in the EDE cosmology is very generic to models resolving the Hubble tension solely by modifying the pre-recombination era [265], and may indicate modifications the late-universe dynamics to fully restore cosmic concordance. Ref. [265] in fact proposes the use of ternary plots to simultaneously visualize independent constraints on key quantities related to H_0 like t_U , r_s , and Ω_m . These quantities representing an over-constrained problem can be used as a diagnostic tool of consistency, and help find solutions to the H_0 tension. For further discussion about the age of the Universe tension and future prospects, we refer to Refs. [262, 264–266].

F. An extended EDE model to restore cosmic concordance

The fact that EDE models cannot explain the low-value of S_8 (and even slightly worsen the tension) is often presented as a major argument against the existence of an EDE-like component in the pre-recombination era. Given that both the Λ CDM cosmology and the EDE cosmology are in tension with S_8 measurements, it is nevertheless reasonable to ask whether there exist EDE extensions that would help in accommodating the low S_8 value. In fact, as discussed in this review, it is striking that at fixed ω_{cdm} , the EDE leads to a decrease in power at small scales that seemingly goes in the right direction to resolve the S_8 tension. The problem arises from the EDE- ω_{cdm} degeneracy that counteracts the effect of the EDE on the gravitational potential wells as seen in the CMB. It is hence possible that a simple extension of the EDE model would mitigate the need for an increase in the CDM density, or alternatively compensate the associated increase in the amplitude of fluctuations.

One of the least ‘theoretically costly’ explanations of the S_8 tension is to invoke massive neutrinos that already lead to a power suppression at small scales which decreases the value of σ_8 . Unfortunately, in practice, the sum of neutrino masses $\sum m_\nu \sim 0.3\text{eV}$ required to resolve the tension is excluded by *Planck* data (e.g. [4, 268]). Moreover, neither DES nor KiDS prefer a non-zero $\sum m_\nu$ [220, 221]. However, constraints on the sum of neutrino masses are substantially broadened in extended cosmologies (e.g. [269, 270]). In the context of EDE, simply adding the neutrino mass as free parameter in an analysis of the EDE model does not change the reconstructed value of S_8 [144, 271]. Adding more complexity, Ref. [80] suggested that the non-relativistic transition of neutrinos could trigger a phase-transition in EDE. Further exploration of any possible connections between EDE and neutrino masses would be interesting.

Another proposal showed that the existence of a dark sector, where DM is composed of $\sim 5\%$ ultra-light axions (ULAs), can help in relieving the S_8 tension without affecting the success of the EDE solution in explaining a high- H_0 [225]. Such a dark sector could be the manifestation of the presence of numerous scalar-fields that are ubiquitous in string theory [207, 272]. Ref. [224] obtained a similar result considering a decaying DM model instead of the ULA component. While these models may seem ‘ad-hoc’, and disfavored from the ‘Occam’s razor’ point-of-view, they demonstrate that H_0 and S_8 solutions can come from different (potentially disconnected) sectors, and therefore that one should not dismiss EDE models on the basis that they cannot simultaneously explain both tensions.

Nevertheless, there exist attempts of connecting S_8 and H_0 resolutions within the same theoretical models. For instance, Ref. [95] points out that the Swampland Distance Conjecture (SDC) implies that the near-Planckian scalar-field excursion required in axion-like EDE models would lead to an exponential sensitivity of the mass m_{DM} of DM, if DM is composed of a scalar-field, $m_{\text{DM}}(\phi) = m_0 \exp(c\phi/M_{\text{Pl}})$ where c is a free parameter. Authors argue that this additional time-dependent mass manifests as an EDE-induced “fifth force” that has the potential of reducing the growth of structure and relieving the tension with LSS data. A similar model was discussed for EDE and AdS-EDE in Ref. [96] and a chameleon-inspired EDE in Ref. [94].

Another EDE-like model designed to resolve both tensions is presented in Ref. [97]. In this string-theory-inspired model, an axion, playing the role of the EDE field, is kinetically coupled to a dilaton field, which syphons off energy density as the axion falls down its potential, allowing it to redshift faster. The introduction of the kinetically-coupled dilaton field allows the use of a standard axion potential for solving the Hubble tension. In addition, the axion with mass $\mathcal{O}(10^{-27})\text{ eV}$ contributes a small fraction ($\sim 1\%$) to dark matter post-recombination, and naturally suppresses power on scales sensitive to σ_8 .

Finally, we mention Ref. [90], where authors studied EDE solutions to both tensions in the generalized Dark Matter (GDM) framework covers more general microphysical descriptions of the EDE component than the simple scalar-field picture described thus far. Interestingly, they found that EDE with an anisotropic sound speed can soften both the H_0 and S_8 tensions while still providing a quality fit to CMB data. Such models will be distinguishable from standard scalar-field EDE with future CMB-S4 data.

The existence of several models based on EDE dynamics that can alleviate both tensions demonstrate that, with current data, one should not dismiss the EDE resolutions of the Hubble tension on the basis that it does not simultaneously address the S_8 tension. Nevertheless, it is clear that there are irreducible features that are signs of an EDE-like component acting pre-recombination, and future CMB and LSS data will be pivotal in settling the fate of

the EDE resolution to the Hubble tension.

VIII. CONCLUSIONS

Early Dark Energy remains one of the most effective models at resolving the Hubble tension [69], the discrepancy between direct and indirect estimates of the Hubble constant, and as such has received a lot of attention in the recent literature. In this review, we present the status of this solution, describing both the qualitative requirement that a successful EDE model must have, and the quantitative results obtained for various EDE models that have been studied so far (described in Sec. III). In a nutshell, EDE refers to an additional component of dark energy active at early times (typically manifested by a scalar-field) that quickly dilutes away at a redshift close to that of matter-radiation equality. The role of EDE is to decrease the sound horizon by briefly contributing to the Hubble rate in the pre-recombination era. Different models (and different perturbation dynamics) of EDE lead to subtle signatures in the CMB and matter power spectra beyond this simple background description. Further details of the phenomenological effects of EDE are presented in Sec. IV.

We summarize the results of analyses of several EDE models in light of a combination of cosmological data that includes *Planck* data (2015 or 2018), BOSS BAO DR12, Pantheon and SH0ES in Fig. 18 and expound on these in Sec. V. EDE models are typically able to reduce the Hubble tension to below the 2σ level, although not all models achieve the same level of success. In fact, while all models behave similarly at the background level, data favor very specific dynamics for their perturbations, which can differentiate various models. For instance, scalar-field power-law potentials are disfavored over potentials that flatten around the initial field value, such as the modified cosine potential in axion-like models. Introducing a non-minimal coupling to the Ricci scalar also improves the results of the quartic potential.

Despite these successes, Bayesian analyses of the EDE models in light of *Planck* data do not indicate a preference for EDE in the absence of information from SH0ES on H_0 . On the other hand, likelihood-profile analyses show a $\sim 2\sigma$ preference for EDE from *Planck* data alone. This illustrates the impact of prior-volume effects inherent to the Bayesian framework, pivotal in disfavoring EDE models, and therefore cautions against naively interpreting results of Bayesian analyses. Such differences between the Bayesian and Frequentist approaches are likely tied to the fairly low constraining power of current data on EDE models, and we anticipate that if the preference for (or against) EDE becomes stronger with higher precision data, both frameworks would provide similar results.

In Sec. VI, we reviewed the recent hints of EDE in ACT data, alone or in combination with restricted *Planck* TT data, with H_0 values that are in good agreement with the SH0ES determination. Although supported by *Planck* polarization data, which also weakly favor the EDE model on their own, the addition of *Planck* high- ℓ temperature data removes the preference for EDE, raising the question of a potential (mild) inconsistency between ACT and *Planck* high- ℓ TT data. Future ACT and SPT data²⁴, expected next year, will be crucial to confirm or exclude the current hints of EDE. Looking forward, it is expected that high-accuracy measurements at high- ℓ 's ($\gtrsim 1000$) will be sensitive to the characteristic increase of power induced by the EDE cosmology (mostly due to the reshuffling of Λ CDM parameters as a consequence of the presence of EDE), while improvements at intermediate ℓ 's ($\sim 50 - 500$) can help probe the details of the EDE perturbative dynamics.

If EDE is responsible for the current Hubble tension, Fig. 18 illustrates that one generically expects a higher DM density ω_{cdm} and primordial tilt n_s . These shifts in parameters have important consequences on the growth of structure at late times, and lead to a very different matter power spectrum (at the 5–10% level in the range $k \sim 0.01 - 1 \text{ h/Mpc}$) than predicted in Λ CDM, which can be used to further probe the model (see Secs. VII C and VII D). In fact, EDE cosmologies predict a slightly larger S_8 parameter than Λ CDM, which is at odds with recent measurements from weak-lensing surveys. We have presented constraints from galaxy weak-lensing and clustering surveys such as KiDS, DES and BOSS on the EDE scenarios, concluding that current surveys generally do not exclude the EDE resolution to the Hubble tension (although they can constrain large EDE contributions), and that current models of EDE cannot explain a low- S_8 . Future constraints with DESI and subsequent surveys will be crucial to test EDE models further. In addition, the existence of an EDE phase may have important consequences for inflation, as the value of n_s reconstructed in EDE models that resolve the Hubble tension favor curvaton models over Starobinsky inflation [189, 190]. There are additional questions associated with EDE cosmologies described in Sec. VII, including a second ‘cosmic coincidence’ problem in the EDE cosmology, a potential ‘age of the Universe’ tension and whether additional dynamics on top of the EDE can explain both the H_0 and S_8 tensions.

With this review, we argue that EDE is a promising mechanism to resolve the H_0 tension, with consequences for a wide variety of observables that will be firmly tested with next-generation surveys. Yet, it is clear that this cannot be

²⁴ As this review was nearing completion, new results by the SPT collaboration have been released [196]. Dedicated analyses of EDE models in light of these data are however still lacking.

'the end of the story' at least in its current form, for various observational and theoretical reasons. Indeed, connections between inflation, late DE and early DE are still largely unexplored, and may provide an interesting path forward for model-building with undetermined consequences for EDE models. Nevertheless, further work is required to find a common solution to recent cosmic tensions, that may or may not be based on some aspects presented in this review, and that will hopefully shed new light on the yet unknown fundamental nature of dark matter and dark energy.

ACKNOWLEDGMENTS

We thank Théo Simon for providing us with the residuals of the galaxy power spectrum calculated with the EFTofLSS between the EDE cosmology and Λ CDM and Alexa Bartlett and Yashvi Patel for computing the EDE profile likelihood. We thank Kim Berghaus, Eoin Colgáin, Francis-Yan Cyr-Racine, Fabio Finelli, Laura Herold, Emil Brinch Holm, Meng-Xiang Lin, Evan McDonough, Florian Niedermann, Yun-Son Piao, Adam Riess, Jeremy Sakstein, Martin Sloth, Mark Trodden for useful comments on the draft. This article is based upon work from COST Action CA21136 Addressing observational tensions in cosmology with systematics and fundamental physics (CosmoVerse) supported by COST (European Cooperation in Science and Technology). This project has received funding from the European Research Council (ERC) under the European Union's HORIZON-ERC-2022 (Grant agreement No. 101076865). This work used the Strelka Computing Cluster, which is run by Swarthmore College. TLS is supported by NSF Grant No. 2009377 and the Research Corporation. TK is supported by NASA ATP Grant 80NSSC18K0694 and by funds provided by the Center for Particle Cosmology at the University of Pennsylvania.

Appendix A: Appendix: Impact of f_{EDE} , a_c and w_f on the power spectra

In this section, we discuss the impacts of varying f_{EDE} , a_c and w_f on the CMB power spectra. We show relative differences with respect to Λ CDM keeping $\{\omega_{\text{cdm}}, \omega_b, A_s, n_s, \tau_{\text{reio}}\}$ fixed for all curves. Finally, we fix either h to emphasize the dominant background effects of EDE (left panels) or fix θ_s to show the role of perturbations (right panels). We refer to the text under Sec. IV for a detailed discussion on the role of the sound speed c_s^2 .

1. Impact of f_{EDE}

Increasing f_{EDE} at fixed $\log_{10}(z_c) = 3.5$ and $w_f = 1/2$ amounts to changing *how much* the EDE contributes to $H(z)$ and therefore the amplitude of the reduction of the sound horizon and damping scale. This leads to enhanced oscillations in the residuals shown in Fig. 29, left panel, and more power in the damping tail. In addition, the EDE contributes more significantly to the acoustic driving of CMB perturbations, and affects the amplitude of the SW term, while leading to a larger residual time-evolution of the gravitational potentials, which affects the amplitude of the eISW term (at $\ell \sim 100$). The latter effects are more clearly visible on the right panel. In the matter and lensing power spectra, we see the effect of a larger Hubble friction that damps matter perturbations, and leads to a suppression at scales that enter or are within the horizon at a_c . Note that, once h is adjusted to fix θ_s (right panel), the small- k branch is largely increased due to the larger $\Omega_m = \omega_{\text{cdm}}/h^2$.

2. Impact of z_c

Increasing $\log_{10}(z_c)$ at fixed $f_{\text{EDE}} = 0.1$ and $w_f = 1/2$ amounts to changing *when* the EDE contributes to $H(z)$. This affects the ability of EDE to reduce the sound horizon and damping scale. For $\log_{10}(z_c) = 4$, one can notice the absence of a shift in the damping tail (left panel). The impact of EDE is mostly visible on the acoustic driving of CMB perturbations, and therefore on the amplitude of the SW term (right panel). For $\log_{10}(z_c) = 3$ on the other hand, EDE does not strongly affect CMB acoustic driving since the universe is essentially matter dominated at that time. The effect is therefore dominated by the background impact of the sound horizon and damping scale. Pushing z_c to much larger values would lead to EDE impacting smaller and smaller scales. Considering much smaller z_c , for which the EDE contributes only in the post-recombination era, would affect the angular diameter distance to recombination, and lead to additional decay of the gravitational potential and an ISW effect, similar to the effect of Dark Energy at late-times.

In the matter and lensing power spectra, the dominant effect is an overall shift of the power suppression, centered around $k_c = H(z_c)/(1 + z_c)$. The amplitude of the suppression is also mildly affected, as the EDE contribution before matter-domination leads to shallower suppression at late times. Note also that when fixing θ_s , the model with

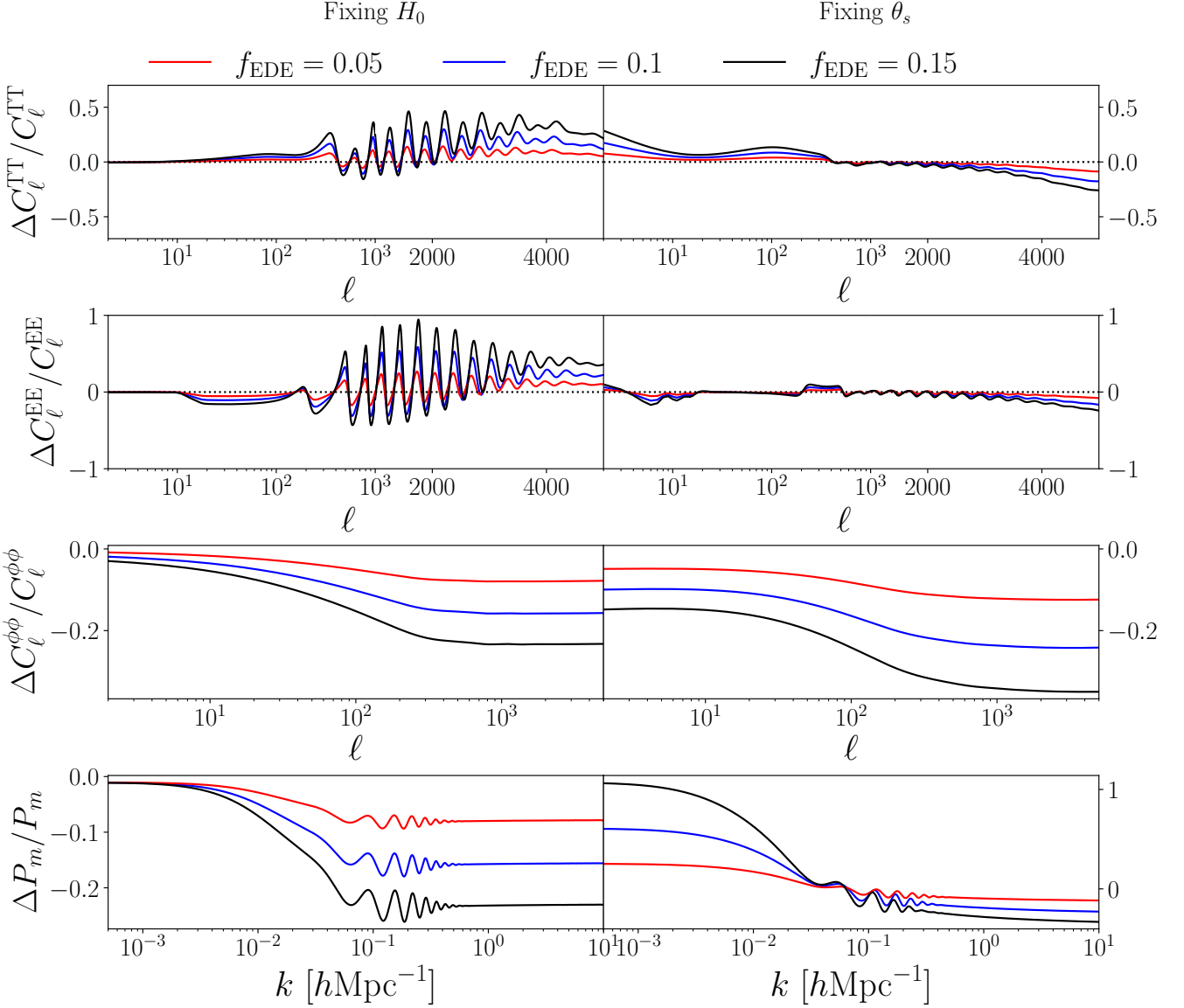


FIG. 29. Impact of changing f_{EDE} at fixed $\log_{10}(z_c) = 3.5$ and $w_f = 1/2$ on the CMB and matter power spectra. We show relative differences with respect to ΛCDM and choose to keep $\{\omega_{\text{cdm}}, \omega_b, A_s, n_s, \tau_{\text{reio}}\}$ fixed along with either h (left panels) or θ_s (right panels) in all models. Note that the y -axis ranges are common across rows for all but the last $\Delta P_m/P_m$ panels that have different ranges as indicated.

$\log_{10}(z_c) = 3$ shows a higher amplitude than when keeping h fixed, compared to other models. This is due to the fact that EDE contributes more here than in other models in the post recombination universe, affecting the angular diameter distance, and limiting the required change in h and therefore Ω_m which scales the overall amplitude of the spectrum [192].

3. Impact of w_f

The impact of changing w_f at fixed $f_{\text{EDE}} = 0.1$ and $\log_{10}(z_c) = 3.5$ is more subtle as it amounts to changing *how long* EDE contributes, and leads to effects that are a combination of those induced by changing f_{EDE} or $\log_{10}(a_c)$. Larger w_f means faster EDE dilution and smaller cumulative contribution to $H(z)$. The dominant effect on the TT and EE spectra is similar to the effect of larger f_{EDE} , namely an overall shift of the peak and more power on small scales, due to a smaller sound horizon and damping scale induced by the larger EDE contribution. However, one

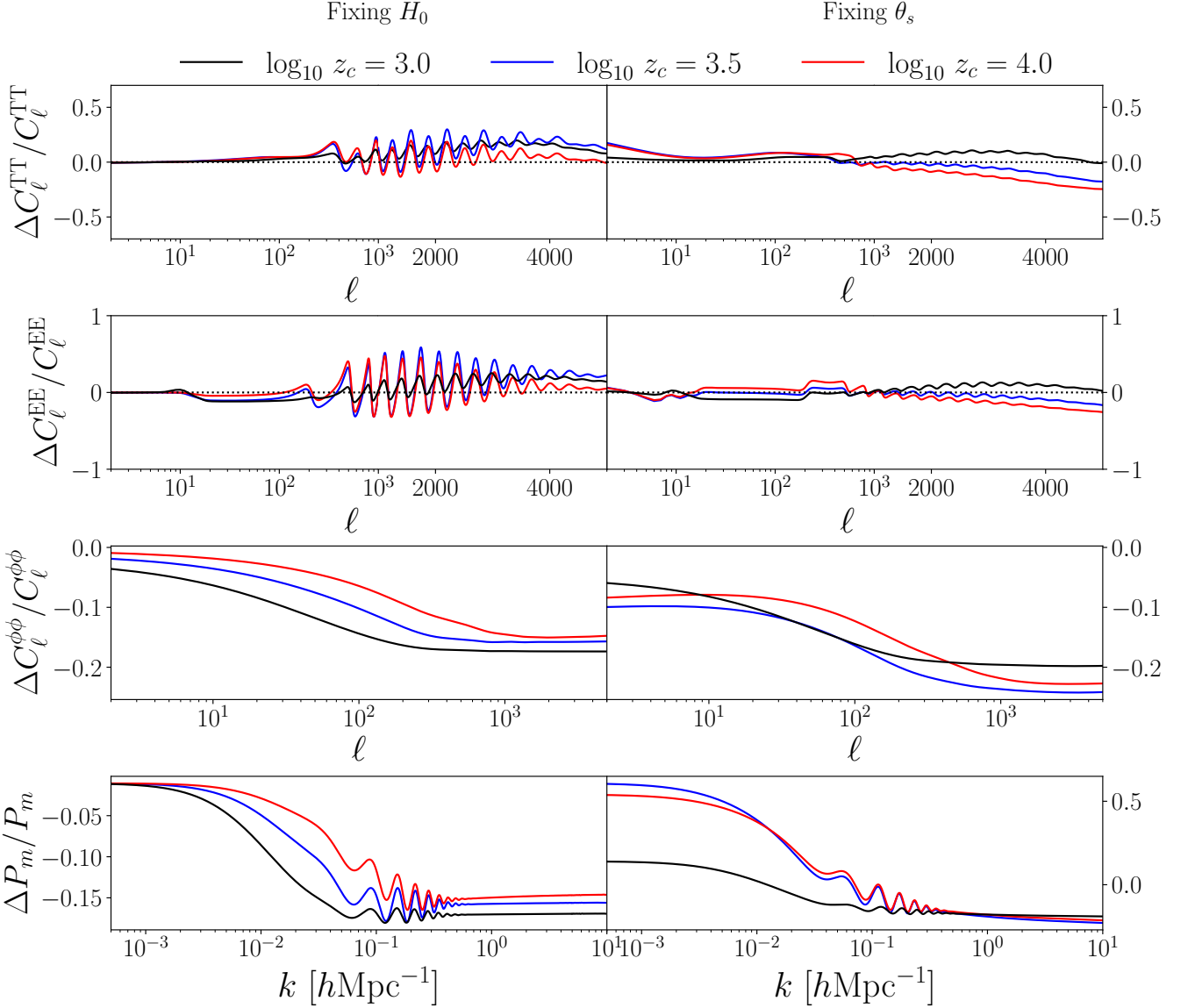


FIG. 30. Same as Fig. 29 but now changing $\log_{10}(z_c)$ at fixed $f_{\text{EDE}} = 0.1$ and $w_f = 1/2$.

can see in the matter and lensing power spectra, that both the amplitude and the shape of the power suppression is affected: at fixed h (left panel), a smaller w_f means both that modes are affected longer (larger suppression), and that more modes can be affected (shift the suppression towards larger scales). Once θ_s is adjusted (right panel), the change in h , and therefore Ω_m , can partly compensate these effects, and even overcome them at large scales.

There are additional subtle effects induced at the level of EDE perturbations, whose growth on super-horizon scales is controlled by w_f , that lead to a correlation with c_s^2 in the data analysis. These are described in more detail in Sec. IV.

-
- [1] Michael S. Turner, “The Road to Precision Cosmology,” (2022), 10.1146/annurev-nucl-111119-041046, arXiv:2201.04741 [astro-ph.CO].
 - [2] Elcio Abdalla et al., “Cosmology intertwined: A review of the particle physics, astrophysics, and cosmology associated with the cosmological tensions and anomalies,” JHEAp **34**, 49–211 (2022), arXiv:2203.06142 [astro-ph.CO].
 - [3] Kenneth C. Wong et al., “H0LiCOW – XIII. A 2.4 per cent measurement of H0 from lensed quasars: 5.3σ tension between early- and late-Universe probes,” Mon. Not. Roy. Astron. Soc. **498**, 1420–1439 (2020), arXiv:1907.04869 [astro-ph.CO].

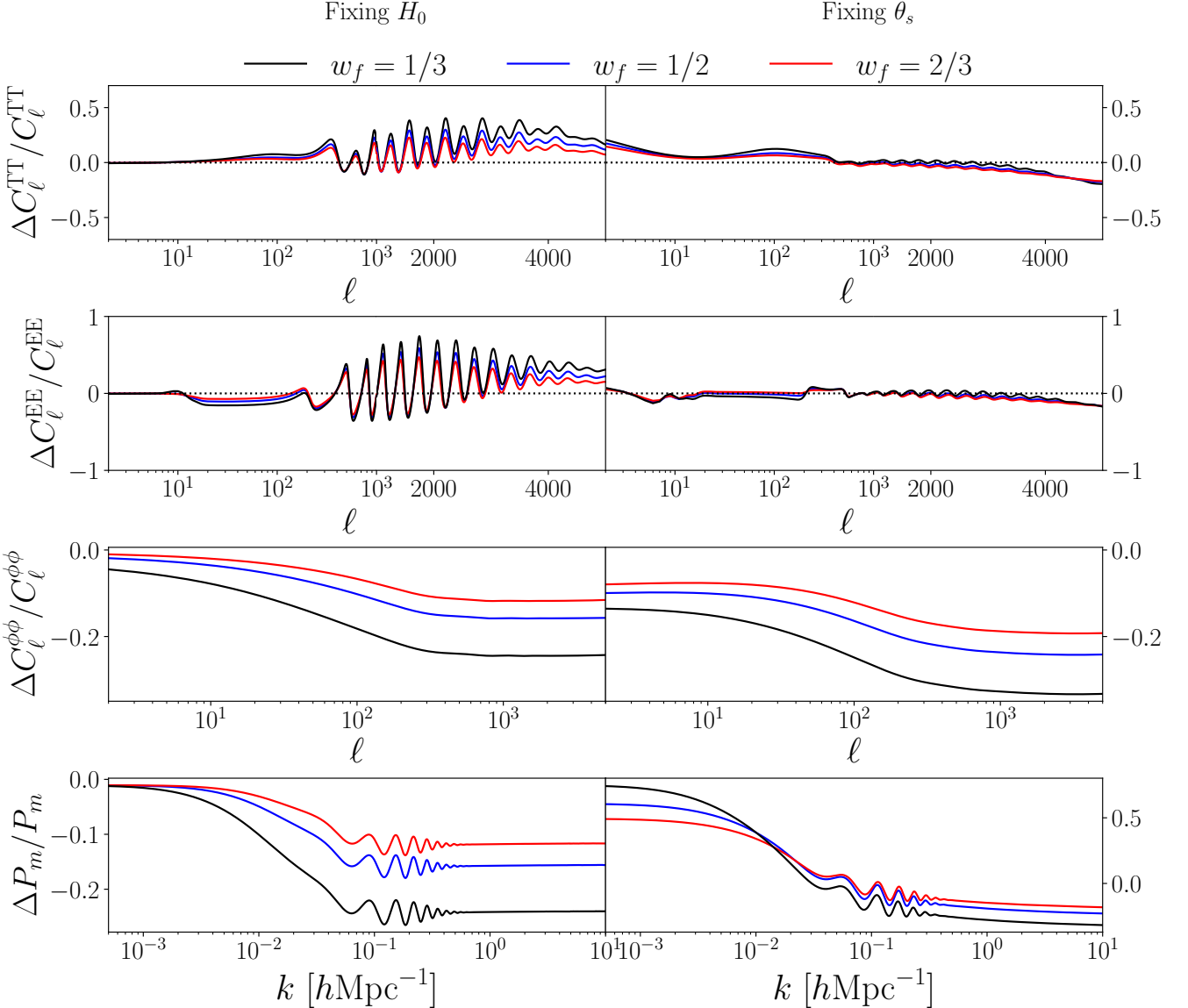


FIG. 31. Same as Fig. 29 but now changing w_f at fixed $f_{\text{EDE}} = 0.1$ and $\log_{10}(z_c) = 3.5$.

- [4] N. Aghanim et al. (Planck), “Planck 2018 results. VI. Cosmological parameters,” *Astron. Astrophys.* **641**, A6 (2020), [Erratum: *Astron. Astrophys.* 652, C4 (2021)], arXiv:1807.06209 [astro-ph.CO].
- [5] Adam G. Riess et al., “A Comprehensive Measurement of the Local Value of the Hubble Constant with 1 km/s/Mpc Uncertainty from the Hubble Space Telescope and the SH0ES Team,” (2021), arXiv:2112.04510 [astro-ph.CO].
- [6] M. Rigault et al., “Confirmation of a Star Formation Bias in Type Ia Supernova Distances and its Effect on Measurement of the Hubble Constant,” *Astrophys. J.* **802**, 20 (2015), arXiv:1412.6501.
- [7] M. Rigault et al. (Nearby Supernova Factory), “Strong Dependence of Type Ia Supernova Standardization on the Local Specific Star Formation Rate,” *Astron. Astrophys.* **644**, A176 (2020), arXiv:1806.03849 [astro-ph.CO].
- [8] G. E. Addison, D. J. Watts, C. L. Bennett, M. Halpern, G. Hinshaw, and J. L. Weiland, “Elucidating Λ CDM: Impact of Baryon Acoustic Oscillation Measurements on the Hubble Constant Discrepancy,” *Astrophys. J.* **853**, 119 (2018), arXiv:1707.06547.
- [9] Christopher R. Burns et al. (CSP), “The Carnegie Supernova Project: Absolute Calibration and the Hubble Constant,” *Astrophys. J.* **869**, 56 (2018), arXiv:1809.06381 [astro-ph.CO].
- [10] D. O. Jones et al., “Should Type Ia Supernova Distances be Corrected for their Local Environments?” *Astrophys. J.* **867**, 108 (2018), arXiv:1805.05911 [astro-ph.CO].
- [11] G. Efstathiou, “A Lockdown Perspective on the Hubble Tension (with comments from the SH0ES team),” arXiv e-prints , arXiv:2007.10716 (2020), arXiv:2007.10716 [astro-ph.CO].

- [12] Dillon Brout and Daniel Scolnic, “It’s Dust: Solving the Mysteries of the Intrinsic Scatter and Host-galaxy Dependence of Standardized Type Ia Supernova Brightnesses,” *Astrophys. J.* **909**, 26 (2021), arXiv:2004.10206 [astro-ph.CO].
- [13] Edvard Mortsell, Ariel Goobar, Joel Johansson, and Suhail Dhawan, “Sensitivity of the Hubble Constant Determination to Cepheid Calibration,” *Astrophys. J.* **933**, 212 (2022), arXiv:2105.11461 [astro-ph.CO].
- [14] Edvard Mortsell, Ariel Goobar, Joel Johansson, and Suhail Dhawan, “The Hubble Tension Revisited: Additional Local Distance Ladder Uncertainties,” *Astrophys. J.* **935**, 58 (2022), arXiv:2106.09400 [astro-ph.CO].
- [15] Wendy L. Freedman, “Measurements of the Hubble Constant: Tensions in Perspective,” arXiv e-prints , arXiv:2106.15656 (2021), arXiv:2106.15656.
- [16] Peter Garnavich, Charlotte M. Wood, Peter Milne, Joseph B. Jensen, John P. Blakeslee, Peter J. Brown, Daniel Scolnic, Benjamin Rose, and Dillon Brout, “Connecting Infrared Surface Brightness Fluctuation Distances to Type Ia Supernova Hosts: Testing the Top Rung of the Distance Ladder,” (2022), arXiv:2204.12060 [astro-ph.CO].
- [17] W. D’Arcy Kenworthy, Adam G. Riess, Daniel Scolnic, Wenlong Yuan, José Luis Bernal, Dillon Brout, Stefano Casertano, David O. Jones, Lucas Macri, and Erik R. Peterson, “Measurements of the Hubble Constant with a Two-rung Distance Ladder: Two Out of Three Ain’t Bad,” *Astrophys. J.* **935**, 83 (2022), arXiv:2204.10866 [astro-ph.CO].
- [18] Adam G. Riess, Louise Breuval, Wenlong Yuan, Stefano Casertano, Lucas M. Macri, J. Bradley Bowers, Dan Scolnic, Tristan Cantat-Gaudin, Richard I. Anderson, and Mauricio Cruz Reyes, “Cluster Cepheids with High Precision Gaia Parallaxes, Low Zero-point Uncertainties, and Hubble Space Telescope Photometry,” *Astrophys. J.* **938**, 36 (2022), arXiv:2208.01045 [astro-ph.CO].
- [19] Stephen M. Feeney, Daniel J. Mortlock, and Niccolò Dalmasso, “Clarifying the Hubble constant tension with a Bayesian hierarchical model of the local distance ladder,” *Mon. Not. Roy. Astron. Soc.* **476**, 3861–3882 (2018), arXiv:1707.00007 [astro-ph.CO].
- [20] Louise Breuval et al., “The Milky Way Cepheid Leavitt law based on Gaia DR2 parallaxes of companion stars and host open cluster populations,” *Astron. Astrophys.* **643**, A115 (2020), arXiv:2006.08763 [astro-ph.SR].
- [21] Behnam Javanmardi, Antoine Merand, Pierre Kervella, Louise Breuval, Alexandre Gallenne, Nicolas Nardetto, Wolfgang Gieren, Grzegorz Pietrzynski, Vincent Hocde, and Simon Borgniet, “Inspecting the Cepheid Distance Ladder: the Hubble Space Telescope Distance to the SN Ia Host Galaxy NGC 5584,” *Astrophys. J.* **911**, 12 (2021), arXiv:2102.12489 [astro-ph.GA].
- [22] Radosław Wojtak and Jens Hjorth, “Intrinsic tension in the supernova sector of the local Hubble constant measurement and its implications,” *Mon. Not. Roy. Astron. Soc.* **515**, 2790–2799 (2022), arXiv:2206.08160 [astro-ph.CO].
- [23] Eleonora Di Valentino, Olga Mena, Supriya Pan, Luca Visinelli, Weiqiang Yang, Alessandro Melchiorri, David F. Mota, Adam G. Riess, and Joseph Silk, “In the realm of the Hubble tension—a review of solutions,” *Class. Quant. Grav.* **38**, 153001 (2021), arXiv:2103.01183 [astro-ph.CO].
- [24] L. Verde, T. Treu, and A. G. Riess, “Tensions between the Early and the Late Universe,” *Nature Astron.* **3**, 891 (2019), arXiv:1907.10625 [astro-ph.CO].
- [25] Nils Schöneberg, Julien Lesgourges, and Deanna C. Hooper, “The BAO+BBN take on the Hubble tension,” *JCAP* **10**, 029 (2019), arXiv:1907.11594 [astro-ph.CO].
- [26] Wendy L. Freedman, Barry F. Madore, Dylan Hatt, Taylor J. Hoyt, In Sung Jang, Rachael L. Beaton, Christopher R. Burns, Myung Gyoon Lee, Andrew J. Monson, Jillian R. Neeley, M. M. Phillips, Jeffrey A. Rich, and Mark Seibert, “The Carnegie-Chicago Hubble Program. VIII. An Independent Determination of the Hubble Constant Based on the Tip of the Red Giant Branch,” *Astrophys. J.* **882**, 34 (2019), arXiv:1907.05922 [astro-ph.CO].
- [27] Gagandeep S. Anand, R. Brent Tully, Luca Rizzi, Adam G. Riess, and Wenlong Yuan, “Comparing Tip of the Red Giant Branch Distance Scales: An Independent Reduction of the Carnegie-Chicago Hubble Program and the Value of the Hubble Constant,” *Astrophys. J.* **932**, 15 (2022), arXiv:2108.00007 [astro-ph.CO].
- [28] Wenlong Yuan, Adam G. Riess, Lucas M. Macri, Stefano Casertano, and Dan Scolnic, “Consistent Calibration of the Tip of the Red Giant Branch in the Large Magellanic Cloud on the Hubble Space Telescope Photometric System and Implications for the Determination of the Hubble Constant,” (2019), arXiv:1908.00993 [astro-ph.GA].
- [29] John Soltis, Stefano Casertano, and Adam G. Riess, “The Parallax of ω Centauri Measured from Gaia EDR3 and a Direct, Geometric Calibration of the Tip of the Red Giant Branch and the Hubble Constant,” *Astrophys. J. Lett.* **908**, L5 (2021), arXiv:2012.09196 [astro-ph.GA].
- [30] Nandita Khetan et al., “A new measurement of the Hubble constant using Type Ia supernovae calibrated with surface brightness fluctuations,” *Astron. Astrophys.* **647**, A72 (2021), arXiv:2008.07754 [astro-ph.CO].
- [31] Caroline D. Huang, Adam G. Riess, Wenlong Yuan, Lucas M. Macri, Nadia L. Zakamska, Stefano Casertano, Patricia A. Whitelock, Samantha L. Hoffmann, Alexei V. Filippenko, and Daniel Scolnic, “Hubble Space Telescope Observations of Mira Variables in the SN Ia Host NGC 1559: An Alternative Candle to Measure the Hubble Constant,” *Astrophys. J.* **889**, 5 (2020).
- [32] James Schombert, Stacy McGaugh, and Federico Lelli, “Using the Baryonic Tully-Fisher Relation to Measure H_0 ,” *Astrophysical Journal* **160**, 71 (2020), arXiv:2006.08615 [astro-ph.CO].
- [33] S. Birrer et al., “TDCOSMO - IV. Hierarchical time-delay cosmography – joint inference of the Hubble constant and galaxy density profiles,” *Astron. Astrophys.* **643**, A165 (2020), arXiv:2007.02941 [astro-ph.CO].
- [34] Anowar J. Shajib et al., “TDCOSMO. XIII. Improved Hubble constant measurement from lensing time delays using spatially resolved stellar kinematics of the lens galaxy,” (2023), arXiv:2301.02656 [astro-ph.CO].
- [35] D. W. Pesce et al., “The Megamaser Cosmology Project. XIII. Combined Hubble constant constraints,” *Astrophys. J. Lett.* **891**, L1 (2020), arXiv:2001.09213 [astro-ph.CO].
- [36] Michele Moresco et al., “Unveiling the Universe with emerging cosmological probes,” *Living Rev. Rel.* **25**, 6 (2022),

- arXiv:2201.07241 [astro-ph.CO].
- [37] Raul Jimenez, Andrea Cimatti, Licia Verde, Michele Moresco, and Benjamin Wandelt, “The local and distant Universe: stellar ages and H_0 ,” *JCAP* **03**, 043 (2019), arXiv:1902.07081 [astro-ph.CO].
- [38] Andrea Cimatti and Michele Moresco, “Revisiting oldest stars as cosmological probes: new constraints on the Hubble constant,” (2023), arXiv:2302.07899 [astro-ph.CO].
- [39] B. P. Abbott et al. (LIGO Scientific, Virgo), “A Gravitational-wave Measurement of the Hubble Constant Following the Second Observing Run of Advanced LIGO and Virgo,” *Astrophys. J.* **909**, 218 (2021), arXiv:1908.06060 [astro-ph.CO].
- [40] Shivam Pandey, Marco Raveri, and Bhuvnesh Jain, “Model independent comparison of supernova and strong lensing cosmography: Implications for the Hubble constant tension,” *Phys. Rev. D* **102**, 023505 (2020), arXiv:1912.04325 [astro-ph.CO].
- [41] Hsin-Yu Chen, Maya Fishbach, and Daniel E. Holz, “A two per cent Hubble constant measurement from standard sirens within five years,” *Nature* **562**, 545–547 (2018), arXiv:1712.06531 [astro-ph.CO].
- [42] Amir Aghamousa et al. (DESI), “The DESI Experiment Part I: Science, Targeting, and Survey Design,” (2016), arXiv:1611.00036 [astro-ph.IM].
- [43] R. Laureijs et al. (EUCLID), “Euclid Definition Study Report,” (2011), arXiv:1110.3193 [astro-ph.CO].
- [44] Peter Ade et al. (Simons Observatory), “The Simons Observatory: Science goals and forecasts,” *JCAP* **02**, 056 (2019), arXiv:1808.07445 [astro-ph.CO].
- [45] Kevork N. Abazajian et al. (CMB-S4), “CMB-S4 Science Book, First Edition,” (2016), arXiv:1610.02743 [astro-ph.CO].
- [46] Adam G. Riess, Stefano Casertano, Wenlong Yuan, Lucas M. Macri, and Dan Scolnic, “Large Magellanic Cloud Cepheid Standards Provide a 1% Foundation for the Determination of the Hubble Constant and Stronger Evidence for Physics beyond Λ CDM,” *Astrophys. J.* **876**, 85 (2019), arXiv:1903.07603 [astro-ph.CO].
- [47] Adam G. Riess, Stefano Casertano, Wenlong Yuan, J. Bradley Bowers, Lucas Macri, Joel C. Zinn, and Dan Scolnic, “Cosmic Distances Calibrated to 1% Precision with Gaia EDR3 Parallaxes and Hubble Space Telescope Photometry of 75 Milky Way Cepheids Confirm Tension with Λ CDM,” *Astrophys. J. Lett.* **908**, L6 (2021), arXiv:2012.08534 [astro-ph.CO].
- [48] Marc Kamionkowski and Adam G. Riess, “The Hubble Tension and Early Dark Energy,” (2022), arXiv:2211.04492 [astro-ph.CO].
- [49] Dan Scolnic et al., “The Pantheon+ Analysis: The Full Dataset and Light-Curve Release,” (2021), arXiv:2112.03863 [astro-ph.CO].
- [50] Shadab Alam et al. (eBOSS), “Completed SDSS-IV extended Baryon Oscillation Spectroscopic Survey: Cosmological implications from two decades of spectroscopic surveys at the Apache Point Observatory,” *Phys. Rev. D* **103**, 083533 (2021), arXiv:2007.08991 [astro-ph.CO].
- [51] Jose Luis Bernal, Licia Verde, and Adam G. Riess, “The trouble with H_0 ,” *JCAP* **1610**, 019 (2016), arXiv:1607.05617.
- [52] Vivian Poulin, Kimberly K. Boddy, Simeon Bird, and Marc Kamionkowski, “Implications of an extended dark energy cosmology with massive neutrinos for cosmological tensions,” *Phys. Rev. D* **97**, 123504 (2018), arXiv:1803.02474.
- [53] David Camarena and Valerio Marra, “On the use of the local prior on the absolute magnitude of Type Ia supernovae in cosmological inference,” *Mon. Not. Roy. Astron. Soc.* **504**, 5164–5171 (2021), arXiv:2101.08641 [astro-ph.CO].
- [54] George Efstathiou, “To H_0 or not to H_0 ?” *Mon. Not. Roy. Astron. Soc.* **505**, 3866–3872 (2021), arXiv:2103.08723 [astro-ph.CO].
- [55] Levon Pogosian, Marco Raveri, Kazuya Koyama, Matteo Martinelli, Alessandra Silvestri, and Gong-Bo Zhao, “Imprints of cosmological tensions in reconstructed gravity,” (2021), arXiv:2107.12992 [astro-ph.CO].
- [56] C. Krishnan, Eoin Ó. Colgáin, Ruchika, Anjan A. Sen, M. M. Sheikh-Jabbari, and Tao Yang, “Is there an early Universe solution to Hubble tension?” *Phys. Rev. D* **102**, 103525 (2020), arXiv:2002.06044 [astro-ph.CO].
- [57] Maria Giovanna Dainotti, Biagio De Simone, Tiziano Schiavone, Giovanni Montani, Enrico Rinaldi, and Gaetano Lambiase, “On the Hubble constant tension in the SNe Ia Pantheon sample,” *Astrophys. J.* **912**, 150 (2021), arXiv:2103.02117 [astro-ph.CO].
- [58] Maria Giovanna Dainotti, Biagio De Simone, Tiziano Schiavone, Giovanni Montani, Enrico Rinaldi, Gaetano Lambiase, Malgorzata Bogdan, and Sahil Ugale, “On the Evolution of the Hubble Constant with the SNe Ia Pantheon Sample and Baryon Acoustic Oscillations: A Feasibility Study for GRB-Cosmology in 2030,” *Galaxies* **10**, 24 (2022), arXiv:2201.09848 [astro-ph.CO].
- [59] Chethan Krishnan, Roya Mohayaee, Eoin Ó. Colgáin, M. M. Sheikh-Jabbari, and Lu Yin, “Does Hubble tension signal a breakdown in FLRW cosmology?” *Class. Quant. Grav.* **38**, 184001 (2021), arXiv:2105.09790 [astro-ph.CO].
- [60] Mohammad Malekjani, Ruairí Mc Conville, Eoin Ó. Colgáin, Saeed Pourojaghi, and M. M. Sheikh-Jabbari, “Negative Dark Energy Density from High Redshift Pantheon+ Supernovae,” (2023), arXiv:2301.12725 [astro-ph.CO].
- [61] Dillon Brout et al., “The Pantheon+ Analysis: Cosmological Constraints,” *Astrophys. J.* **938**, 110 (2022), arXiv:2202.04077 [astro-ph.CO].
- [62] Giampaolo Benevento, Wayne Hu, and Marco Raveri, “Can Late Dark Energy Transitions Raise the Hubble constant?” *Phys. Rev. D* **101**, 103517 (2020), arXiv:2002.11707 [astro-ph.CO].
- [63] Kevin Aylor, Mackenzie Joy, Lloyd Knox, Marius Millea, Srinivasan Raghunathan, and W. L. Kimmy Wu, “Sounds Discordant: Classical Distance Ladder & Λ CDM-based Determinations of the Cosmological Sound Horizon,” (2018), arXiv:1811.00537.
- [64] Jarah Evslin, Anjan A. Sen, and Ruchika, “Price of shifting the Hubble constant,” *Phys. Rev. D* **97**, 103511 (2018), arXiv:1711.01051.
- [65] Karsten Jedamzik and Levon Pogosian, “Relieving the Hubble tension with primordial magnetic fields,” *Phys. Rev. Lett.*

- 125**, 181302 (2020), arXiv:2004.09487 [astro-ph.CO].
- [66] Luke Hart and Jens Chluba, “Updated fundamental constant constraints from Planck 2018 data and possible relations to the Hubble tension,” *Mon. Not. Roy. Astron. Soc.* **493**, 3255–3263 (2020), arXiv:1912.03986 [astro-ph.CO].
- [67] Luke Hart and Jens Chluba, “Varying fundamental constants principal component analysis: additional hints about the Hubble tension,” *Mon. Not. Roy. Astron. Soc.* **510**, 2206–2227 (2022), arXiv:2107.12465 [astro-ph.CO].
- [68] Toyokazu Sekiguchi and Tomo Takahashi, “Early recombination as a solution to the H_0 tension,” *Phys. Rev. D* **103**, 083507 (2021), arXiv:2007.03381 [astro-ph.CO].
- [69] Nils Schöneberg, Guillermo Franco Abellán, Andrea Pérez Sánchez, Samuel J. Witte, Vivian Poulin, and Julien Lesgourges, “The H_0 Olympics: A fair ranking of proposed models,” (2021), arXiv:2107.10291 [astro-ph.CO].
- [70] Gen Ye, Bin Hu, and Yun-Song Piao, “Implication of the Hubble tension for the primordial Universe in light of recent cosmological data,” *Phys. Rev. D* **104**, 063510 (2021), arXiv:2103.09729 [astro-ph.CO].
- [71] Michael Doran, Matthew J. Lilley, Jan Schwindt, and Christof Wetterich, “Quintessence and the separation of CMB peaks,” *Astrophys. J.* **559**, 501–506 (2001), arXiv:astro-ph/0012139.
- [72] Christof Wetterich, “Phenomenological parameterization of quintessence,” *Phys. Lett. B* **594**, 17–22 (2004), arXiv:astro-ph/0403289.
- [73] Michael Doran and Georg Robbers, “Early dark energy cosmologies,” *JCAP* **06**, 026 (2006), arXiv:astro-ph/0601544.
- [74] Tanvi Karwal and Marc Kamionkowski, “Dark energy at early times, the Hubble parameter, and the string axiverse,” *Phys. Rev. D* **94**, 103523 (2016), arXiv:1608.01309.
- [75] Vivian Poulin, Tristan L. Smith, Tanvi Karwal, and Marc Kamionkowski, “Early Dark Energy Can Resolve The Hubble Tension,” *Phys. Rev. Lett.* **122**, 221301 (2019), arXiv:1811.04083.
- [76] Tristan L. Smith, Vivian Poulin, and Mustafa A. Amin, “Oscillating scalar fields and the Hubble tension: a resolution with novel signatures,” *Phys. Rev. D* **101**, 063523 (2020), arXiv:1908.06995 [astro-ph.CO].
- [77] Prateek Agrawal, Francis-Yan Cyr-Racine, David Pinner, and Lisa Randall, “Rock ‘n’ Roll Solutions to the Hubble Tension,” (2019), arXiv:1904.01016.
- [78] Meng-Xiang Lin, Giampaolo Benevento, Wayne Hu, and Marco Raveri, “Acoustic Dark Energy: Potential Conversion of the Hubble Tension,” *Phys. Rev. D* **100**, 063542 (2019), arXiv:1905.12618 [astro-ph.CO].
- [79] Stephon Alexander and Evan McDonough, “Axion-Dilaton Destabilization and the Hubble Tension,” *Phys. Lett. B* **797**, 134830 (2019), arXiv:1904.08912 [astro-ph.CO].
- [80] Jeremy Sakstein and Mark Trodden, “Early Dark Energy from Massive Neutrinos as a Natural Resolution of the Hubble Tension,” *Phys. Rev. Lett.* **124**, 161301 (2020), arXiv:1911.11760 [astro-ph.CO].
- [81] Antareep Gogoi, Ravi Kumar Sharma, Prolay Chanda, and Subinoy Das, “Early Mass-varying Neutrino Dark Energy: Nugget Formation and Hubble Anomaly,” *Astrophysical Journal* **915**, 132 (2021), arXiv:2005.11889 [astro-ph.CO].
- [82] Florian Niedermann and Martin S. Sloth, “New early dark energy,” *Phys. Rev. D* **103**, L041303 (2021), arXiv:1910.10739 [astro-ph.CO].
- [83] Florian Niedermann and Martin S. Sloth, “Resolving the Hubble tension with new early dark energy,” *Phys. Rev. D* **102**, 063527 (2020), arXiv:2006.06686 [astro-ph.CO].
- [84] Florian Niedermann and Martin S. Sloth, “Hot new early dark energy,” *Phys. Rev. D* **105**, 063509 (2022), arXiv:2112.00770 [hep-ph].
- [85] Gen Ye and Yun-Song Piao, “Is the Hubble tension a hint of AdS phase around recombination?” *Phys. Rev. D* **101**, 083507 (2020), arXiv:2001.02451 [astro-ph.CO].
- [86] Kim V. Berghaus and Tanvi Karwal, “Thermal Friction as a Solution to the Hubble Tension,” *Phys. Rev. D* **101**, 083537 (2020), arXiv:1911.06281 [astro-ph.CO].
- [87] Katherine Freese and Martin Wolfgang Winkler, “Chain early dark energy: A Proposal for solving the Hubble tension and explaining today’s dark energy,” *Phys. Rev. D* **104**, 083533 (2021), arXiv:2102.13655 [astro-ph.CO].
- [88] Matteo Braglia, William T. Emond, Fabio Finelli, A. Emir Gumrukcuoglu, and Kazuya Koyama, “Unified framework for early dark energy from α -attractors,” *Phys. Rev. D* **102**, 083513 (2020), arXiv:2005.14053 [astro-ph.CO].
- [89] Vivian I. Sabla and Robert R. Caldwell, “No H_0 assistance from assisted quintessence,” *Phys. Rev. D* **103**, 103506 (2021), arXiv:2103.04999 [astro-ph.CO].
- [90] Vivian I. Sabla and Robert R. Caldwell, “Microphysics of early dark energy,” *Phys. Rev. D* **106**, 063526 (2022), arXiv:2202.08291 [astro-ph.CO].
- [91] Adrià Gómez-Valent, Ziyang Zheng, Luca Amendola, Valeria Pettorino, and Christof Wetterich, “Early dark energy in the pre- and postrecombination epochs,” *Phys. Rev. D* **104**, 083536 (2021), arXiv:2107.11065 [astro-ph.CO].
- [92] Adam Moss, Edmund Copeland, Steven Bamford, and Thomas Clarke, “A model-independent reconstruction of dark energy to very high redshift,” (2021), arXiv:2109.14848 [astro-ph.CO].
- [93] Eduardo Guendelman, Ramón Herrera, and David Benisty, “Unifying inflation with early and late dark energy with multiple fields: Spontaneously broken scale invariant two measures theory,” *Phys. Rev. D* **105**, 124035 (2022), arXiv:2201.06470 [gr-qc].
- [94] Tanvi Karwal, Marco Raveri, Bhuvnesh Jain, Justin Khoury, and Mark Trodden, “Chameleon Early Dark Energy and the Hubble Tension,” arXiv e-prints , arXiv:2106.13290 (2021), arXiv:2106.13290.
- [95] Evan McDonough, Meng-Xiang Lin, J. Colin Hill, Wayne Hu, and Shengjia Zhou, “The Early Dark Sector, the Hubble Tension, and the Swampland,” (2021), arXiv:2112.09128 [astro-ph.CO].
- [96] Hao Wang and Yun-Song Piao, “A fraction of dark matter faded with early dark energy ?” (2022), arXiv:2209.09685 [astro-ph.CO].
- [97] Stephon Alexander, Heliudson Bernardo, and Michael W. Toomey, “Addressing the Hubble and S_8 Tensions with a

- Kinetically Mixed Dark Sector,” (2022), arXiv:2207.13086 [astro-ph.CO].
- [98] Evan McDonough and Marco Scalisi, “Towards Early Dark Energy in String Theory,” (2022), arXiv:2209.00011 [hep-th].
- [99] Shota Nakagawa, Fuminobu Takahashi, and Wen Yin, “Early dark energy by dark Higgs, and axion-induced non-thermal trapping,” (2022), arXiv:2209.01107 [astro-ph.CO].
- [100] Adrià Gómez-Valent, Ziyang Zheng, Luca Amendola, Christof Wetterich, and Valeria Pettorino, “Coupled and uncoupled early dark energy, massive neutrinos and the cosmological tensions,” (2022), arXiv:2207.14487 [astro-ph.CO].
- [101] H. Mohseni Sadjadi and V. Anari, “Early dark energy and the screening mechanism,” (2022), arXiv:2205.15693 [gr-qc].
- [102] Kentaro Kojima and Yuri Okubo, “Early dark energy from a higher-dimensional gauge theory,” Phys. Rev. D **106**, 063540 (2022), arXiv:2205.13777 [astro-ph.CO].
- [103] Tom Rudelius, “Constraints on Early Dark Energy from the Axion Weak Gravity Conjecture,” (2022), arXiv:2203.05575 [hep-th].
- [104] V. K. Oikonomou, “Unifying inflation with early and late dark energy epochs in axion $F(R)$ gravity,” Phys. Rev. D **103**, 044036 (2021), arXiv:2012.00586 [astro-ph.CO].
- [105] S. X. Tian and Zong-Hong Zhu, “Early dark energy in k -essence,” Phys. Rev. D **103**, 043518 (2021), arXiv:2102.06399 [gr-qc].
- [106] Michael Maziashvili, “Inflaton-driven early dark energy,” Astropart. Phys. **145**, 102792 (2023), arXiv:2111.07288 [astro-ph.CO].
- [107] Diego Blas, Julien Lesgourgues, and Thomas Tram, “The Cosmic Linear Anisotropy Solving System (CLASS) II: Approximation schemes,” JCAP **1107**, 034 (2011), arXiv:1104.2933.
- [108] Hiroyuki Abe, Tatsuo Kobayashi, and Hajime Otsuka, “Natural inflation with and without modulations in type IIB string theory,” JHEP **04**, 160 (2015), arXiv:1411.4768 [hep-th].
- [109] Kiwoon Choi and Hyungjin Kim, “Aligned natural inflation with modulations,” Phys. Lett. B **759**, 520–527 (2016), arXiv:1511.07201 [hep-th].
- [110] Rolf Kappl, Hans Peter Nilles, and Martin Wolfgang Winkler, “Modulated Natural Inflation,” Phys. Lett. B **753**, 653–659 (2016), arXiv:1511.05560 [hep-th].
- [111] Nemanja Kaloper, “Dark energy, H_0 and weak gravity conjecture,” Int. J. Mod. Phys. D **28**, 1944017 (2019), arXiv:1903.11676 [hep-th].
- [112] Michael Czerny, Tetsutaro Higaki, and Fuminobu Takahashi, “Multi-Natural Inflation in Supergravity and BICEP2,” Phys. Lett. B **734**, 167–172 (2014), arXiv:1403.5883 [hep-ph].
- [113] Djuna Croon and Verónica Sanz, “Saving Natural Inflation,” JCAP **02**, 008 (2015), arXiv:1411.7809 [hep-ph].
- [114] Tetsutaro Higaki and Fuminobu Takahashi, “Elliptic inflation: interpolating from natural inflation to R^2 -inflation,” JHEP **03**, 129 (2015), arXiv:1501.02354 [hep-ph].
- [115] Michele Cicoli, Matteo Licheri, Ratul Mahanta, Evan McDonough, Francisco G. Pedro, and Marco Scalisi, “Early Dark Energy in Type IIB String Theory,” (2023), arXiv:2303.03414 [hep-th].
- [116] Vivian Poulin, Tristan L. Smith, Daniel Grin, Tanvi Karwal, and Marc Kamionkowski, “Cosmological implications of ultralight axionlike fields,” Phys. Rev. **D98**, 083525 (2018), arXiv:1806.10608.
- [117] J. Colin Hill, Evan McDonough, Michael W. Toomey, and Stephon Alexander, “Early dark energy does not restore cosmological concordance,” Phys. Rev. D **102**, 043507 (2020), arXiv:2003.07355 [astro-ph.CO].
- [118] Florian Niedermann and Martin S. Sloth, “Hot New Early Dark Energy: Towards a Unified Dark Sector of Neutrinos, Dark Energy and Dark Matter,” (2021), arXiv:2112.00759 [hep-ph].
- [119] Kim V. Bergmann and Tanvi Karwal, “Thermal Friction as a Solution to the Hubble and Large-Scale Structure Tensions,” (2022), arXiv:2204.09133 [astro-ph.CO].
- [120] Mark Gonzalez, Mark P. Hertzberg, and Fabrizio Rompineve, “Ultralight Scalar Decay and the Hubble Tension,” JCAP **10**, 028 (2020), arXiv:2006.13959 [astro-ph.CO].
- [121] Justin Khoury and Amanda Weltman, “Chameleon fields: Awaiting surprises for tests of gravity in space,” Phys. Rev. Lett. **93**, 171104 (2004), arXiv:astro-ph/0309300.
- [122] Justin Khoury and Amanda Weltman, “Chameleon cosmology,” Phys. Rev. D **69**, 044026 (2004), arXiv:astro-ph/0309411.
- [123] Meng-Xiang Lin, Evan McDonough, J. Colin Hill, and Wayne Hu, “A Dark Matter Trigger for Early Dark Energy Coincidence,” (2022), arXiv:2212.08098 [astro-ph.CO].
- [124] Eric V. Linder, “Dark Energy from α -Attractors,” Phys. Rev. D **91**, 123012 (2015), arXiv:1505.00815 [astro-ph.CO].
- [125] Carlos García-García, Eric V. Linder, Pilar Ruiz-Lapuente, and Miguel Zumalacárregui, “Dark energy from α -attractors: phenomenology and observational constraints,” JCAP **08**, 022 (2018), arXiv:1803.00661 [astro-ph.CO].
- [126] Francisco X. Linares Cedeño, Ariadna Montiel, Juan Carlos Hidalgo, and Gabriel Germán, “Bayesian evidence for α -attractor dark energy models,” JCAP **08**, 002 (2019), arXiv:1905.00834 [gr-qc].
- [127] Konstantinos Dimopoulos and Charlotte Owen, “Quintessential Inflation with α -attractors,” JCAP **06**, 027 (2017), arXiv:1703.00305 [gr-qc].
- [128] Yashar Akrami, Renata Kallosh, Andrei Linde, and Valeri Vardanyan, “Dark energy, α -attractors, and large-scale structure surveys,” JCAP **06**, 041 (2018), arXiv:1712.09693 [hep-th].
- [129] Lucy Brissenden, Konstantinos Dimopoulos, and Samuel Sánchez López, “Non-oscillating Early Dark Energy and Quintessence from Alpha-Attractors,” (2023), arXiv:2301.03572 [astro-ph.CO].
- [130] C. Umiltà, M. Ballardini, F. Finelli, and D. Paoletti, “CMB and BAO constraints for an induced gravity dark energy model with a quartic potential,” JCAP **08**, 017 (2015), arXiv:1507.00718 [astro-ph.CO].
- [131] Massimo Rossi, Mario Ballardini, Matteo Braglia, Fabio Finelli, Daniela Paoletti, Alexei A. Starobinsky, and Caterina Umiltà, “Cosmological constraints on post-Newtonian parameters in effectively massless scalar-tensor theories of gravity,”

- Phys. Rev. D **100**, 103524 (2019), arXiv:1906.10218 [astro-ph.CO].
- [132] Guillermo Ballesteros, Alessio Notari, and Fabrizio Rompineve, “The H_0 tension: ΔG_N vs. ΔN_{eff} ,” JCAP **11**, 024 (2020), arXiv:2004.05049 [astro-ph.CO].
- [133] Matteo Braglia, Mario Ballardini, William T. Emond, Fabio Finelli, A. Emir Gumrukcuoglu, Kazuya Koyama, and Daniela Paoletti, “Larger value for H_0 by an evolving gravitational constant,” Phys. Rev. D **102**, 023529 (2020), arXiv:2004.11161 [astro-ph.CO].
- [134] Miguel Zumalacarregui, “Gravity in the Era of Equality: Towards solutions to the Hubble problem without fine-tuned initial conditions,” Phys. Rev. D **102**, 023523 (2020), arXiv:2003.06396 [astro-ph.CO].
- [135] Tal Abadi and Ely D. Kovetz, “Can conformally coupled modified gravity solve the Hubble tension?” Phys. Rev. D **103**, 023530 (2021), arXiv:2011.13853 [astro-ph.CO].
- [136] Mario Ballardini, Matteo Braglia, Fabio Finelli, Daniela Paoletti, Alexei A. Starobinsky, and Caterina Umiłtā, “Scalar-tensor theories of gravity, neutrino physics, and the H_0 tension,” JCAP **10**, 044 (2020), arXiv:2004.14349 [astro-ph.CO].
- [137] Matteo Braglia, Mario Ballardini, Fabio Finelli, and Kazuya Koyama, “Early modified gravity in light of the H_0 tension and LSS data,” Phys. Rev. D **103**, 043528 (2021), arXiv:2011.12934 [astro-ph.CO].
- [138] Renée Hlozek, David J. E. Marsh, and Daniel Grin, “Using the Full Power of the Cosmic Microwave Background to Probe Axion Dark Matter,” Mon. Not. Roy. Astron. Soc. **476**, 3063–3085 (2018), arXiv:1708.05681.
- [139] Mariana Carrillo González, Qiuyue Liang, Jeremy Sakstein, and Mark Trodden, “Neutrino-Assisted Early Dark Energy: Theory and Cosmology,” JCAP **04**, 063 (2021), arXiv:2011.09895 [astro-ph.CO].
- [140] Samuel Brieden, Héctor Gil-Marín, and Licia Verde, “Model-agnostic interpretation of 10 billion years of cosmic evolution traced by BOSS and eBOSS data,” JCAP **08**, 024 (2022), arXiv:2204.11868 [astro-ph.CO].
- [141] Théo Simon, Pierre Zhang, and Vivian Poulin, “Cosmological inference from the EFTofLSS: the eBOSS QSO full-shape analysis,” (2022), arXiv:2210.14931 [astro-ph.CO].
- [142] Guillermo Franco Abellán, Zackaria Chacko, Abhish Dev, Peizhi Du, Vivian Poulin, and Yuhsin Tsai, “Improved cosmological constraints on the neutrino mass and lifetime,” JHEP **08**, 076 (2022), arXiv:2112.13862 [hep-ph].
- [143] Ivan Esteban and Jordi Salvado, “Long Range Interactions in Cosmology: Implications for Neutrinos,” JCAP **05**, 036 (2021), arXiv:2101.05804 [hep-ph].
- [144] Riccardo Murgia, Guillermo F. Abellán, and Vivian Poulin, “Early dark energy resolution to the Hubble tension in light of weak lensing surveys and lensing anomalies,” Phys. Rev. D **103**, 063502 (2021), arXiv:2009.10733 [astro-ph.CO].
- [145] Alexander Reeves, Laura Herold, Sunny Vagnozzi, Blake D. Sherwin, and Elisa G. M. Ferreira, “Restoring cosmological concordance with early dark energy and massive neutrinos?” (2022), arXiv:2207.01501 [astro-ph.CO].
- [146] Andrei D. Linde, “Eternal extended inflation and graceful exit from old inflation without Jordan-Brans-Dicke,” Phys. Lett. B **249**, 18–26 (1990).
- [147] Fred C. Adams and Katherine Freese, “Double field inflation,” Phys. Rev. D **43**, 353–361 (1991), arXiv:hep-ph/0504135.
- [148] Gen Ye, Jun Zhang, and Yun-Song Piao, “Alleviating both H_0 and S8 tensions: Early dark energy lifts the CMB-lockdown on ultralight axion,” Phys. Lett. B **839**, 137770 (2023), arXiv:2107.13391 [astro-ph.CO].
- [149] Luz Ángela García, Leonardo Castañeda, and Juan Manuel Tejeiro, “A novel early dark energy model,” New Astronomy **84**, 101503 (2021).
- [150] Scott Dodelson, Manoj Kaplinghat, and Ewan Stewart, “Solving the coincidence problem : Tracking oscillating energy,” Phys. Rev. Lett. **85**, 5276–5279 (2000), arXiv:astro-ph/0002360 [astro-ph].
- [151] Soo A. Kim, Andrew R. Liddle, and Shinji Tsujikawa, “Dynamics of assisted quintessence,” Phys. Rev. D **72**, 043506 (2005), arXiv:astro-ph/0506076.
- [152] Wayne Hu, “Structure formation with generalized dark matter,” Astrophys. J. **506**, 485–494 (1998), arXiv:astro-ph/9801234.
- [153] Michael S. Turner, “Coherent Scalar Field Oscillations in an Expanding Universe,” Phys. Rev. D**28**, 1243 (1983).
- [154] Chung-Pei Ma and Edmund Bertschinger, “Cosmological perturbation theory in the synchronous and conformal Newtonian gauges,” Astrophys. J. **455**, 7–25 (1995), arXiv:astro-ph/9506072 [astro-ph].
- [155] Matthew C. Johnson and Marc Kamionkowski, “Dynamical and Gravitational Instability of Oscillating-Field Dark Energy and Dark Matter,” Phys. Rev. D**78**, 063010 (2008), arXiv:0805.1748 [astro-ph].
- [156] Xiaolei Li and Arman Shafieloo, “A Simple Phenomenological Emergent Dark Energy Model can Resolve the Hubble Tension,” Astrophys. J. Lett. **883**, L3 (2019), arXiv:1906.08275 [astro-ph.CO].
- [157] Sunny Vagnozzi, “Consistency tests of Λ CDM from the early ISW effect: implications for early-time new physics and the Hubble tension,” arXiv e-prints , arXiv:2105.10425 (2021), arXiv:2105.10425.
- [158] P. A. R. Ade et al. (Planck), “Planck 2015 results. XV. Gravitational lensing,” Astron. Astrophys. **594**, A15 (2016), arXiv:1502.01591 [astro-ph.CO].
- [159] Shadab Alam et al. (BOSS), “The clustering of galaxies in the completed SDSS-III Baryon Oscillation Spectroscopic Survey: cosmological analysis of the DR12 galaxy sample,” Mon. Not. Roy. Astron. Soc. **470**, 2617–2652 (2017), arXiv:1607.03155.
- [160] Ashley J. Ross, Lado Samushia, Cullan Howlett, Will J. Percival, Angela Burden, and Marc Manera, “The clustering of the SDSS DR7 main Galaxy sample – I. A 4 per cent distance measure at $z = 0.15$,” Mon. Not. Roy. Astron. Soc. **449**, 835–847 (2015), arXiv:1409.3242.
- [161] Florian Beutler, Chris Blake, Matthew Colless, D. Heath Jones, Lister Staveley-Smith, Lachlan Campbell, Quentin Parker, Will Saunders, and Fred Watson, “The 6dF Galaxy Survey: Baryon Acoustic Oscillations and the Local Hubble Constant,” Mon. Not. Roy. Astron. Soc. **416**, 3017–3032 (2011), arXiv:1106.3366.

- [162] D. M. Scolnic et al., “The Complete Light-curve Sample of Spectroscopically Confirmed SNe Ia from Pan-STARRS1 and Cosmological Constraints from the Combined Pantheon Sample,” *Astrophys. J.* **859**, 101 (2018), arXiv:1710.00845.
- [163] Théo Simon, Pierre Zhang, Vivian Poulin, and Tristan L. Smith, “Updated constraints from the effective field theory analysis of BOSS power spectrum on Early Dark Energy,” *Phys. Rev. D* **In press** (2022), arXiv:2208.05930 [astro-ph.CO].
- [164] Antony Lewis and Sarah Bridle, “Cosmological parameters from CMB and other data: A Monte Carlo approach,” *Phys. Rev. D* **66**, 103511 (2002), arXiv:astro-ph/0205436.
- [165] Benjamin Audren, Julien Lesgourgues, Karim Benabed, and Simon Prunet, “Conservative Constraints on Early Cosmology: an illustration of the Monte Python cosmological parameter inference code,” *JCAP* **02**, 001 (2013), arXiv:1210.7183 [astro-ph.CO].
- [166] S. Henrot-Versillé, O. Perdereau, S. Plaszczynski, B. Rouillé d’Orfeuil, M. Spinelli, and M. Tristram, “Agnostic cosmology in the CAMEL framework,” (2016), arXiv:1607.02964 [astro-ph.CO].
- [167] Laura Herold, Elisa G. M. Ferreira, and Eiichiro Komatsu, “New constraint on Early Dark Energy from Planck and BOSS data using the profile likelihood,” (2021), arXiv:2112.12140 [astro-ph.CO].
- [168] Tristan L. Smith, Vivian Poulin, José Luis Bernal, Kimberly K. Boddy, Marc Kamionkowski, and Riccardo Murgia, “Early dark energy is not excluded by current large-scale structure data,” *Phys. Rev. D* **103**, 123542 (2021), arXiv:2009.10740 [astro-ph.CO].
- [169] Marco Raveri and Wayne Hu, “Concordance and Discordance in Cosmology,” (2018), arXiv:1806.04649.
- [170] Adrià Gómez-Valent, “Fast test to assess the impact of marginalization in Monte Carlo analyses and its application to cosmology,” *Phys. Rev. D* **106**, 063506 (2022), arXiv:2203.16285 [astro-ph.CO].
- [171] Boryana Hadzhiyska, Kevin Wolz, Susanna Azzoni, David Alonso, Carlos García-García, Jaime Ruiz-Zapatero, and Anže Slosar, “Cosmology with 6 parameters in the Stage-IV era: efficient marginalisation over nuisance parameters,” (2023), arXiv:2301.11895 [astro-ph.CO].
- [172] Laura Herold and Elisa G. M. Ferreira, “Resolving the Hubble tension with Early Dark Energy,” (2022), arXiv:2210.16296 [astro-ph.CO].
- [173] Emil Brinch Holm, Laura Herold, Steen Hannestad, Andreas Nygaard, and Thomas Tram, “Decaying dark matter with profile likelihoods,” *Phys. Rev. D* **107**, L021303 (2023), arXiv:2211.01935 [astro-ph.CO].
- [174] J. Neyman, “Outline of a Theory of Statistical Estimation Based on the Classical Theory of Probability,” *Phil. Trans. Roy. Soc. Lond. A* **236**, 333–380 (1937).
- [175] Gary J. Feldman and Robert D. Cousins, “A Unified approach to the classical statistical analysis of small signals,” *Phys. Rev. D* **57**, 3873–3889 (1998), arXiv:physics/9711021.
- [176] P. A. R. Ade et al. (Planck), “Planck intermediate results. XVI. Profile likelihoods for cosmological parameters,” *Astron. Astrophys.* **566**, A54 (2014), arXiv:1311.1657 [astro-ph.CO].
- [177] Robert E. Kass and Adrian E. Raftery, “Bayes Factors,” *J. Am. Statist. Assoc.* **90**, 773–795 (1995).
- [178] Marco Raveri and Cyrille Doux, “Non-Gaussian estimates of tensions in cosmological parameters,” arXiv e-prints , arXiv:2105.03324 (2021), arXiv:2105.03324.
- [179] Gideon Schwarz, “Estimating the Dimension of a Model,” *The Annals of Statistics* **6**, 461 – 464 (1978).
- [180] Licia Verde, Pavlos Protopapas, and Raul Jimenez, “Planck and the local Universe: Quantifying the tension,” *Physics of the Dark Universe* **2**, 166–175 (2013), arXiv:1306.6766 [astro-ph.CO].
- [181] Will Handley and Pablo Lemos, “Quantifying tensions in cosmological parameters: Interpreting the DES evidence ratio,” *Phys. Rev. D* **100**, 043504 (2019), arXiv:1902.04029 [astro-ph.CO].
- [182] Lukas T. Hergt, Will J. Handley, Michael P. Hobson, and Anthony N. Lasenby, “Bayesian evidence for the tensor-to-scalar ratio r and neutrino masses m_ν : Effects of uniform vs logarithmic priors,” *Phys. Rev. D* **103**, 123511 (2021), arXiv:2102.11511 [astro-ph.CO].
- [183] S. S. Wilks, “The Large-Sample Distribution of the Likelihood Ratio for Testing Composite Hypotheses,” *Annals Math. Statist.* **9**, 60–62 (1938).
- [184] Eilam Gross and Ofer Vitells, “Trial factors for the look elsewhere effect in high energy physics,” *Eur. Phys. J. C* **70**, 525–530 (2010), arXiv:1005.1891 [physics.data-an].
- [185] Giacchino Ranucci, “The Profile likelihood ratio and the look elsewhere effect in high energy physics,” *Nucl. Instrum. Meth. A* **661**, 77–85 (2012), arXiv:1201.4604 [physics.data-an].
- [186] Adrian E. Bayer and Uros Seljak, “The look-elsewhere effect from a unified Bayesian and frequentist perspective,” *JCAP* **10**, 009 (2020), arXiv:2007.13821 [physics.data-an].
- [187] Tristan L. Smith, Matteo Lucca, Vivian Poulin, Guillermo F. Abellán, Lennart Balkenhol, Karim Benabed, Silvia Galli, and Riccardo Murgia, “Hints of Early Dark Energy in Planck, SPT, and ACT data: new physics or systematics?” (2022), arXiv:2202.09379 [astro-ph.CO].
- [188] J. Colin Hill et al., “The Atacama Cosmology Telescope: Constraints on Pre-Recombination Early Dark Energy,” (2021), arXiv:2109.04451 [astro-ph.CO].
- [189] Fuminobu Takahashi and Wen Yin, “Cosmological implications of ns 1 in light of the Hubble tension,” *Phys. Lett. B* **830**, 137143 (2022), arXiv:2112.06710 [astro-ph.CO].
- [190] Juan S. Cruz, Florian Niedermann, and Martin S. Sloth, “A grounded perspective on New Early Dark Energy using ACT, SPT, and BICEP/Keck,” (2022), arXiv:2209.02708 [astro-ph.CO].
- [191] Matteo Lucca, “The role of CMB spectral distortions in the Hubble tension: a proof of principle,” *Phys. Lett. B* **810**, 135791 (2020), arXiv:2008.01115 [astro-ph.CO].
- [192] Julien Lesgourgues, Gianpiero Mangano, Gennaro Miele, and Sergio Pastor, *Neutrino Cosmology* (Cambridge University Press, 2013).

- [193] Meng-Xiang Lin, Wayne Hu, and Marco Raveri, “Testing H_0 in Acoustic Dark Energy with Planck and ACT Polarization,” Phys. Rev. D **102**, 123523 (2020), arXiv:2009.08974 [astro-ph.CO].
- [194] Simone Aiola et al. (ACT), “The Atacama Cosmology Telescope: DR4 Maps and Cosmological Parameters,” JCAP **12**, 047 (2020), arXiv:2007.07288 [astro-ph.CO].
- [195] D. Dutcher, L. Balkenhol, P. A. R. Ade, Z. Ahmed, E. Anderes, A. J. Anderson, M. Archipley, J. S. Avva, K. Aylor, P. S. Barry, R. Basu Thakur, K. Benabed, A. N. Bender, B. A. Benson, F. Bianchini, L. E. Bleem, F. R. Bouchet, L. Bryant, K. Byrum, J. E. Carlstrom, F. W. Carter, T. W. Cecil, C. L. Chang, P. Chaubal, G. Chen, H. M. Cho, T. L. Chou, J. F. Cliche, T. M. Crawford, A. Cukierman, C. Daley, T. de Haan, E. V. Denison, K. Dibert, J. Ding, M. A. Dobbs, W. Everett, C. Feng, K. R. Ferguson, A. Foster, J. Fu, S. Galli, A. E. Gambrel, R. W. Gardner, N. Goeckner-Wald, R. Gualtieri, S. Guns, N. Gupta, R. Guyser, N. W. Halverson, A. H. Harke-Hosemann, N. L. Harrington, J. W. Henning, G. C. Hilton, E. Hivon, G. P. Holder, W. L. Holzapfel, J. C. Hood, D. Howe, N. Huang, K. D. Irwin, O. B. Jeong, M. Jonas, A. Jones, T. S. Khaire, L. Knox, A. M. Kofman, M. Korman, D. L. Kubik, S. Kuhlmann, C. L. Kuo, A. T. Lee, E. M. Leitch, A. E. Lowitz, C. Lu, S. S. Meyer, D. Michalik, M. Millea, J. Montgomery, A. Nadolski, T. Natoli, H. Nguyen, G. I. Noble, V. Novosad, Y. Omori, S. Padin, Z. Pan, P. Paschos, J. Pearson, C. M. Posada, K. Prabhu, W. Quan, S. Raghunathan, A. Rahlin, C. L. Reichardt, D. Riebel, B. Riedel, M. Rouble, J. E. Ruhl, J. T. Sayre, E. Schiappucci, E. Shirokoff, G. Smecher, J. A. Sobrin, A. A. Stark, J. Stephen, K. T. Story, A. Suzuki, K. L. Thompson, B. Thorne, C. Tucker, C. Umlita, L. R. Vale, K. Vanderlinde, J. D. Vieira, G. Wang, N. Whitehorn, W. L. K. Wu, V. Yefremenko, K. W. Yoon, and M. R. Young, “Measurements of the E-Mode Polarization and Temperature-E-Mode Correlation of the CMB from SPT-3G 2018 Data,” arXiv e-prints , arXiv:2101.01684 (2021), arXiv:2101.01684.
- [196] L. Balkenhol et al. (SPT-3G), “A Measurement of the CMB Temperature Power Spectrum and Constraints on Cosmology from the SPT-3G 2018 TT/TE/EE Data Set,” (2022), arXiv:2212.05642 [astro-ph.CO].
- [197] Adrien La Posta, Thibaut Louis, Xavier Garrido, and J. Colin Hill, “Constraints on Pre-Recombination Early Dark Energy from SPT-3G Public Data,” (2021), arXiv:2112.10754 [astro-ph.CO].
- [198] Anton Chudaykin, Dmitry Gorbunov, and Nikita Nedelko, “Combined analysis of Planck and SPTPol data favors the early dark energy models,” JCAP **08**, 013 (2020), arXiv:2004.13046 [astro-ph.CO].
- [199] Anton Chudaykin, Dmitry Gorbunov, and Nikita Nedelko, “Exploring an early dark energy solution to the Hubble tension with Planck and SPTPol data,” Phys. Rev. D **103**, 043529 (2021), arXiv:2011.04682 [astro-ph.CO].
- [200] Tristan L. Smith, Vivian Poulin, and Théo Simon, “Assessing the robustness of sound horizon-free determinations of the Hubble constant,” (2022), arXiv:2208.12992 [astro-ph.CO].
- [201] Will Handley and Pablo Lemos, “Quantifying the global parameter tensions between ACT, SPT and Planck,” Phys. Rev. D **103**, 063529 (2021), arXiv:2007.08496 [astro-ph.CO].
- [202] Eleonora Di Valentino, William Giarè, Alessandro Melchiorri, and Joseph Silk, “A health checkup test of the standard cosmological model in view of recent Cosmic Microwave Background Anisotropies experiments,” (2022), arXiv:2209.12872 [astro-ph.CO].
- [203] G. E. Addison, Y. Huang, D. J. Watts, C. L. Bennett, M. Halpern, G. Hinshaw, and J. L. Weiland, “Quantifying discordance in the 2015 Planck CMB spectrum,” Astrophys. J. **818**, 132 (2016), arXiv:1511.00055.
- [204] N. Aghanim et al. (Planck), “Planck intermediate results. LI. Features in the cosmic microwave background temperature power spectrum and shifts in cosmological parameters,” Astron. Astrophys. **607**, A95 (2017), arXiv:1608.02487 [astro-ph.CO].
- [205] Vivian Poulin, Tristan L. Smith, and Alexa Bartlett, “Dark energy at early times and ACT data: A larger Hubble constant without late-time priors,” Phys. Rev. D **104**, 123550 (2021), arXiv:2109.06229 [astro-ph.CO].
- [206] Kim Griest, “Toward a possible solution to the cosmic coincidence problem,” Phys. Rev. D **66**, 123501 (2002), arXiv:astro-ph/0202052.
- [207] Asimina Arvanitaki, Savas Dimopoulos, Sergei Dubovsky, Nemanja Kaloper, and John March-Russell, “String Axiverse,” Phys. Rev. D **81**, 123530 (2010), arXiv:0905.4720 [hep-th].
- [208] Marc Kamionkowski, Josef Pradler, and Devin G. E. Walker, “Dark energy from the string axiverse,” Phys. Rev. Lett. **113**, 251302 (2014), arXiv:1409.0549 [hep-ph].
- [209] Eric V. Linder and Tristan L. Smith, “Dark Before Light: Testing the Cosmic Expansion History through the Cosmic Microwave Background,” JCAP **1104**, 001 (2011), arXiv:1009.3500.
- [210] Johan Samsing, Eric V. Linder, and Tristan L. Smith, “Model Independent Early Expansion History and Dark Energy,” Phys. Rev. D **86**, 123504 (2012), arXiv:1208.4845 [astro-ph.CO].
- [211] Alireza Hojjati, Eric V. Linder, and Johan Samsing, “New Constraints on the Early Expansion History of the Universe,” Phys. Rev. Lett. **111**, 041301 (2013), arXiv:1304.3724.
- [212] Daniel Aloni, Asher Berlin, Melissa Joseph, Martin Schmaltz, and Neal Weiner, “A Step in Understanding the Hubble Tension,” (2021), arXiv:2111.00014 [astro-ph.CO].
- [213] Melissa Joseph, Daniel Aloni, Martin Schmaltz, Eashwar N. Sivarajan, and Neal Weiner, “A Step in Understanding the S_8 Tension,” (2022), arXiv:2207.03500 [astro-ph.CO].
- [214] Manuel A. Buen-Abad, Zackaria Chacko, Can Kilic, Gustavo Marques-Tavares, and Taewook Youn, “Stepped Partially Acoustic Dark Matter, Large Scale Structure, and the Hubble Tension,” (2022), arXiv:2208.05984 [hep-ph].
- [215] Y. Akrami et al. (Planck), “Planck 2018 results. X. Constraints on inflation,” Astron. Astrophys. **641**, A10 (2020), arXiv:1807.06211 [astro-ph.CO].
- [216] Minsu Park, Marco Raveri, and Bhuvnesh Jain, “Reconstructing Quintessence,” Phys. Rev. D **103**, 103530 (2021), arXiv:2101.04666 [astro-ph.CO].
- [217] Samuel Goldstein, Minsu Park, Marco Raveri, Bhuvnesh Jain, and Lado Samushia, “Beyond dark energy Fisher forecasts:

- how DESI will constrain LCDM and quintessence models,” (2022), arXiv:2207.01612 [astro-ph.CO].
- [218] Catherine Heymans et al., “CFHTLenS: The Canada-France-Hawaii Telescope Lensing Survey,” *Mon. Not. Roy. Astron. Soc.* **427**, 146 (2012), arXiv:1210.0032.
- [219] P. A. R. Ade et al. (Planck), “Planck 2015 results. XXIV. Cosmology from Sunyaev-Zeldovich cluster counts,” *Astron. Astrophys.* **594**, A24 (2016), arXiv:1502.01597 [astro-ph.CO].
- [220] Catherine Heymans et al., “KiDS-1000 Cosmology: Multi-probe weak gravitational lensing and spectroscopic galaxy clustering constraints,” (2020) arXiv:2007.15632 [astro-ph.CO].
- [221] T. M. C. Abbott et al. (DES), “Dark Energy Survey Year 3 results: Cosmological constraints from galaxy clustering and weak lensing,” *Phys. Rev. D* **105**, 023520 (2022), arXiv:2105.13549 [astro-ph.CO].
- [222] Chiaki Hikage et al. (HSC), “Cosmology from cosmic shear power spectra with Subaru Hyper Suprime-Cam first-year data,” *Publ. Astron. Soc. Jap.* **71**, Publications of the Astronomical Society of Japan, Volume 71, Issue 2, April 2019, 43, <https://doi.org/10.1093/pasj/psz010> (2019), arXiv:1809.09148 [astro-ph.CO].
- [223] Karsten Jedamzik, Levon Pogosian, and Gong-Bo Zhao, “Why reducing the cosmic sound horizon alone can not fully resolve the Hubble tension,” *Commun. in Phys.* **4**, 123 (2021), arXiv:2010.04158 [astro-ph.CO].
- [224] Steven J. Clark, Kyriakos Vattis, JiJi Fan, and Savvas M. Koushiappas, “The H_0 and S_8 tensions necessitate early and late time changes to Λ CDM,” (2021), arXiv:2110.09562 [astro-ph.CO].
- [225] Itamar J. Allali, Mark P. Hertzberg, and Fabrizio Rompineve, “Dark sector to restore cosmological concordance,” *Phys. Rev. D* **104**, L081303 (2021), arXiv:2104.12798 [astro-ph.CO].
- [226] Anatoly Klypin, Vivian Poulin, Francisco Prada, Joel Primack, Marc Kamionkowski, Vladimir Avila-Reese, Aldo Rodriguez-Puebla, Peter Behroozi, Doug Hellinger, and Tristan L. Smith, “Clustering and Halo Abundances in Early Dark Energy Cosmological Models,” *Mon. Not. Roy. Astron. Soc.* **504**, 769–781 (2021), arXiv:2006.14910 [astro-ph.CO].
- [227] Lucas F. Secco, Tanvi Karwal, Wayne Hu, and Elisabeth Krause, “The Role of the Hubble Scale in the Weak Lensing vs. CMB Tension,” (2022), arXiv:2209.12997 [astro-ph.CO].
- [228] Guido D’Amico, Yaniv Donath, Matthew Lewandowski, Leonardo Senatore, and Pierre Zhang, “The BOSS bispectrum analysis at one loop from the Effective Field Theory of Large-Scale Structure,” (2022), arXiv:2206.08327 [astro-ph.CO].
- [229] Daniel Baumann, Alberto Nicolis, Leonardo Senatore, and Matias Zaldarriaga, “Cosmological Non-Linearities as an Effective Fluid,” *JCAP* **07**, 051 (2012), arXiv:1004.2488 [astro-ph.CO].
- [230] John Joseph M. Carrasco, Mark P. Hertzberg, and Leonardo Senatore, “The Effective Field Theory of Cosmological Large Scale Structures,” *JHEP* **09**, 082 (2012), arXiv:1206.2926 [astro-ph.CO].
- [231] Leonardo Senatore and Matias Zaldarriaga, “The IR-resummed Effective Field Theory of Large Scale Structures,” *JCAP* **1502**, 013 (2015), arXiv:1404.5954 [astro-ph.CO].
- [232] Leonardo Senatore, “Bias in the Effective Field Theory of Large Scale Structures,” *JCAP* **1511**, 007 (2015), arXiv:1406.7843 [astro-ph.CO].
- [233] Leonardo Senatore and Matias Zaldarriaga, “Redshift Space Distortions in the Effective Field Theory of Large Scale Structures,” (2014), arXiv:1409.1225 [astro-ph.CO].
- [234] Ashley Perko, Leonardo Senatore, Elise Jennings, and Risa H. Wechsler, “Biased Tracers in Redshift Space in the EFT of Large-Scale Structure,” (2016), arXiv:1610.09321 [astro-ph.CO].
- [235] Shadab Alam et al. (BOSS), “The clustering of galaxies in the completed SDSS-III Baryon Oscillation Spectroscopic Survey: cosmological analysis of the DR12 galaxy sample,” *Mon. Not. Roy. Astron. Soc.* **470**, 2617–2652 (2017), arXiv:1607.03155 [astro-ph.CO].
- [236] Guido D’Amico, Jérôme Gleyzes, Nickolas Kokron, Dida Markovic, Leonardo Senatore, Pierre Zhang, Florian Beutler, and Héctor Gil-Marín, “The Cosmological Analysis of the SDSS/BOSS data from the Effective Field Theory of Large-Scale Structure,” *JCAP* **05**, 005 (2020), arXiv:1909.05271 [astro-ph.CO].
- [237] Mikhail M. Ivanov, Marko Simonović, and Matias Zaldarriaga, “Cosmological Parameters from the BOSS Galaxy Power Spectrum,” (2019), arXiv:1909.05277 [astro-ph.CO].
- [238] Thomas Colas, Guido D’Amico, Leonardo Senatore, Pierre Zhang, and Florian Beutler, “Efficient Cosmological Analysis of the SDSS/BOSS data from the Effective Field Theory of Large-Scale Structure,” *JCAP* **06**, 001 (2020), arXiv:1909.07951 [astro-ph.CO].
- [239] Guido D’Amico, Leonardo Senatore, and Pierre Zhang, “Limits on w CDM from the EFTofLSS with the PyBird code,” (2020), arXiv:2003.07956 [astro-ph.CO].
- [240] Guido D’Amico, Yaniv Donath, Leonardo Senatore, and Pierre Zhang, “Limits on Clustering and Smooth Quintessence from the EFTofLSS,” (2020), arXiv:2012.07554 [astro-ph.CO].
- [241] Théo Simon, Guillermo Franco Abellán, Peizhi Du, Vivian Poulin, and Yuhsin Tsai, “Constraining decaying dark matter with BOSS data and the effective field theory of large-scale structures,” *Phys. Rev. D* **106**, 023516 (2022), arXiv:2203.07440 [astro-ph.CO].
- [242] Shi-Fan Chen, Zvonimir Vlah, and Martin White, “A new analysis of galaxy 2-point functions in the BOSS survey, including full-shape information and post-reconstruction BAO,” *JCAP* **02**, 008 (2022), arXiv:2110.05530 [astro-ph.CO].
- [243] Pierre Zhang, Guido D’Amico, Leonardo Senatore, Cheng Zhao, and Yifu Cai, “BOSS Correlation Function analysis from the Effective Field Theory of Large-Scale Structure,” *JCAP* **02**, 036 (2022), arXiv:2110.07539 [astro-ph.CO].
- [244] Oliver H. E. Philcox and Mikhail M. Ivanov, “BOSS DR12 full-shape cosmology: Λ CDM constraints from the large-scale galaxy power spectrum and bispectrum monopole,” *Phys. Rev. D* **105**, 043517 (2022), arXiv:2112.04515 [astro-ph.CO].
- [245] Suresh Kumar, Rafael C. Nunes, and Priya Yadav, “Updating non-standard neutrinos properties with Planck-CMB data and full-shape analysis of BOSS and eBOSS galaxies,” (2022), arXiv:2205.04292 [astro-ph.CO].
- [246] Rafael C. Nunes, Sunny Vagnozzi, Suresh Kumar, Eleonora Di Valentino, and Olga Mena, “New tests of dark sector

- interactions from the full-shape galaxy power spectrum,” Phys. Rev. D **105**, 123506 (2022), arXiv:2203.08093 [astro-ph.CO].
- [247] Alex Laguë, J. Richard Bond, Renée Hložek, Keir K. Rogers, David J. E. Marsh, and Daniel Grin, “Constraining Ultralight Axions with Galaxy Surveys,” (2021), arXiv:2104.07802 [astro-ph.CO].
- [248] Mikhail M. Ivanov, Evan McDonough, J. Colin Hill, Marko Simonović, Michael W. Toomey, Stephon Alexander, and Matias Zaldarriaga, “Constraining Early Dark Energy with Large-Scale Structure,” Phys. Rev. D **102**, 103502 (2020), arXiv:2006.11235 [astro-ph.CO].
- [249] Guido D’Amico, Leonardo Senatore, Pierre Zhang, and Henry Zheng, “The Hubble Tension in Light of the Full-Shape Analysis of Large-Scale Structure Data,” JCAP **05**, 072 (2021), arXiv:2006.12420 [astro-ph.CO].
- [250] Florian Niedermann and Martin S. Sloth, “New Early Dark Energy is compatible with current LSS data,” Phys. Rev. D **103**, 103537 (2021), arXiv:2009.00006 [astro-ph.CO].
- [251] Oliver H. E. Philcox, Blake D. Sherwin, Gerrit S. Farren, and Eric J. Baxter, “Determining the Hubble Constant without the Sound Horizon: Measurements from Galaxy Surveys,” Phys. Rev. D **103**, 023538 (2021), arXiv:2008.08084 [astro-ph.CO].
- [252] Gerrit S. Farren, Oliver H. E. Philcox, and Blake D. Sherwin, “Determining the Hubble constant without the sound horizon: Perspectives with future galaxy surveys,” Phys. Rev. D **105**, 063503 (2022), arXiv:2112.10749 [astro-ph.CO].
- [253] Oliver H. E. Philcox, Gerrit S. Farren, Blake D. Sherwin, Eric J. Baxter, and Dillon J. Brout, “Determining the Hubble constant without the sound horizon: A 3.6% constraint on H_0 from galaxy surveys, CMB lensing, and supernovae,” Phys. Rev. D **106**, 063530 (2022), arXiv:2204.02984 [astro-ph.CO].
- [254] Ryan Endsley, Peter Behroozi, Daniel P Stark, Christina C Williams, Brant E Robertson, Marcia Rieke, Stefan Gottlöber, and Gustavo Yepes, “Clustering with JWST: Constraining galaxy host halo masses, satellite quenching efficiencies, and merger rates at $z = 4\text{--}10$,” Monthly Notices of the Royal Astronomical Society **493**, 1178–1196 (2020), <https://academic.oup.com/mnras/article-pdf/493/1/1178/32533876/staa324.pdf>.
- [255] Michael Boylan-Kolchin, “Stress Testing Λ CDM with High-redshift Galaxy Candidates,” (2022), arXiv:2208.01611 [astro-ph.CO].
- [256] Samuel Goldstein, J. Colin Hill, Vid Iršič, and Blake D. Sherwin, “Canonical Hubble-Tension-Resolving Early Dark Energy Cosmologies are Inconsistent with the Lyman- α Forest,” (2023), arXiv:2303.00746 [astro-ph.CO].
- [257] Solène Chabanier et al., “The one-dimensional power spectrum from the SDSS DR14 Ly α forests,” JCAP **07**, 017 (2019), arXiv:1812.03554 [astro-ph.CO].
- [258] Vid Iršič et al., “The Lyman α forest power spectrum from the XQ-100 Legacy Survey,” Mon. Not. Roy. Astron. Soc. **466**, 4332–4345 (2017), arXiv:1702.01761 [astro-ph.CO].
- [259] Matteo Viel, George D. Becker, James S. Bolton, and Martin G. Haehnelt, “Warm dark matter as a solution to the small scale crisis: New constraints from high redshift Lyman- α forest data,” Phys. Rev. D **88**, 043502 (2013), arXiv:1306.2314 [astro-ph.CO].
- [260] Nathalie Palanque-Delabrouille, Christophe Yèche, Nils Schöneberg, Julien Lesgourgues, Michael Walther, Solène Chabanier, and Eric Armengaud, “Hints, neutrino bounds and WDM constraints from SDSS DR14 Lyman- α and Planck full-survey data,” JCAP **04**, 038 (2020), arXiv:1911.09073 [astro-ph.CO].
- [261] Deanna C. Hooper and Matteo Lucca, “Hints of dark matter-neutrino interactions in Lyman- α data,” Phys. Rev. D **105**, 103504 (2022), arXiv:2110.04024 [astro-ph.CO].
- [262] Michael Boylan-Kolchin and Daniel R. Weisz, “Uncertain times: the redshift-time relation from cosmology and stars,” Mon. Not. Roy. Astron. Soc. **505**, 2764–2783 (2021), arXiv:2103.15825 [astro-ph.CO].
- [263] David Valcin, José Luis Bernal, Raul Jimenez, Licia Verde, and Benjamin D. Wandelt, “Inferring the Age of the Universe with Globular Clusters,” JCAP **12**, 002 (2020), arXiv:2007.06594 [astro-ph.CO].
- [264] David Valcin, Raul Jimenez, Licia Verde, José Luis Bernal, and Benjamin D. Wandelt, “The age of the Universe with globular clusters: reducing systematic uncertainties,” JCAP **08**, 017 (2021), arXiv:2102.04486 [astro-ph.GA].
- [265] José Luis Bernal, Licia Verde, Raul Jimenez, Marc Kamionkowski, David Valcin, and Benjamin D. Wandelt, “The trouble beyond H_0 and the new cosmic triangles,” Phys. Rev. D **103**, 103533 (2021), arXiv:2102.05066 [astro-ph.CO].
- [266] Sunny Vagnozzi, Fabio Pacucci, and Abraham Loeb, “Implications for the Hubble tension from the ages of the oldest astrophysical objects,” JHEAp **36**, 27–35 (2022), arXiv:2105.10421 [astro-ph.CO].
- [267] Sunny Vagnozzi, Abraham Loeb, and Michele Moresco, “Eppur è piatto? The Cosmic Chronometers Take on Spatial Curvature and Cosmic Concordance,” Astrophys. J. **908**, 84 (2021), arXiv:2011.11645 [astro-ph.CO].
- [268] Guillermo F. Abellan, Riccardo Murgia, Vivian Poulin, and Julien Lavalle, “Hints for decaying dark matter from S_8 measurements,” (2020), arXiv:2008.09615 [astro-ph.CO].
- [269] Zackaria Chacko, Abhish Dev, Peizhi Du, Vivian Poulin, and Yuhsin Tsai, “Cosmological Limits on the Neutrino Mass and Lifetime,” JHEP **04**, 020 (2020), arXiv:1909.05275 [hep-ph].
- [270] Isabel M. Oldengott, Gabriela Barenboim, Sarah Kahlen, Jordi Salvado, and Dominik J. Schwarz, “How to relax the cosmological neutrino mass bound,” JCAP **04**, 049 (2019), arXiv:1901.04352 [astro-ph.CO].
- [271] Emanuele Fondi, Alessandro Melchiorri, and Luca Pagano, “No evidence for EDE from Planck data in extended scenarios,” Astrophys. J. Lett. **931**, L18 (2022), arXiv:2203.12930 [astro-ph.CO].
- [272] Peter Svrcek and Edward Witten, “Axions In String Theory,” JHEP **06**, 051 (2006), arXiv:hep-th/0605206 [hep-th].